NASA CONTRACTOR REPORT

NASA CR-1483

THREE-STAGE POTASSIUM TURBINE PERFORMANCE TEST SUMMARY

by G. C. Wesling

Prepared by
GENERAL ELECTRIC CO.
Cincinnati, Ohio
for Lewis Research Center

NATIONAL AERONAUTICS AND SPACE ADMINISTRATION • WASHINGTON, D. C. • DECEMBER 1969

THREE-STAGE POTASSIUM TURBINE PERFORMANCE TEST SUMMARY

By G. C. Wesling

Issued by Originator as Report No. GESP-271

Prepared under Contract No. NAS 3-10606 by
GENERAL ELECTRIC CO.
Cincinnati, Ohio

for Lewis Research Center

NATIONAL AERONAUTICS AND SPACE ADMINISTRATION

For sale by the Clearinghouse for Federal Scientific and Technical Information
Springfield, Virginia 22151 – Price $3.00

FOREWORD

The research described herein was conducted at the General Electric Company under NASA Contract NAS 3-10606. The project was managed by Mr. Joseph P. Joyce, Space Power Systems Division, NASA Lewis Research Center, with Mr. George M. Kaplan, Space Power Systems Division, NASA Lewis Research Center, as technical advisor. The report was originally issued as General Electric report GESP-271.

CONTENTS

SUMMARY

The three-stage turbine was tested in potassium vapor at rotative speeds from 15,000 to 20,000 rpm, inlet vapor temperatures of 1450 and 1550°F, and turbine pressure ratios from 3 to 10. The measured total to total efficiency of 76 percent at the design conditions of 18,250 rpm, 1550°F inlet temperature and a total pressure ratio of 7.9 agreed with the performance predictions. The performance calculation model was changed from assumed supersaturated expansion through each stage, with reversion to equilibrium properties at each stage exit, to equilibrium properties at each point in the turbine expansion, based on the results of these performance tests.

INTRODUCTION

Latter stages of Rankine Cycle potassium turbines will operate in the wet vapor region for the life of the space power system, e.g., 3 to 5 years. Based on steam turbine experience, it is known that turbine metal corrosion and rotor blade impact damage could occur in these latter stages where blade tip speeds are greatest. A two-stage potassium vapor turbine[1,2]* was designed, built and tested under NASA Contract NAS5-1143. This turbine had about four percent liquid entering the second stage which had a rotor tip velocity of 770 ft/sec at the endurance test conditions. After 5000 hours of testing at these conditions, there was no evidence of impact damage on the turbine rotor blades[3].

Under NASA Contract NAS3-8520 a three-stage potassium vapor turbine was designed to achieve higher levels of moisture and tip velocity. A vapor wetness of between 8 and 10 percent was specified at the inlet of the third stage since it was:

1) Considered achievable by proper loading of the prior stages,

2) Representative of the quality considered in Rankine Cycle system studies, and

3) Deep enough in the wet region to demonstrate possible problems of turbine metal corrosion and rotor blade impact damage.

Major program objectives were to determine whether impact erosion would be a problem for potassium vapor turbines and to refine the fluid design methods for vapor turbines operating in the wet region.

---

* Numbers in parentheses indicate references listed in this report.

The turbine design calculations were based on a calculation model which assumed supersaturated vapor expansions in each turbine stage with reversion to equilibrium conditions after each rotor blade row. The test results of the two-stage turbine[2] supported the selection of this model. For example, the standard deviation of all the experimental power output data from the predicted values was 5.8 KW. The standard deviation of all the efficiency data from the calculated values was 4.4 percentage points. The fluid design of the three-stage turbine was carried out by adding a third stage to the two-stage turbine design[4].

This report presents the results of the performance testing of the three-stage potassium vapor turbine. Test results are presented in terms of blading power output, vapor flow rate, turbine efficiency and turbine pressure ratio. Also presented are the static pressure distributions through the turbine. The predicted turbine performance was calculated with an off design program and is shown for comparison with the test results.

PREDICTED PERFORMANCE

The performance predictions for the three-stage potassium turbine were calculated using an off-design computer program. In this program, the design incidence total-pressure loss coefficient for each blade row is input as a function of turning angle, maximum and trailing edge thickness, and degree of reaction. The total pressure loss coefficient for each blade row is varied in the program according to the incidence angle of the vapor flow relative to the blade, using the design incidence value as a base. The initial off design calculations were based on the supersaturated expansion model with reversion to equilibrium after each stage. Values are input to the program for the following:

a) Flow path dimensions and blading angles.

b) Nozzle flow coefficients determined by air tests.

c) Rotor blade coefficients, calculated from drawings and inspection reports.

d) Total pressure loss coefficients, calculated from experimental results[5].

These include the profile losses, secondary flow and tip clearance losses. Moisture losses were handled separately in two ways; only the vapor flow was assumed to be working fluid and the condensed liquid was assumed to absorb energy from the rotor by being accelerated to rotor tip speed.

The calculated flow rate, blading power and turbine efficiency are shown in Figures 1 through 6, for 15,400, 18,250, and 20,000 rpm, and inlet vapor temperatures of 1450 and 1550°F. Shown in Figures 7 and 8 are the calculated values of vapor quality at the exit of each rotor.

PERFORMANCE TEST

A performance test of the three-stage potassium turbine was conducted with inlet vapor temperatures of 1450 and 1550°F, six rotative speeds between 15,400 and 20,000 rpm, and six pressure ratios between 3 and 10. About half of the points were taken twice so that the repeatability could be established, and a total of 96 data points were taken. A drawing of the potassium turbine is shown in Figure 9. The vapor enters the turbine from the duct on the left side and flows down out of the scroll into a condenser. The turbine power is absorbed by a water brake which is connected to the turbine shaft on the right side.

Vapor pressures were measured at 54 locations and vapor temperatures were measured at 28 locations in the turbine during the performance testing. An instrumentation list is shown in Table I and the measuring stations are identified in Figure 10. The average pressure and temperature at each station were used to analyze the turbine performance. Other performance test measurements were output shaft torque, rotative speed, vapor flow rate and inlet vapor quality. For each data point, these measurements were recorded on digital readout equipment and these data were converted to engineering parameters by means of a data reduction program.

An error analysis made previously for the testing of the two-stage potassium turbine indicated that the largest source of uncertainty in the calculated test efficiency was the measurement of turbine exit pressure. For this reason, new transducers were obtained for the three-stage turbine, with several pressure ranges, to achieve better accuracy at the low exit pressures. Using the influence coefficients from the two-stage

turbine[2], and the manufacturer's specifications for the transducers, the probable errors in efficiency were calculated to be 2.66 percent and 4.21 percent for the 1550°F and 1450°F inlet temperatures, respectively, at a turbine pressure ratio of 8.

The probable errors in flow measurement were estimated to be 2.25 percent and 2.95 percent for inlet temperatures of 1550°F and 1450°F, respectively. The probable errors in power measurement were estimated to be 2 percent and 3 percent for inlet temperatures of 1550°F and 1450°F, respectively.

Prior to the performance testing, the water brake was driven by a steam turbine with the potassium turbine disconnected to check that the two torque meters indicated the same torque. This was done to insure that no torque is transmitted through the flexible hoses to the water brake and steam turbine.

Because one objective of the testing is to improve fluid dynamic design and performance calculation methods, the power output of the turbine blading is desired. Therefore, the parasitic torque of the turbine bearings and the hydrodynamic seal must be obtained. Then the sum of measured shaft output torque and the parasitic torque is the torque output of the turbine blading. The parasitic torque is determined by driving the test turbine shaft, including the water brake, with the steam turbine at various speeds and argon pressures in the loop. The results are shown in Figure 11 as a function of argon density and rotative speed. The argon causes windage losses during parasitic testing which are a function of argon density in the turbine. If the test data are extrapolated to zero density, the windage torque on the turbine blades

is zero and the remaining torque is the desired bearing and seal parasitic torque at the rotative speeds used. These bearing and seal torque values are plotted in Figure 12, for tests run on three dates. The middle line, dated 5/13, was used for the performance tests.

Comparison of the test results were made with the performance predictions, including total to static and total to total efficiency, vapor flow rate, blading power output and turbine static pressures. On each figure the test results are shown by individual points and the predictions are shown by a solid line.

The total to static turbine efficiency is shown in Figures 13 through 16 for 18,250 and 15,400 rpm and inlet vapor temperatures of 1450 and 1550°F. The predictions are in agreement with the test data at 18,250 rpm, but are about 4 points higher than the test data at 15,400 rpm. The scatter in the data at 1450°F is due to the scatter in flow measurement, as will be seen in plots of power output and flow rate. The flow rate data has more scatter than the power output, and efficiency is determined from the ratio of power output to ideal power output, which includes the flow rate.

The total to total turbine efficiency is shown in Figures 17 through 20. Again the agreement between the predictions and the test data is excellent at 18,250 rpm, but the predictions are about 4 points higher than the test data at 15,400 rpm. The scatter due to flow rate measurement is evident in the data at 1450°F.

The vapor flow rate is shown in Figures 21 through 24. The predicted values are about 2 percent greater than the test data at 18,250 rpm, but in agreement with the data at 15,400 rpm.

The blading power output is shown in Figures 25 through 28. The predicted power is about 3 to 4 percent greater than the test data at

18,250 rpm and 8 percent greater than the test data at 15,400 rpm. Although the data are lower than the predictions, they do not have the scatter that was evident in the flow rate data.

The turbine static pressures are shown in Figures 29 through 32. The two top lines for the first stage stator and rotor indicate that the test data are significantly higher than predicted. The next two lines indicate better agreement for the second stage, with the rotor exit pressure greater than predictions at high turbine pressure ratios. The lower lines for the third stage stator and rotor agree with the predicted values.

In general, the measured efficiency agrees with the predictions at the design speed, 18,250 rpm, but the flow and power levels are 2 to 3 percent lower than the predicted values. The static pressures did not agree with the predictions, especially for the first stage.

A verification of the requirement to have a moisture fraction at the third stage inlet of about 8 to 10 percent is desirable. However, it is possible to measure vapor quality only at the turbine inlet where a throttling calorimeter is used. The exit vapor quality can be calculated, however, from the potassium vapor properties[6], the measured inlet conditions of pressure and vapor quality, the measured speed, weight-flow rate and torque, and the measured exit static and total pressures. Shown in Figure 33 is the comparison of the turbine exit vapor quality calculated as indicated above from experimental measurements with the values calculated from the turbine off-design computer program. The experimental data agree with the predictions within 0.33 percentage points, indicating that the vapor quality at the third stage inlet, if it could be measured, would agree with the values presented in Figures 7 and 8.

EVALUATION

Based on the calculation model of supersaturated vapor expansions with reversions to equilibrium conditions after each rotor, it was expected that supersaturation would be evidenced by subcooling below the saturation temperature corresponding to the measured pressure. The test results did not clearly support this model as shown in Figures 34 and 35. The ordinate of these plots is the ratio of measured static pressure to the vapor pressure corresponding to the measured temperature. At stations 4, 6 and 8 which are stator blade exit locations, the supersaturation is negligible. Only at station 7, after the second stage rotor, was there any indicated supersaturation, and even there the subcooling of about 40°F is relatively small. Based on the condensation calculation model[7], it was predicted that subcooling up to 140°F would be experienced in the three-stage turbine. The actual measured subcooling was a maximum of 40°F as shown in Figure 36. The small amounts of measured subcooling seemed to indicate that the turbine expansions were close to equilibrium throughout the turbine.

Because the small amount of subcooling seemed to indicate that the turbine vapor expansions are closer to equilibrium than supersaturated, turbine off design performance was recalculated with a calculation model based on equilibrium expansions. Comparisons with the test results are shown in Figures 37 and 38 for 18,250 rpm and 1550°F inlet vapor temperature. The flow rate in Figure 37 for the equilibrium model agrees with the test results, where the flow calculated with the supersaturated expansion model was about 2 percent higher than the test results, as seen in Figure 21. The static pressure distribution in Figure 38 for the equilibrium model is in better agreement with the test results than the supersaturated model, shown in Figure 29, especially for the first stage where the discrepancy was the greatest. The static pressure variation and the small amount of observed subcooling were major factors in the selection of the equilibrium expansion calculation model.

CALCULATION MODEL

For the supersaturated expansion calculation model it was assumed that only the vapor expanded through the turbine and did work; the condensed liquid was only used to calculate a droplet drag based on accelerating the liquid to the wheel speed of the respective rotor stage. When the equilibrium expansion calculation model was first considered there was some question about how to account for moisture losses. If all the mass flow was assumed to be working fluid, the calculated power and efficiency were higher than the test results. If only the vapor fraction of the mass flow was assumed to be working fluid, the calculated power and efficiency were in good agreement with the test results.

Although the equilibrium calculations were in good agreement with the test results when only the vapor fraction was used as working fluid, it was thought that the moisture losses were not being handled properly in the calculation model. Specifically, the droplet drag was based on accelerating all of the liquid present up to the wheel speed of the respective rotor stage. This is considered unrealistic because only part of the liquid, the part in larger drop sizes, comes into contact with the rotating blades. Also, it was felt that all of the vapor should be used as working fluid, and that the moisture losses are approximately one percent per percent of moisture present.

In steam turbine practice, the moisture losses are considered proportional to the average amount of condensate that is present in a turbine stage or group of stages[8]. A moisture loss of this kind was applied to the equilibrium calculation model instead of using only the vapor fraction and then subtracting droplet drag. The calculation of power and efficiency

agreed with the test results when it was assumed that each percent of liquid present reduced the stage work by 1.2 percent. A comparison of test results with the calculation model is shown in Figures 39 and 58 for the two rotative speeds and two values of inlet vapor temperature. These figures are comparable to Figures 13 through 32 for the original supersaturated expansion calculation model.

Comparing Figures 13-16 and 39-42, it is seen that either model gives an adequate representation of turbine efficiency at the design speed of 18,250 rpm and pressure ratio of 7.9, and neither model is preferable for off-design conditions. Total to total efficiency calculations are practically identical for the two models, as seen by comparing Figures 17-20 and 43-46. Comparing Figures 21-24 and 47-50 it is seen that the supersaturated expansion model calculated flow rates 2 to 3 percent higher than the test results, and the equilibrium expansion model calculates flow rates within 1 percent of the test results, except for 15,400 rpm at 1550°F inlet vapor temperature, which is not simulated well by either calculation model.

Comparing the blading power output in Figures 25-28 and 51-54, it is seen that the equilibrium calculation model is closer to the test results in all cases. Where as the supersaturated expansion calculations were 3 to 8 percent greater than the measured results, the equilibrium expansion model agreed with the test results at the design point and was a maximum of 4 percent greater than the test results at other conditions.

Comparing the static pressure distributions in Figures 29-32 and 55-58, it is seen that the equilibrium model gives better agreement with the measured pressures, especially for the first stage, when the supersaturated model was about 8 percent lower than the test results at the design condi-

tion. Neither calculation model gives a perfect simulation of pressure distribution in all stages, but it is felt that the equilibrium expansion model is generally a better representation of the actual turbine performance.

CONCLUDING REMARKS

The principal surprise in the test results of the three-stage potassium turbine is that the expected subcooling due to supersaturation was not observed. When a calculation model based on equilibrium fluid expansions was used to calculate off design performance of the turbine, the results were in greater agreement with the test results than the calculations which had previously been made with a model based on supersaturated expansions with reversion to equilibrium conditions after each rotor blade row. The value of 1.2 percent loss per percent liquid present used in the moisture loss calculation is consistent with Table I in reference 8, which lists moisture loss factors for steam turbines from ten sources.

REFERENCES

1. "Space Vehicle Rankine Cycle Power Plant Potassium Turbine Development". R. J. Rossbach, ASME 63-WA-326, November 1963.

2. "Two-Stage Potassium Test Turbine, Volume I, Fluid Dynamic Design and Performance." R. J. Rossbach and G. C. Wesling, NASA CR-922, February 1968.

3. "Two-Stage Potassium Test Turbine, Volume IV, Materials Support of Performance and Endurance Tests." W. F. Zimmerman, R. B. Hand, D. S. Engleby, J. W. Semmel, Jr., NASA CR-925, February 1968.

4. "Three-Stage Potassium Test Turbine, Final Design - Volume I - Fluid Design." R. J. Rossbach, G. C. Wesling, W. F. Lemond, NASA CR-72249.

5. "A Method of Performance Estimation for Axial Flow Turbines." D. G. Ainley and G.C.R. Mathieson, A.R.C. (British) R. and M. No. 2074, December 1951.

6. "High-Temperature Properties of Potassium." C.T. Ewing, J.P. Stone, J. R. Spann, E. W. Steinkuller, D. D. Williams and R. R. Miller, NRL Report 6233, September 24, 1965.

7. "Condensation of Wet Vapors in Turbines." WANL-TME-1668, October 15, 1967.

8. "Wetness in Steam Cycles." B. Wood, Proc. Inst. Mech. Engrs., Volume 174, No. 14, 1960.

TABLE I

THREE-STAGE TURBINE INSTRUMENTATION

Station	Total Pressure	Static Pressure	Thermocouple	Taylor Gage
1 - Inlet Duct	2	2	4	1
3 - Bulletnose	4	4	4	
4 - First Nozzle Exit		5	2	
5 - First Rotor Exit		3	2	
6 - Second Nozzle Exit		5	2	
7 - Second Rotor Exit		3	2	
8 - Third Nozzle Exit		5	2	
9 - Third Rotor Exit	4	4	2	1
9.5 - Diffuser Exit	2	4	2	
9.6 - Scroll		4	2	
10 - Exit Duct	2	1	4	1
Total	14	40	28	3

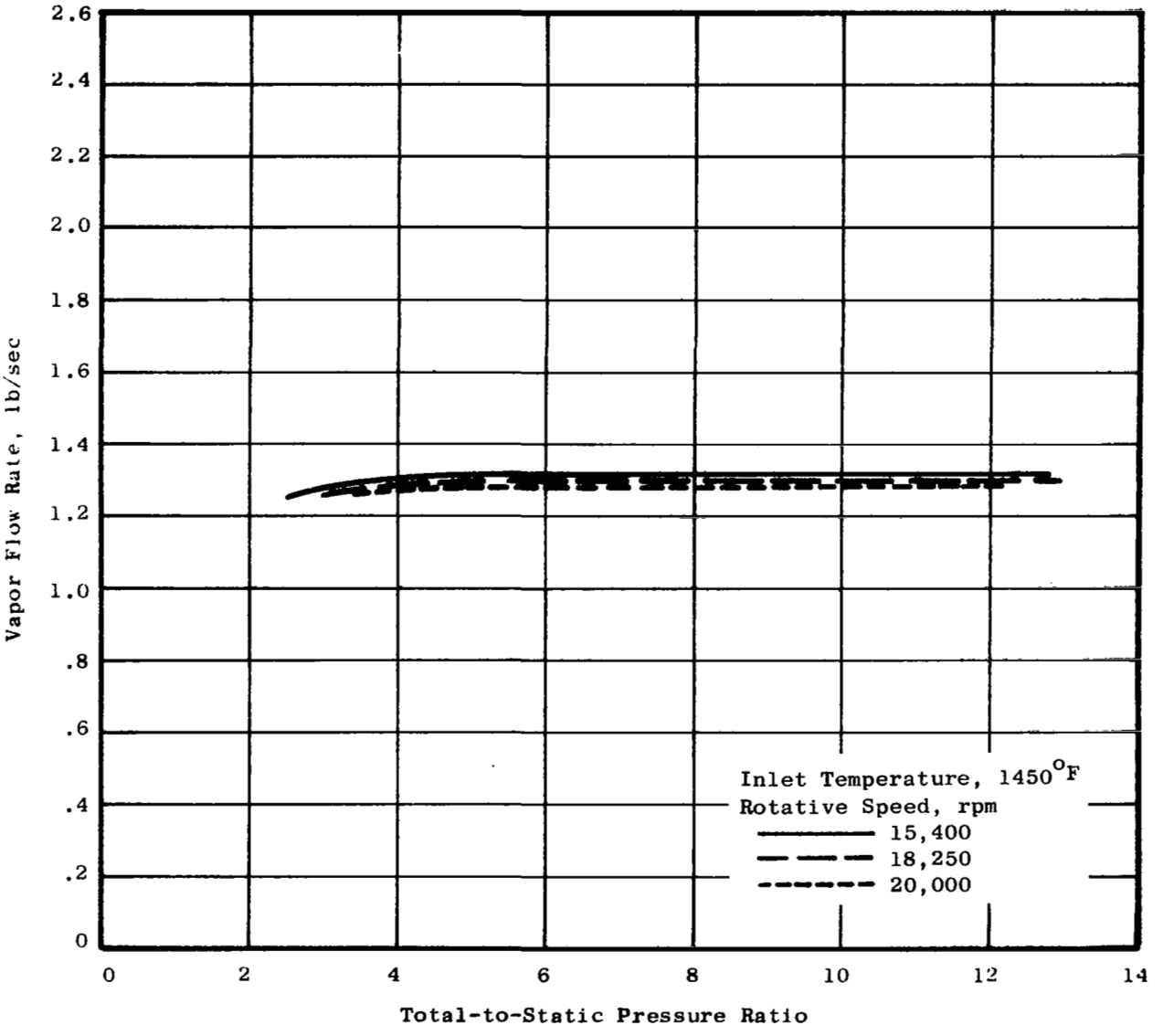

Figure 1. Calculated Vapor Flow Rate.

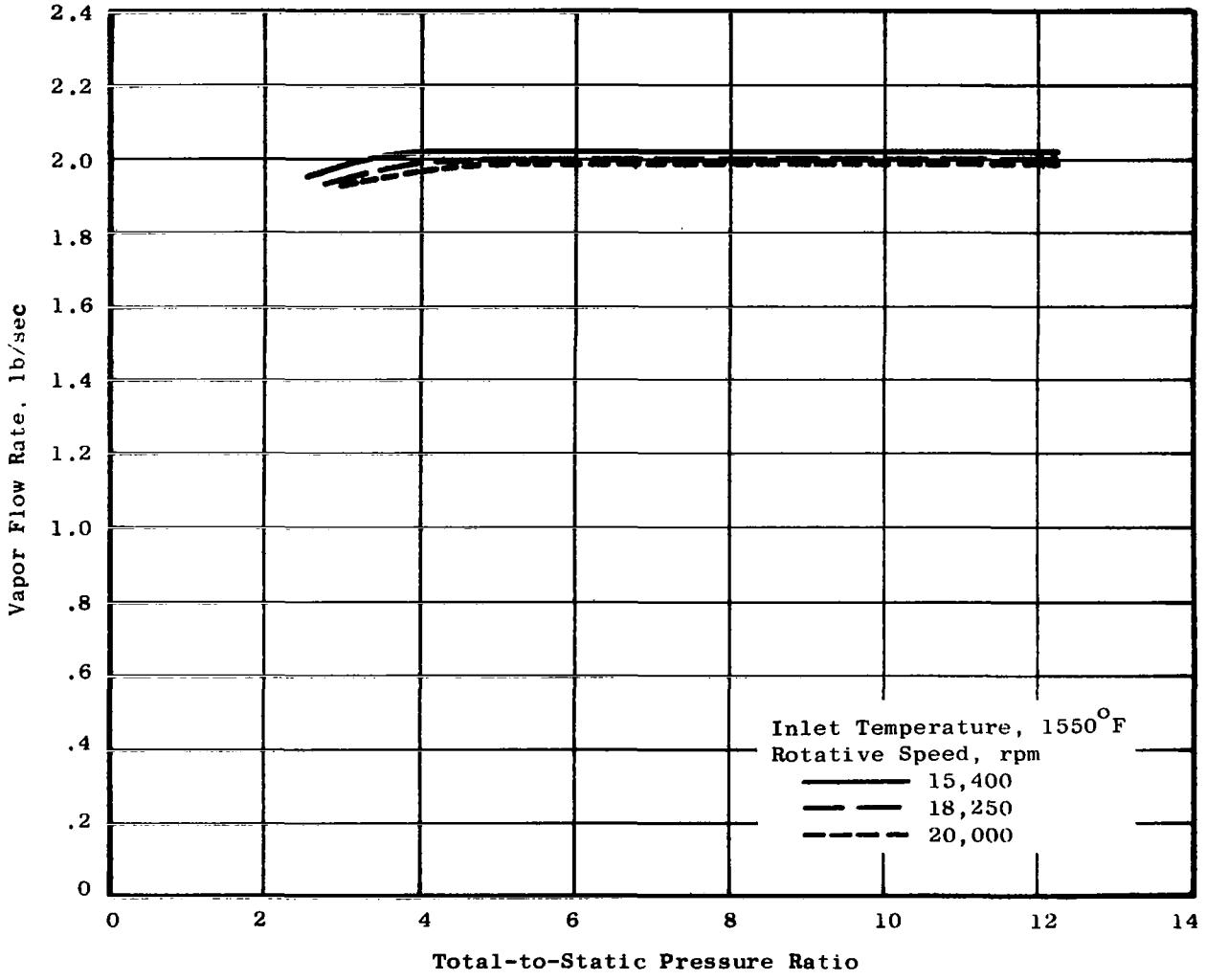

Figure 2. Calculated Vapor Flow Rate.

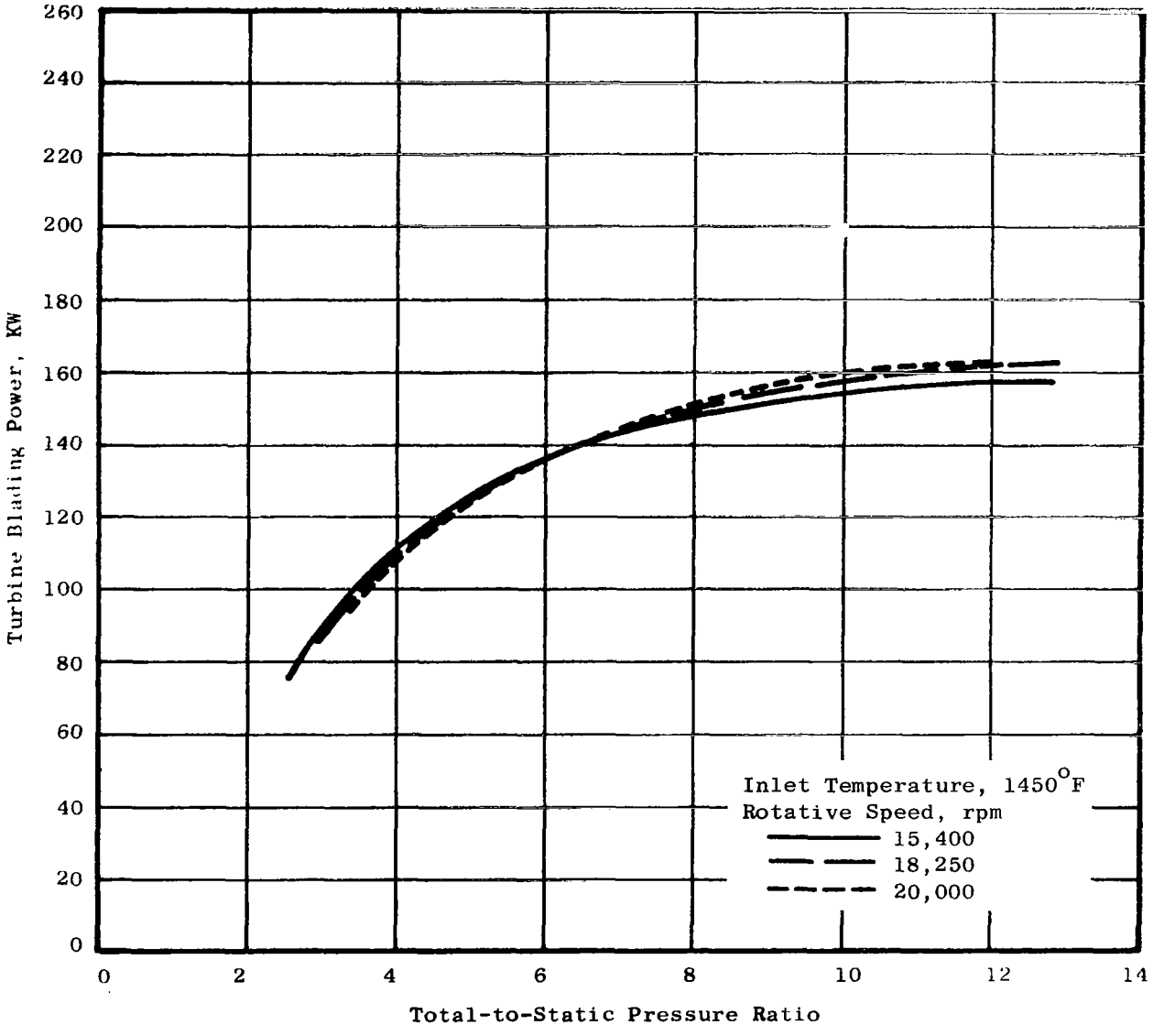

Figure 3. Calculated Turbine Blading Power.

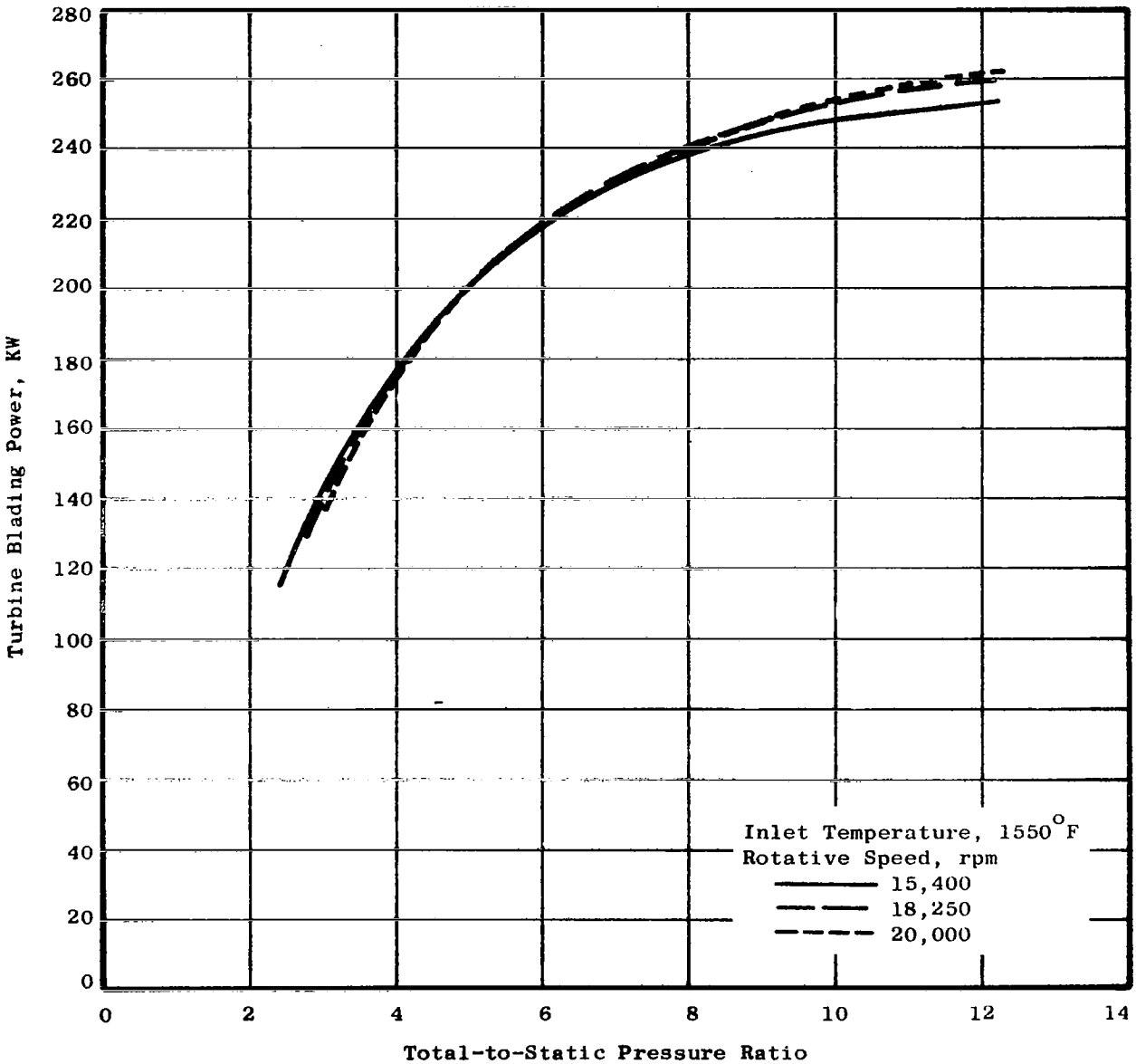

Figure 4. Calculated Turbine Blading Power.

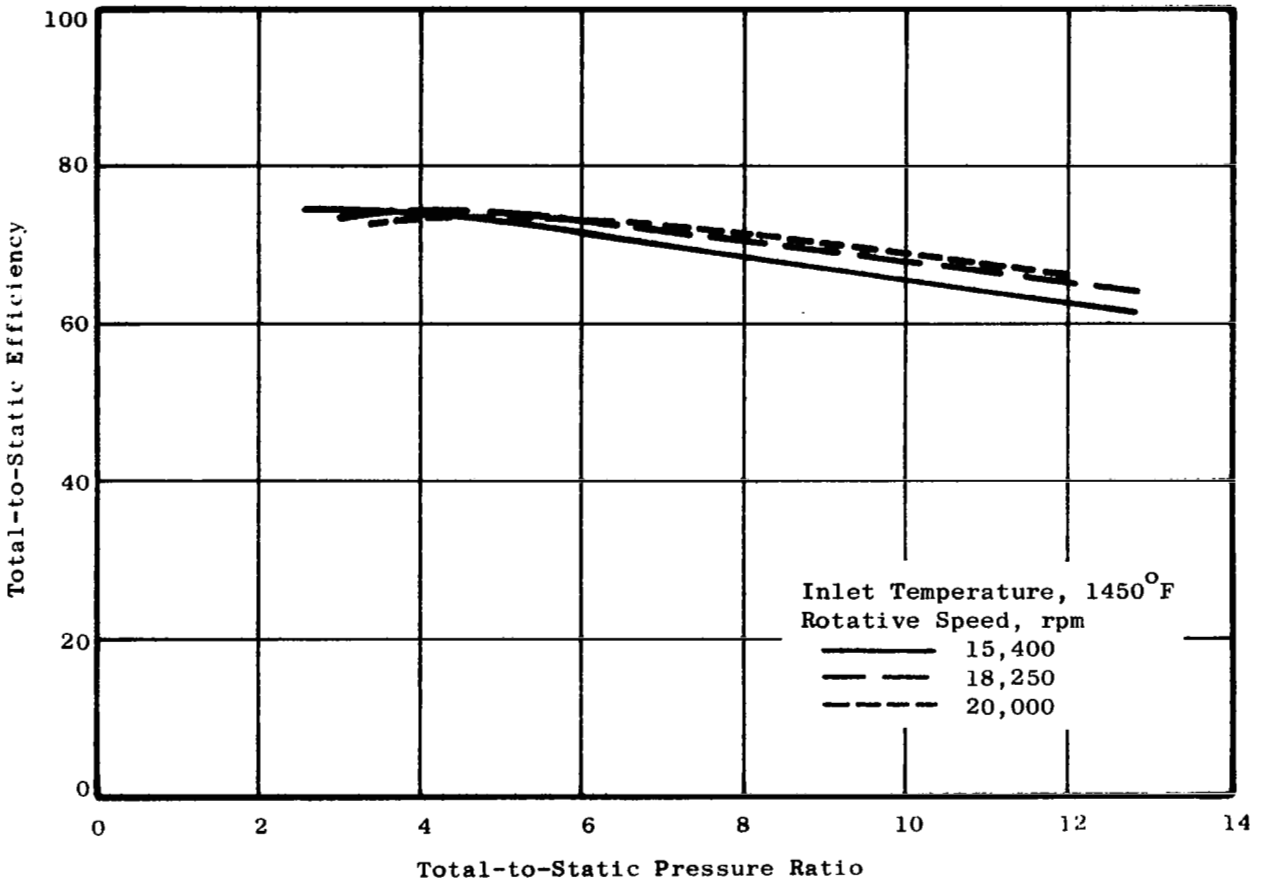

Figure 5. Calculated Total-to-Static Efficiency.

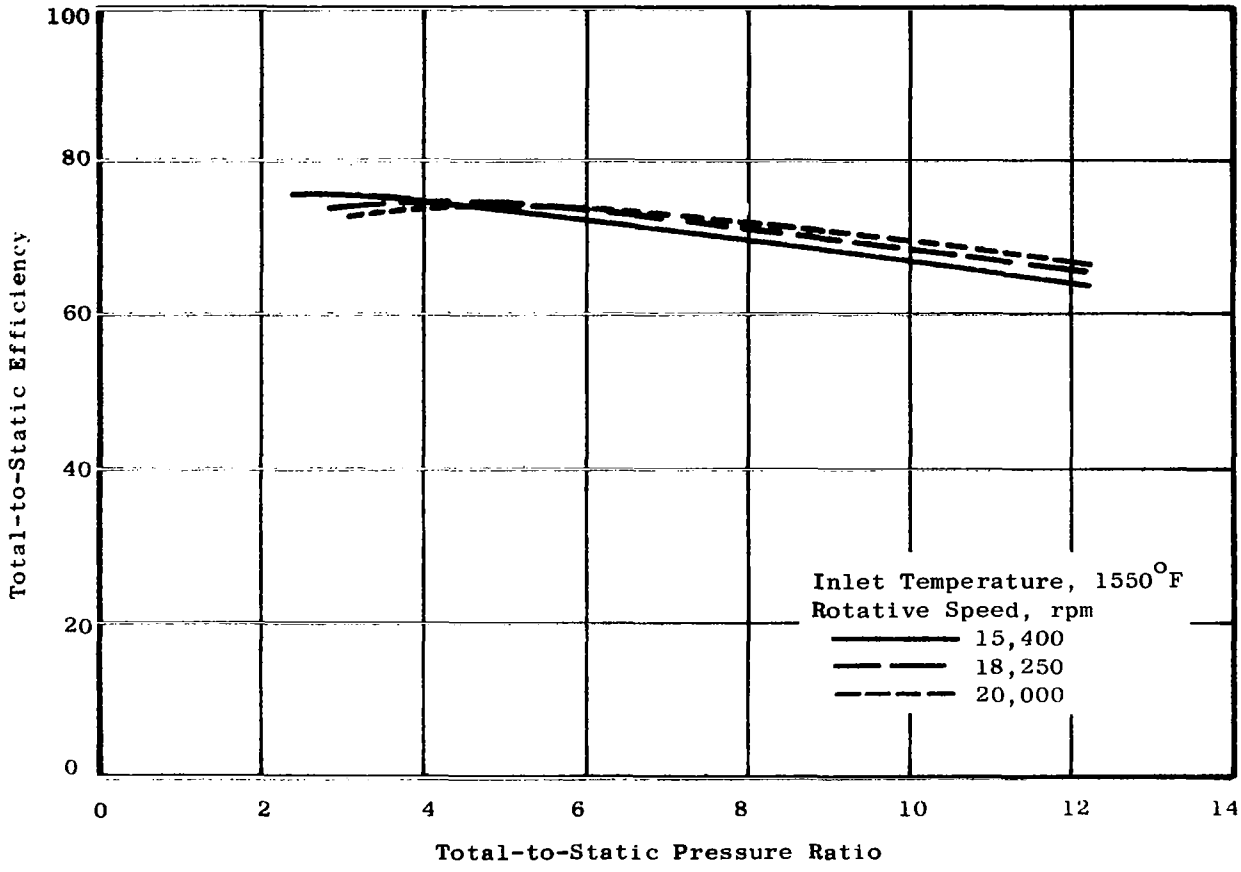

Figure 6. Calculated Total-to-Static Efficiency.

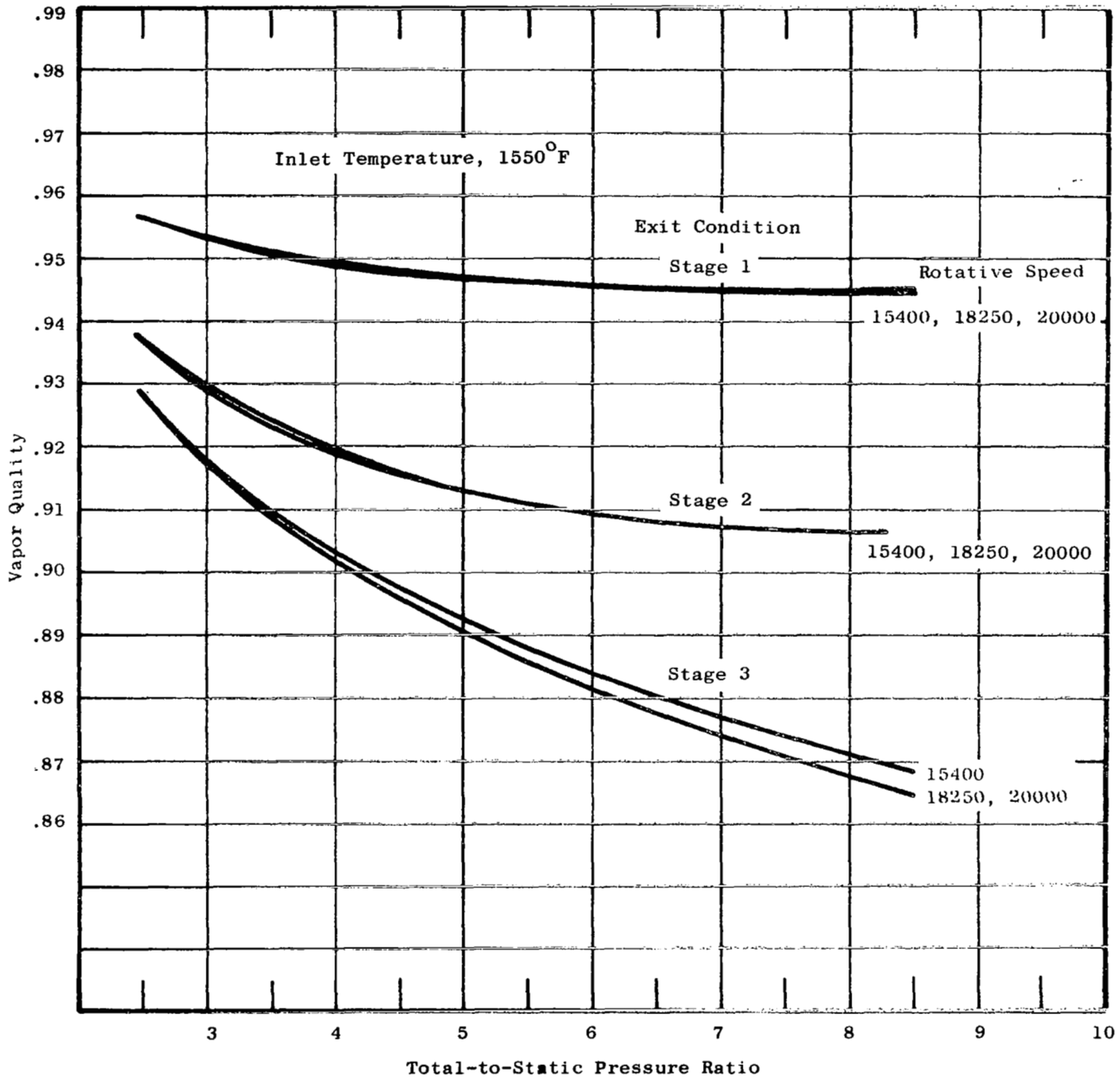

Figure 7. Calculated Vapor Quality.

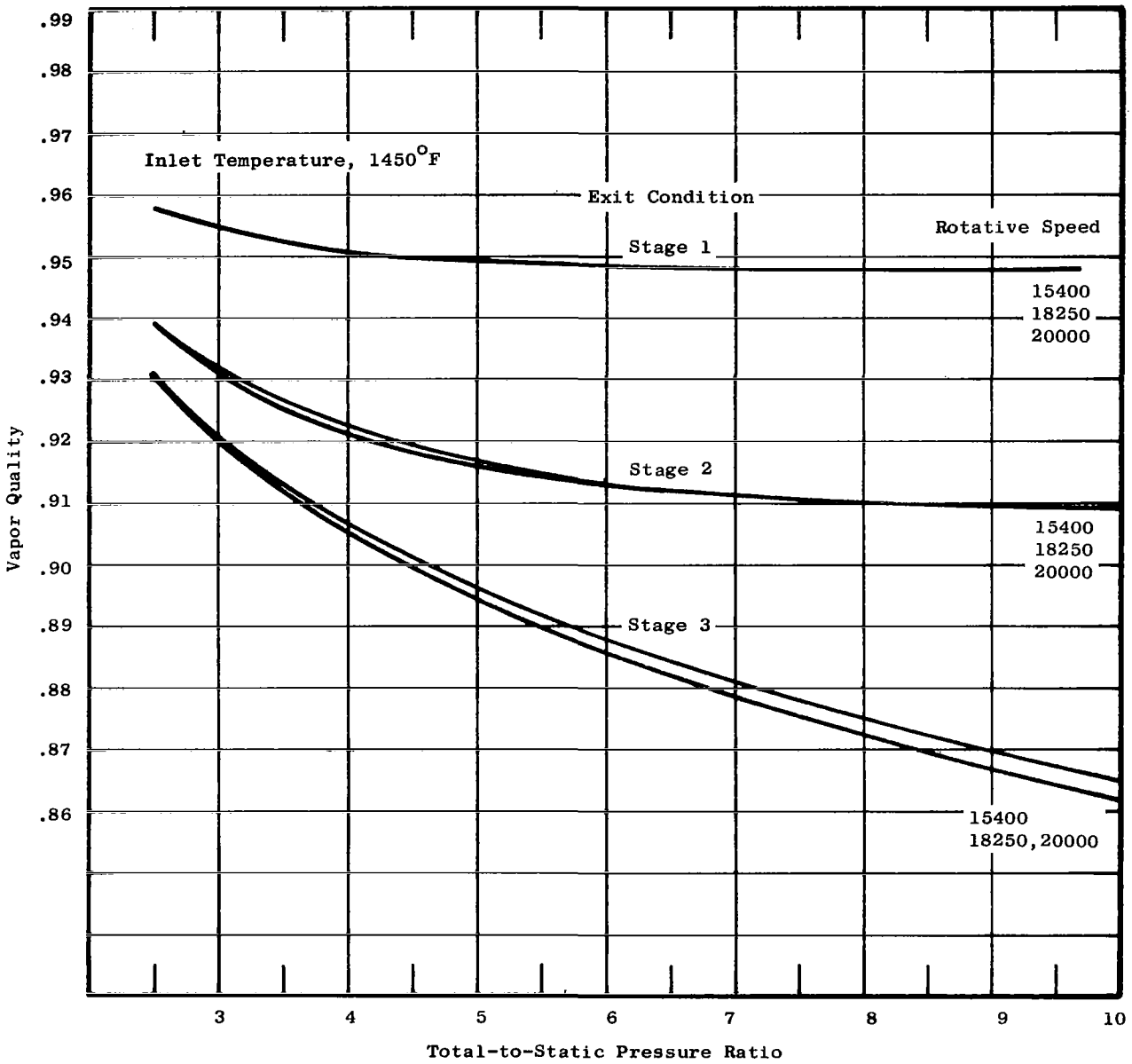

Figure 8. Calculated Vapor Quality.

3 STAGE POTASSIUM TURBINE LOAD TRAIN

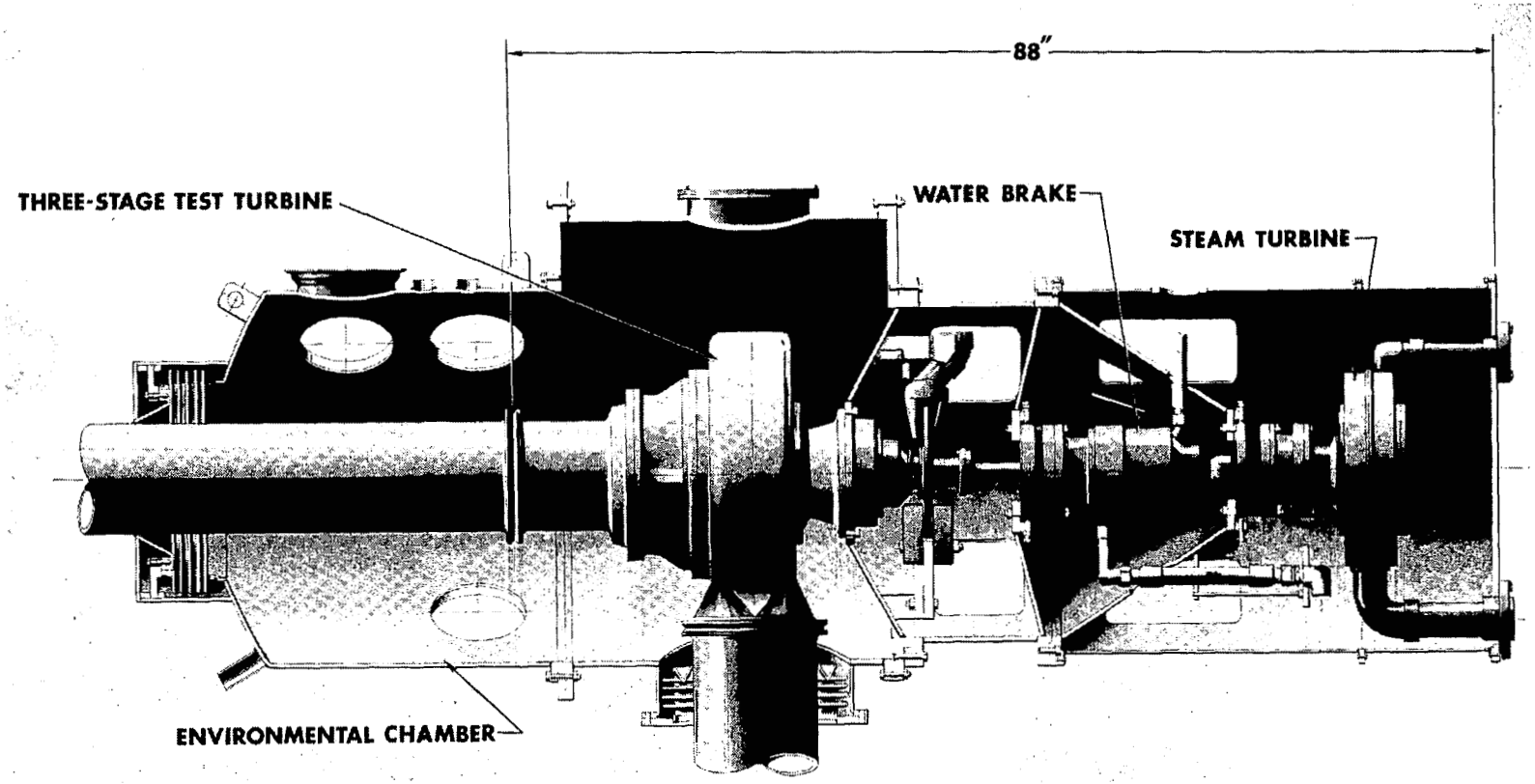

Figure 9. Three Stage Turbine and Load Train.

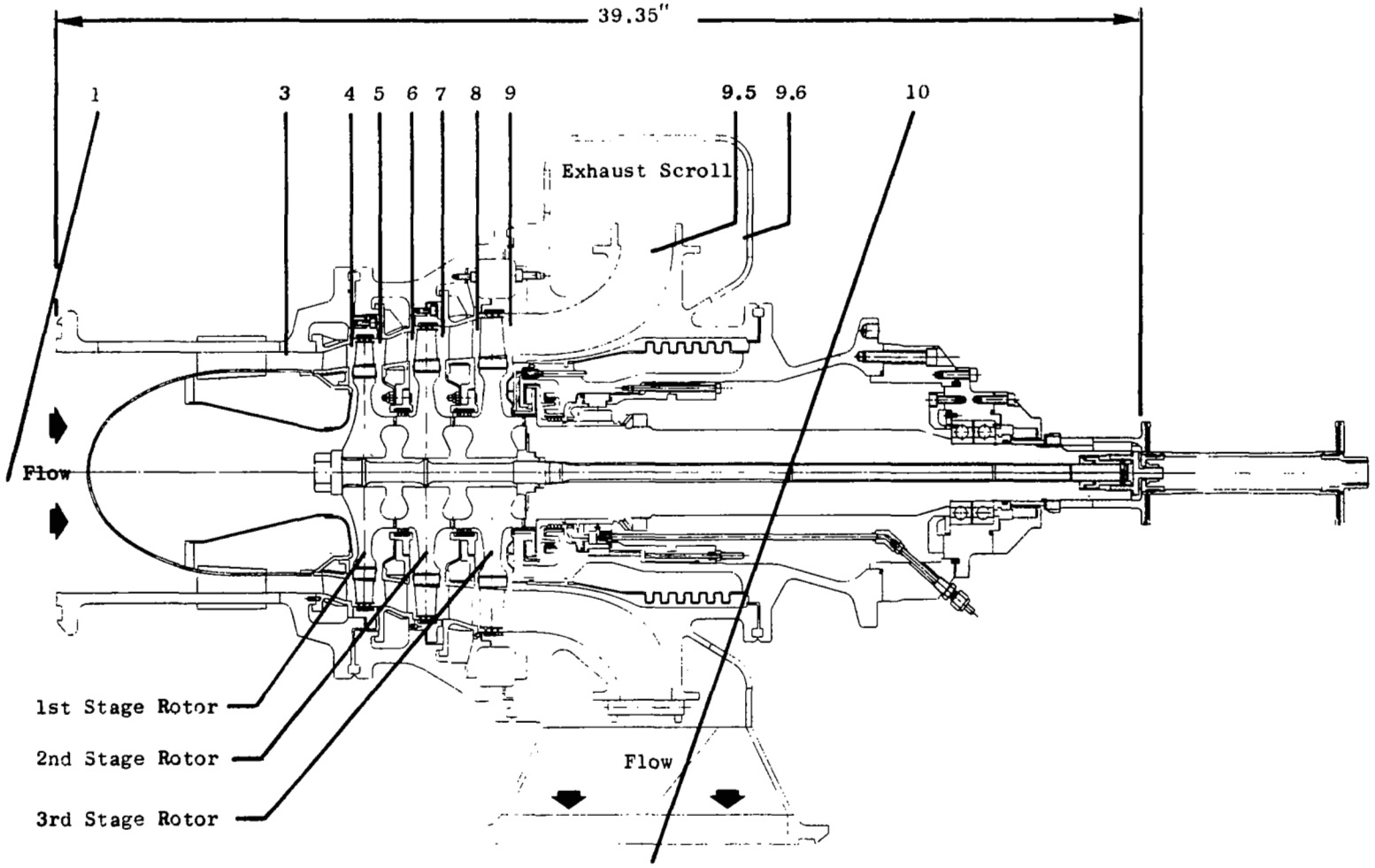

Figure 10. Instrumentation Stations.

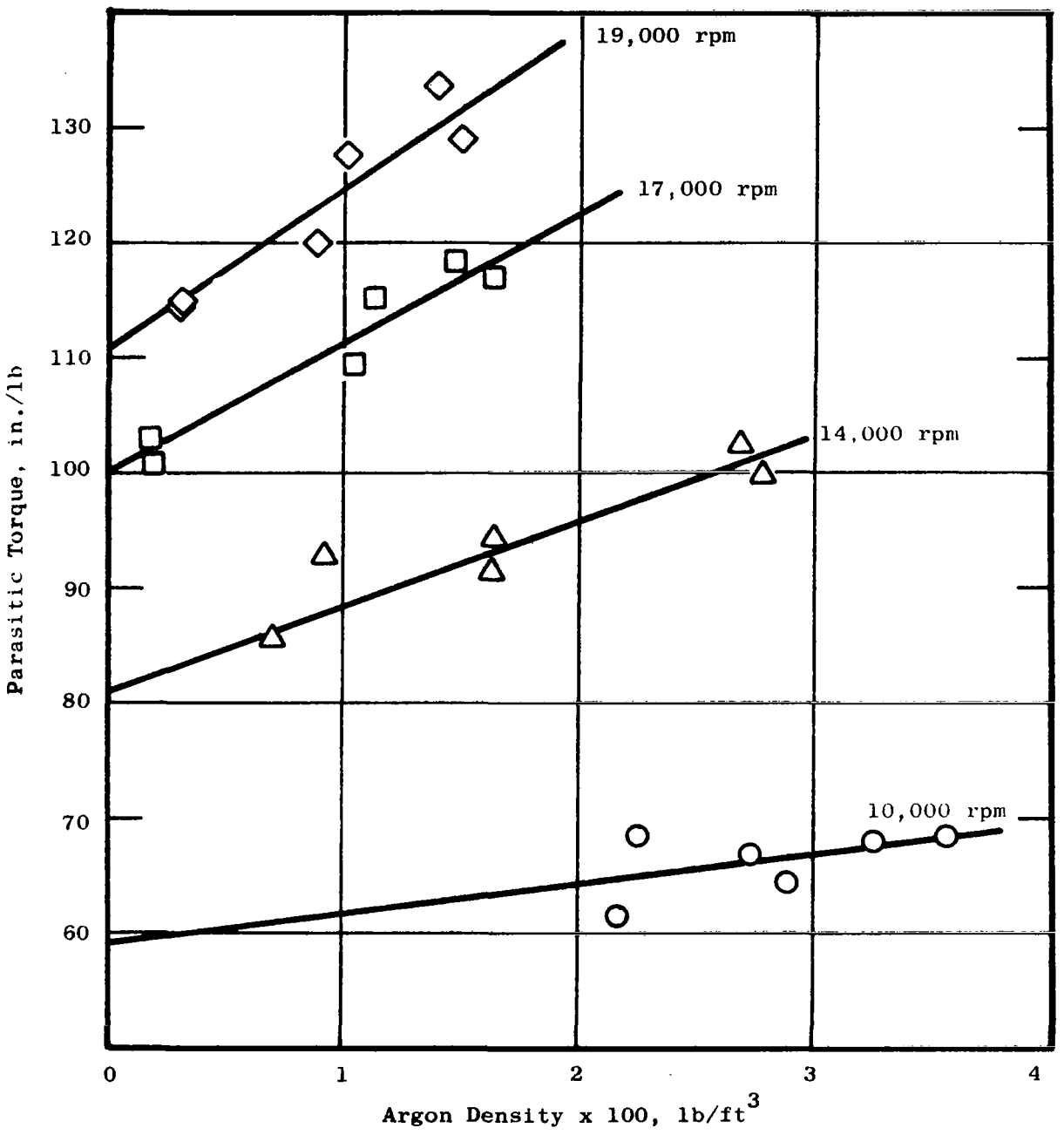

Figure 11. Parasitic Torque Variation with Speed and Density.

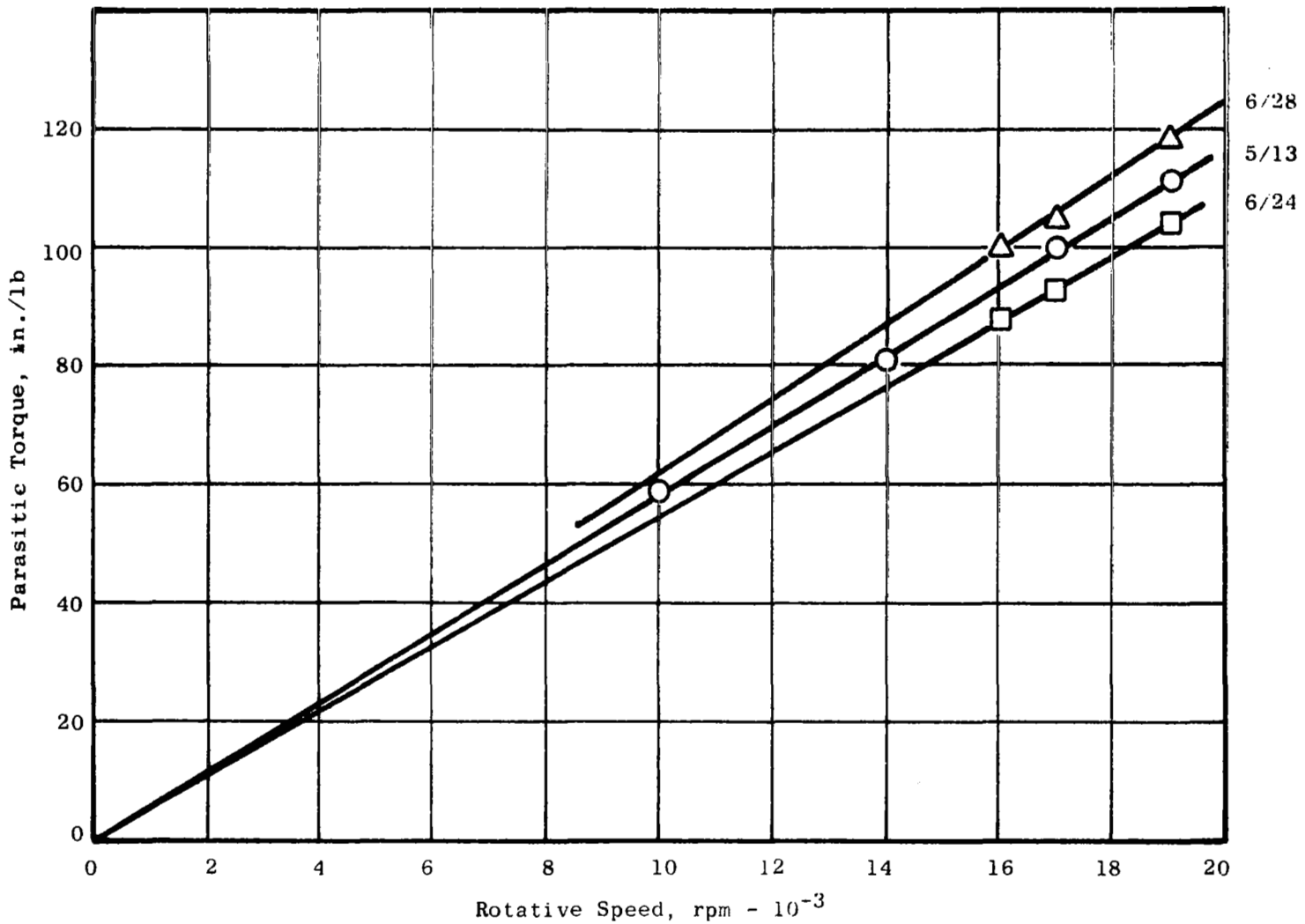

Figure 12. Parasitic Torque Variation with Rotative Speed.

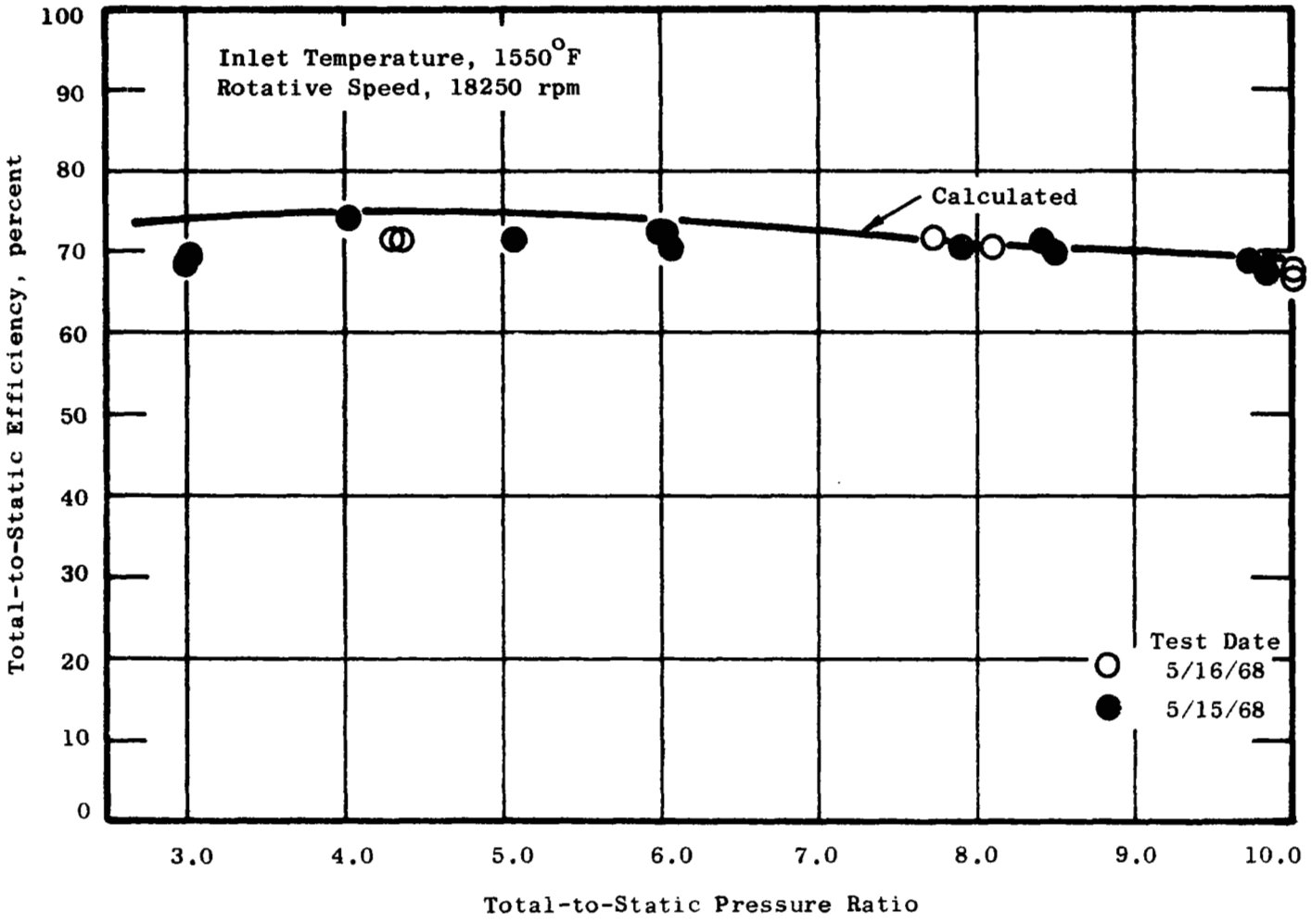

Figure 13. Comparison of Measured and Calculated Efficiency. (Supersaturated Model)

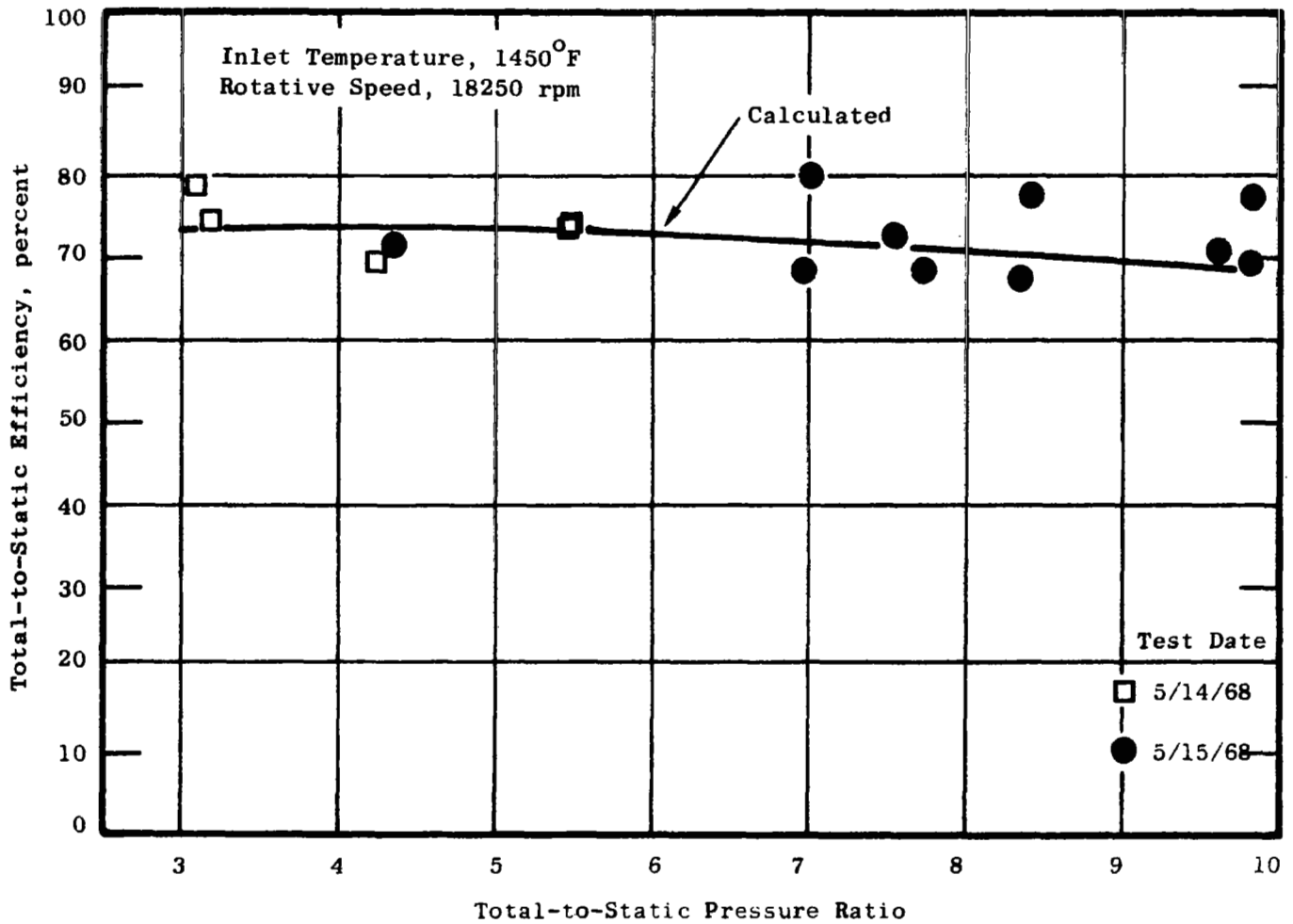

Figure 14. Comparison of Measured and Calculated Efficiency. (Supersaturated Model)

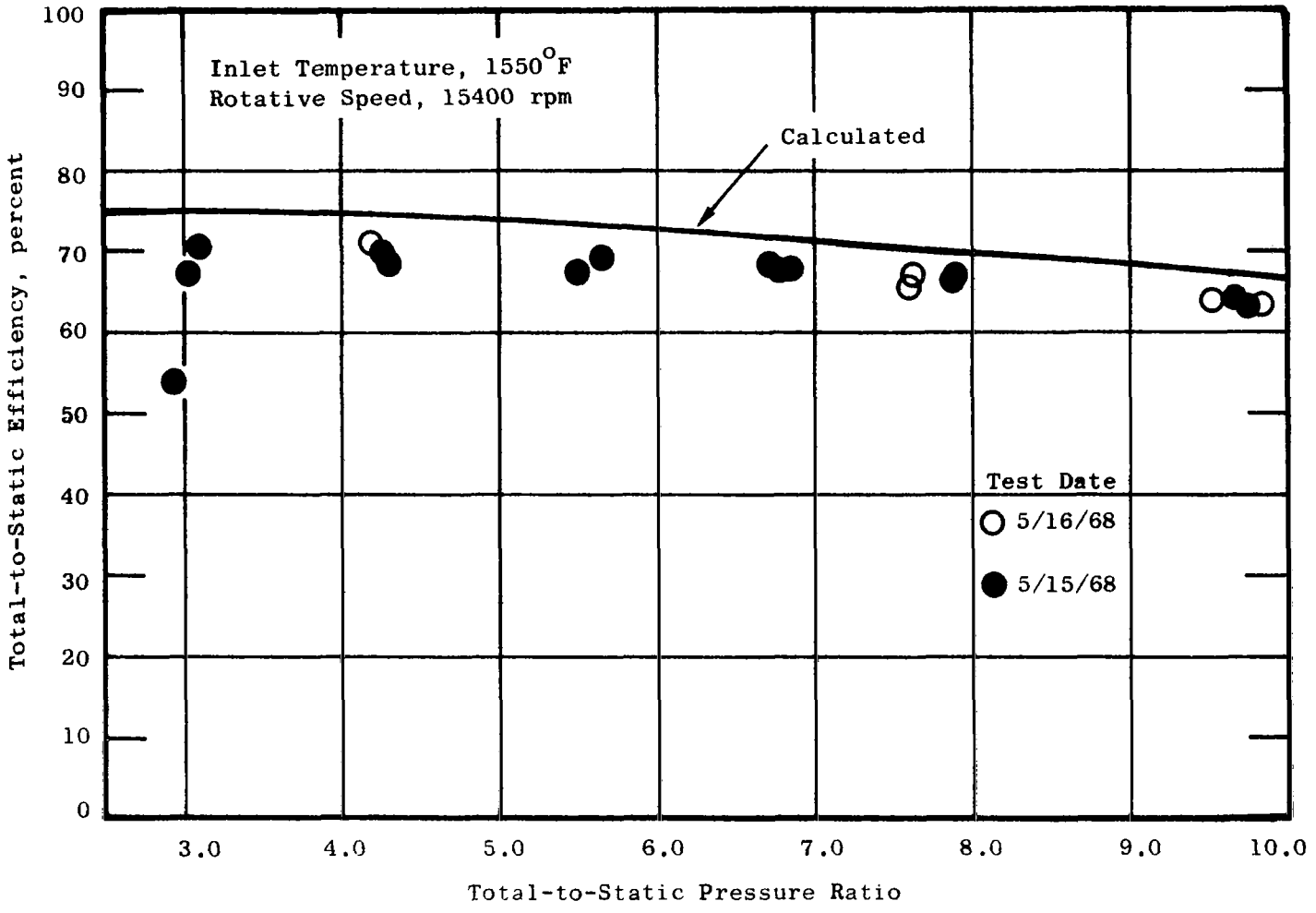

Figure 15. Comparison of Measured and Calculated Efficiency. (Supersaturated Model)

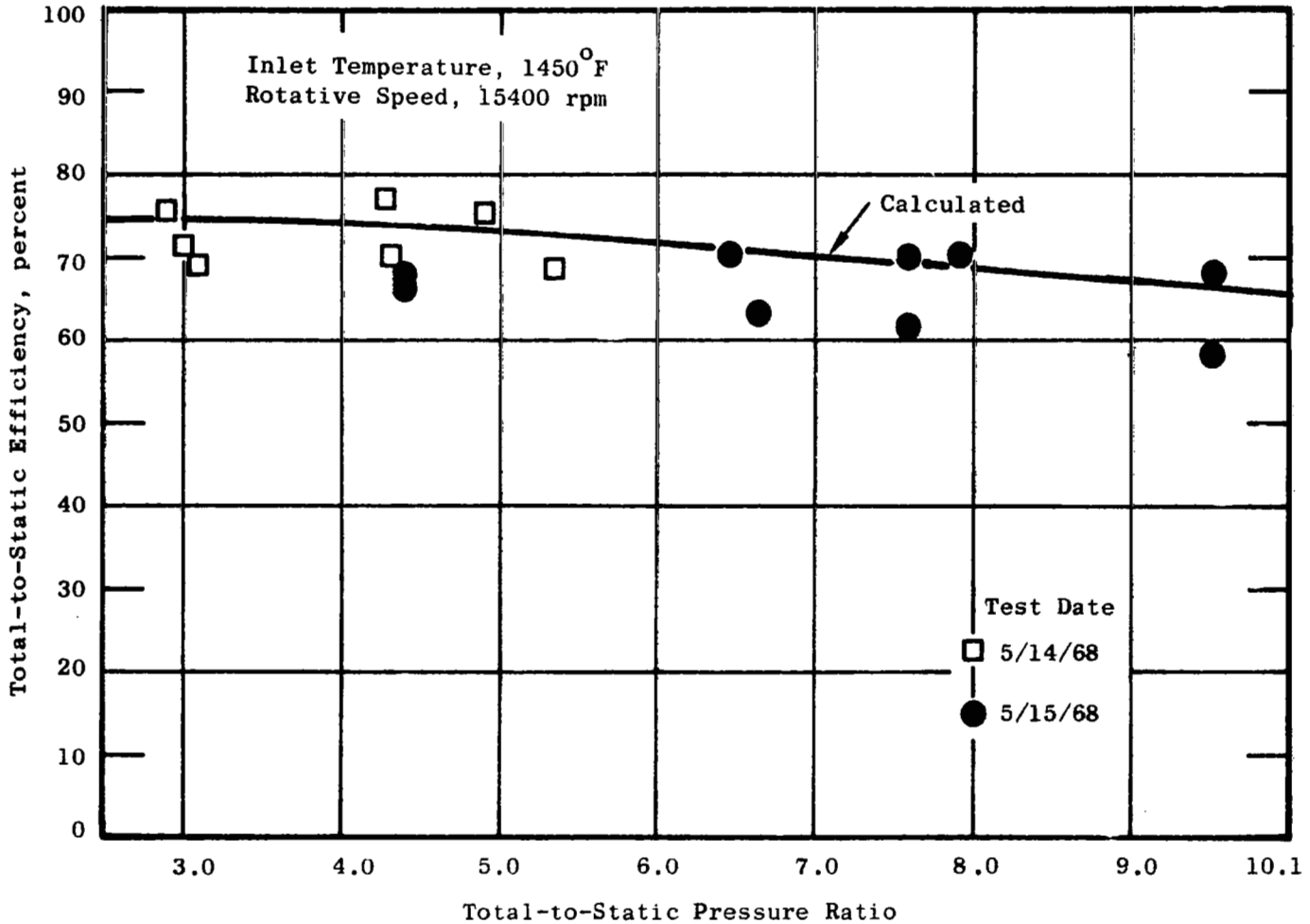

Figure 16. Comparison of Measured and Calculated Efficiency. (Supersaturated Model)

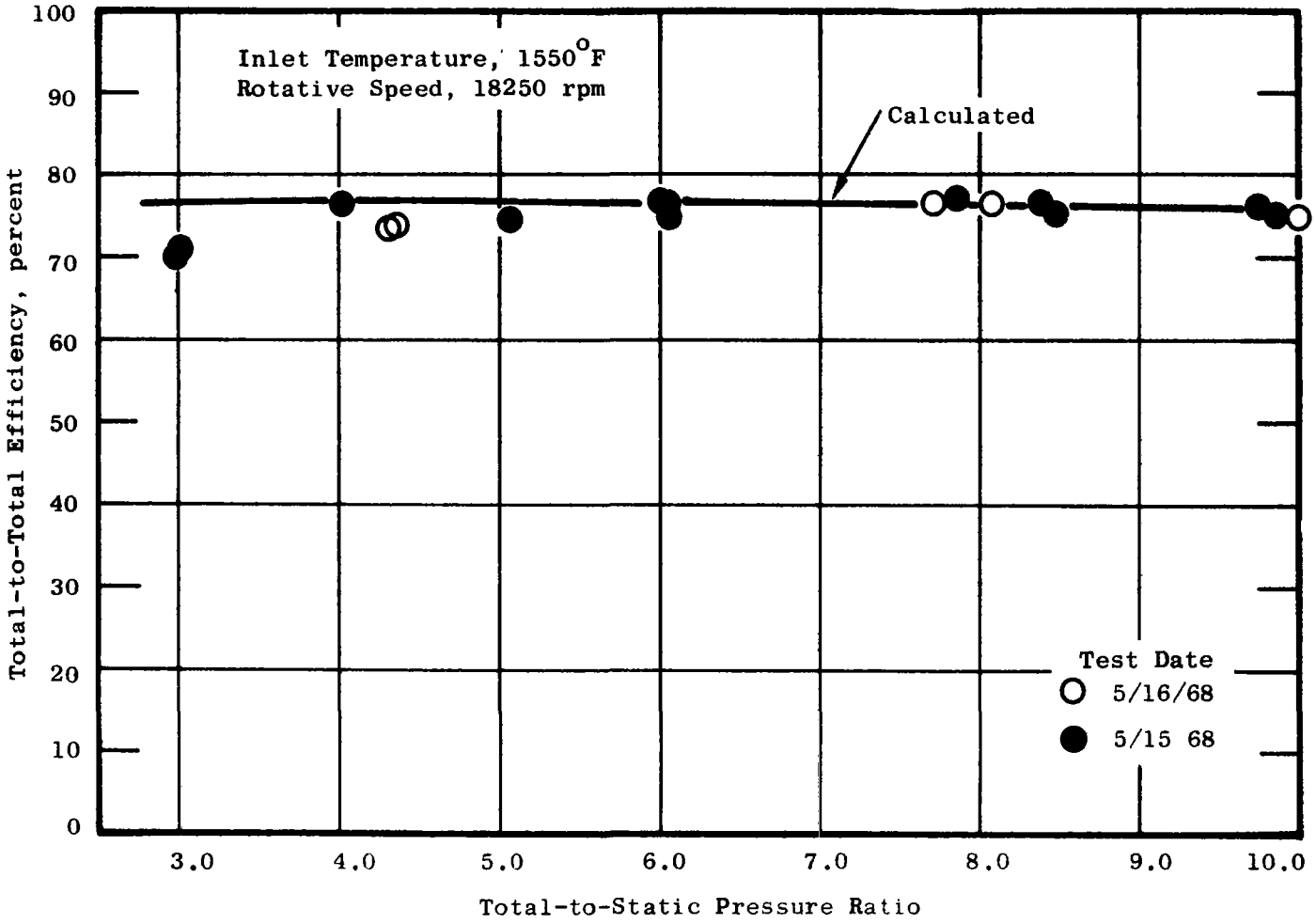

Figure 17. Comparison of Measured and Calculated Efficiency. (Supersaturated Model)

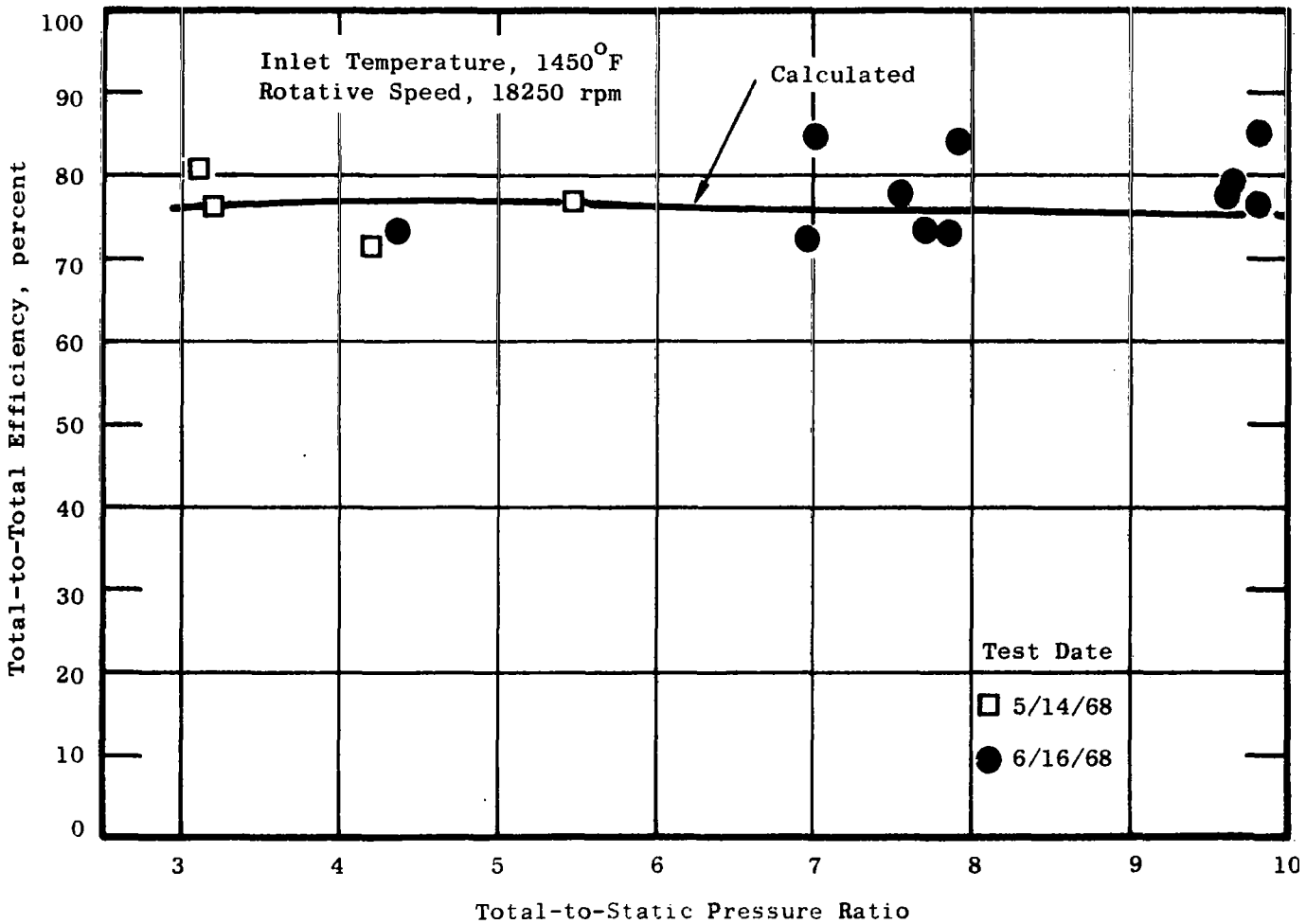

Figure 18. Comparison of Measured and Calculated Efficiency. (Supersaturated Model)

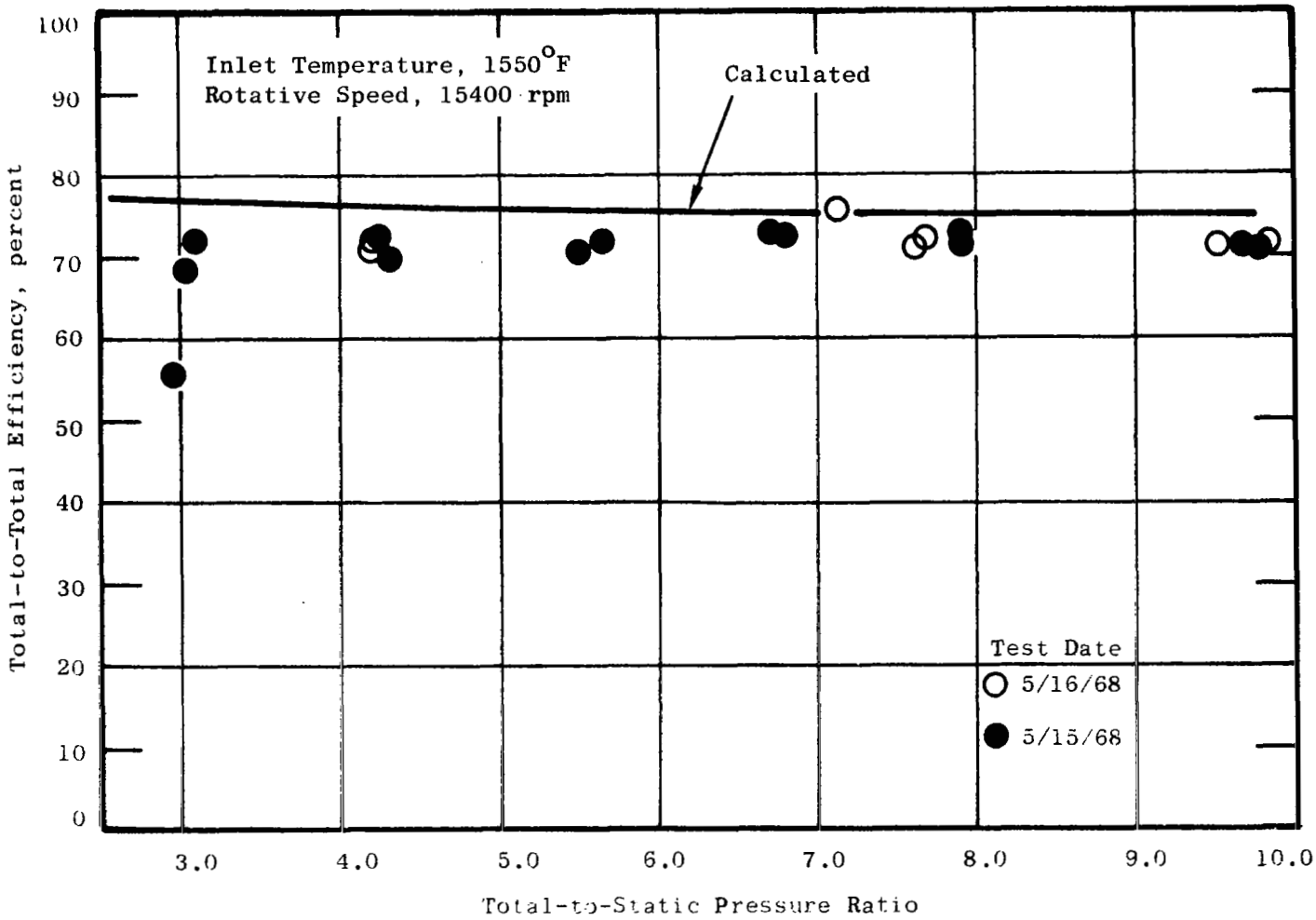

Figure 19. Comparison of Measured and Calculated Efficiency. (Supersaturated Model)

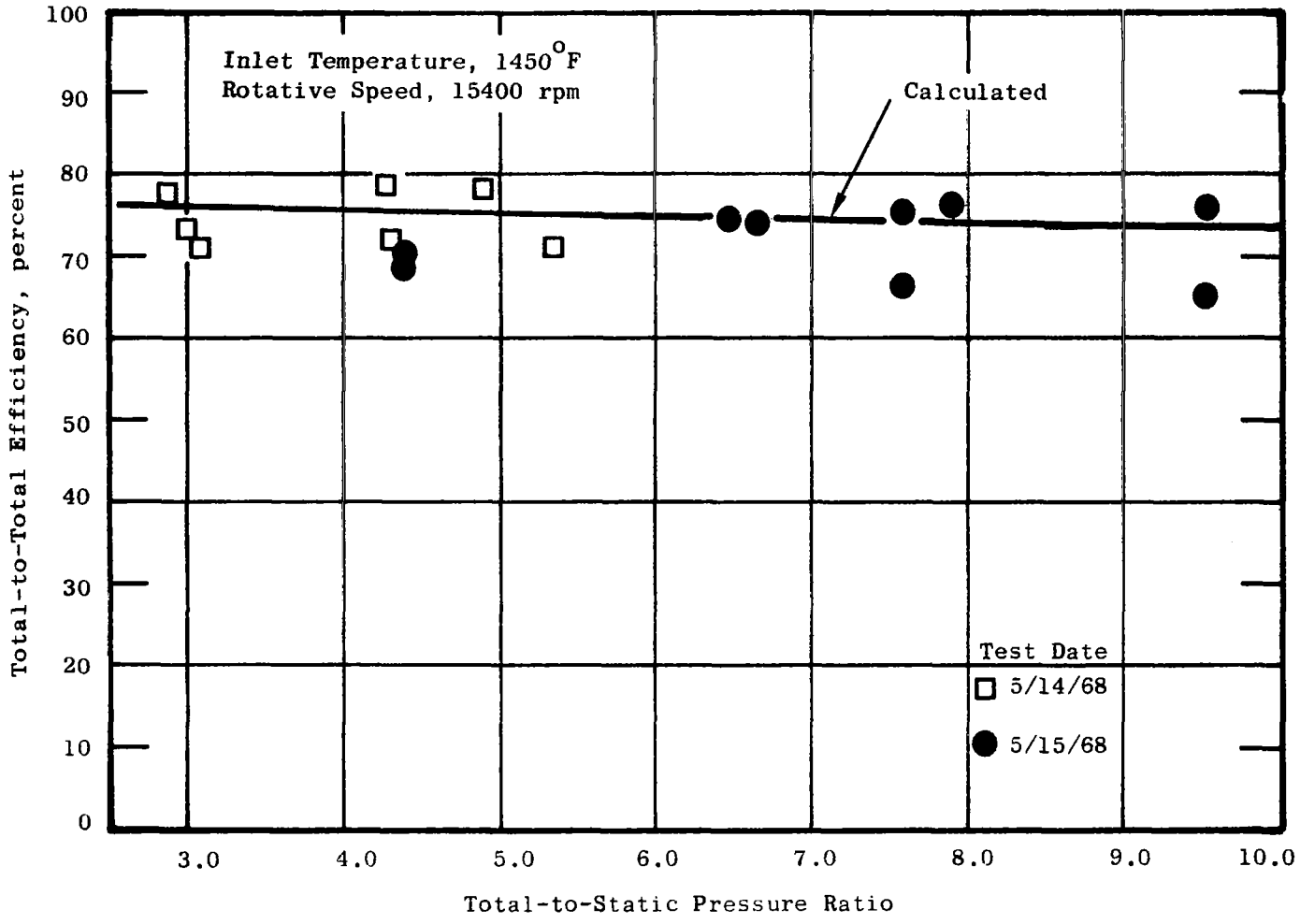

Figure 20. Comparison of Measured and Calculated Efficiency. (Supersaturated Model)

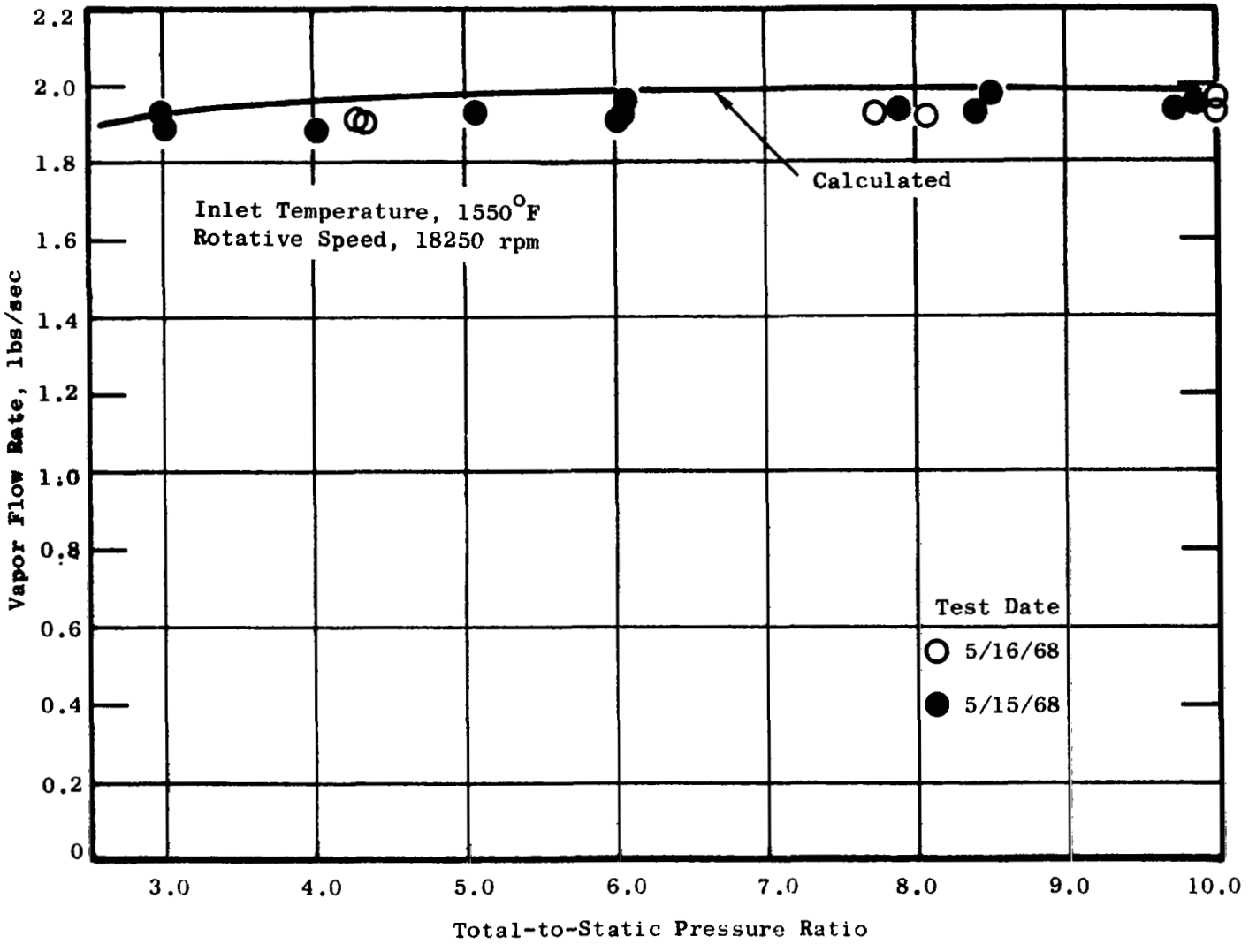

Figure 21. Comparison of Measured and Calculated Vapor Flow Rate. (Supersaturated Model)

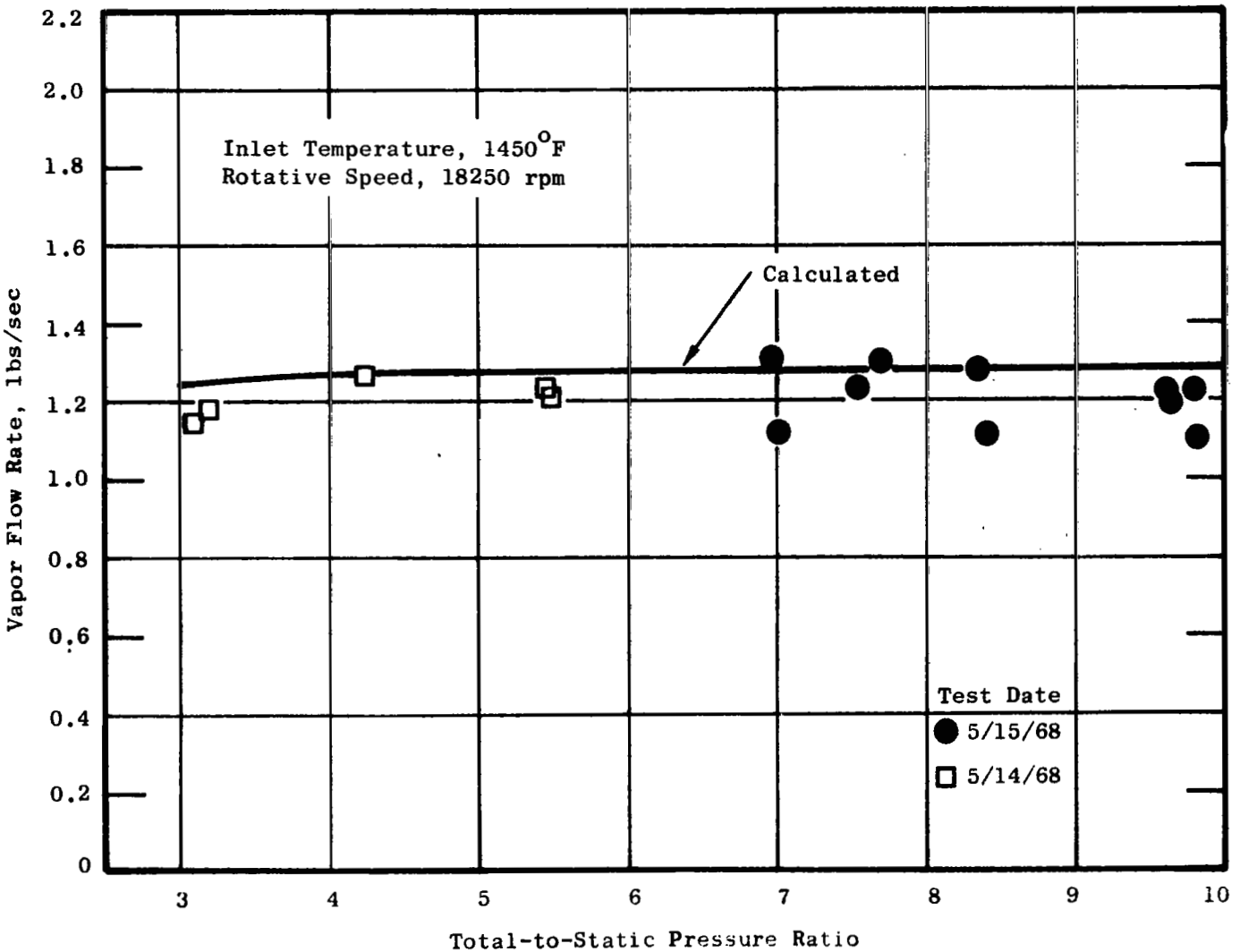

Figure 22. Comparison of Measured and Calculated Vapor Flow Rate. (Supersaturated Model)

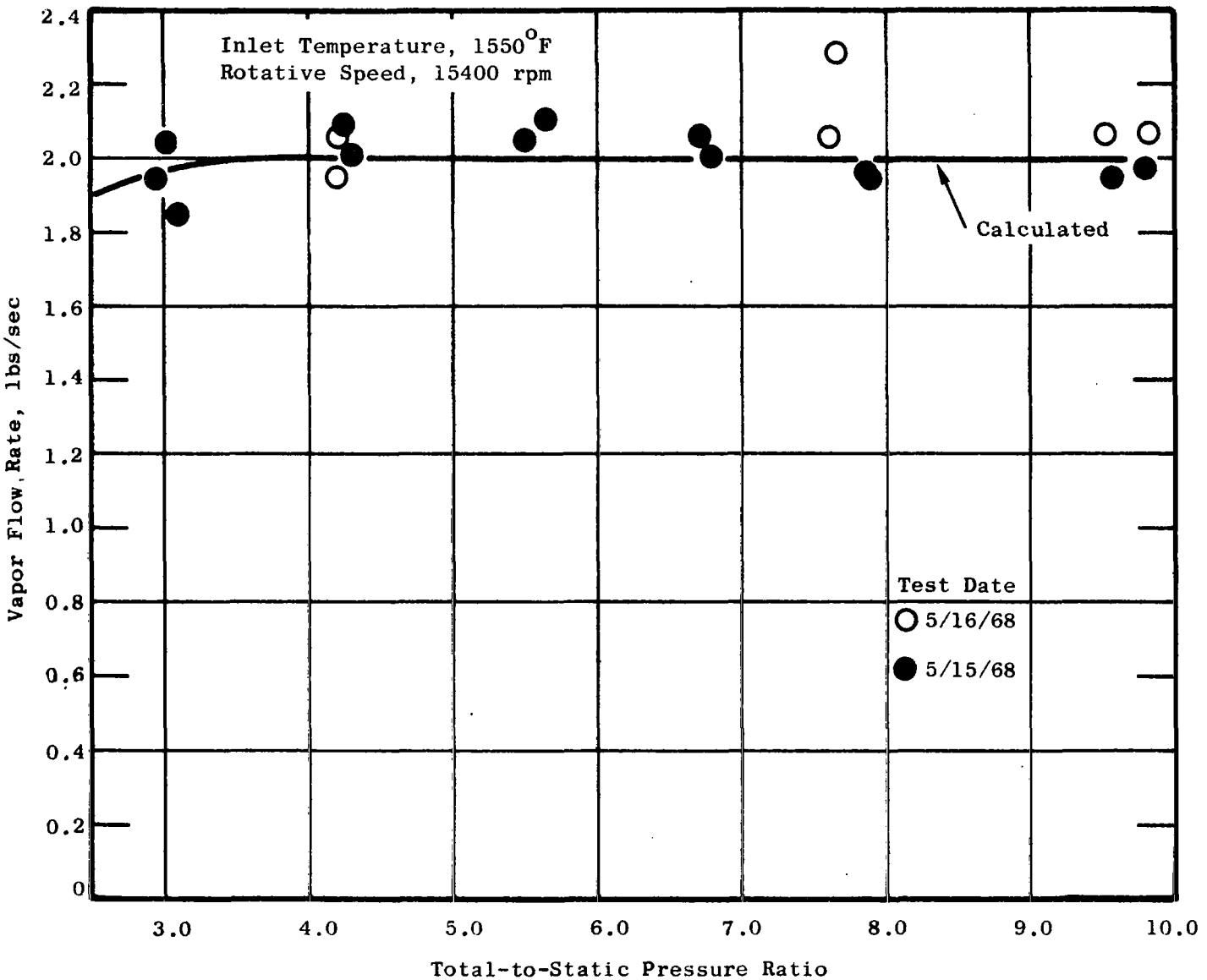

Figure 23. Comparison of Measured and Calculated Vapor Flow Rate. (Supersaturated Model)

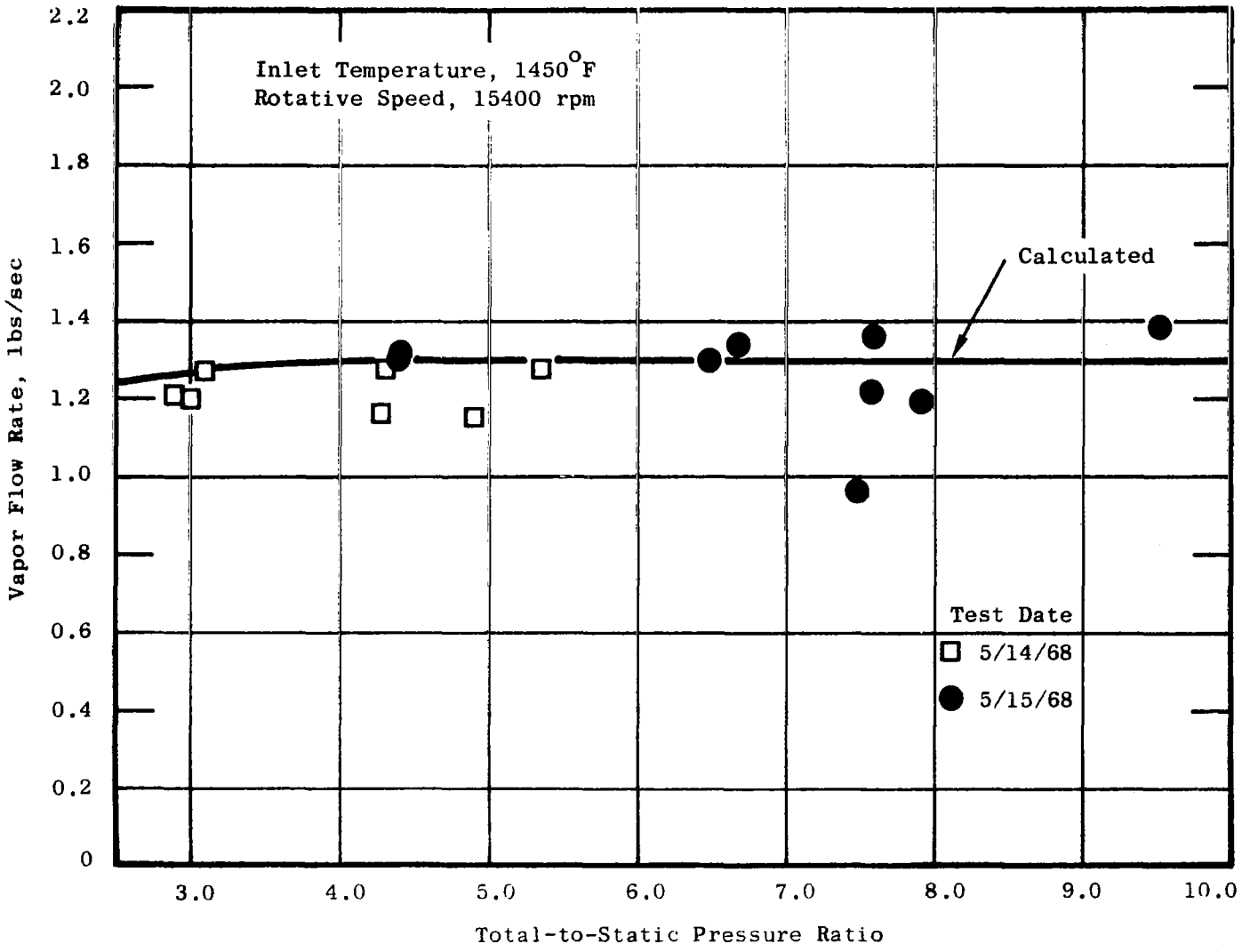

Figure 24. Comparison of Measured and Calculated Vapor Flow Rate. (Supersaturated Model)

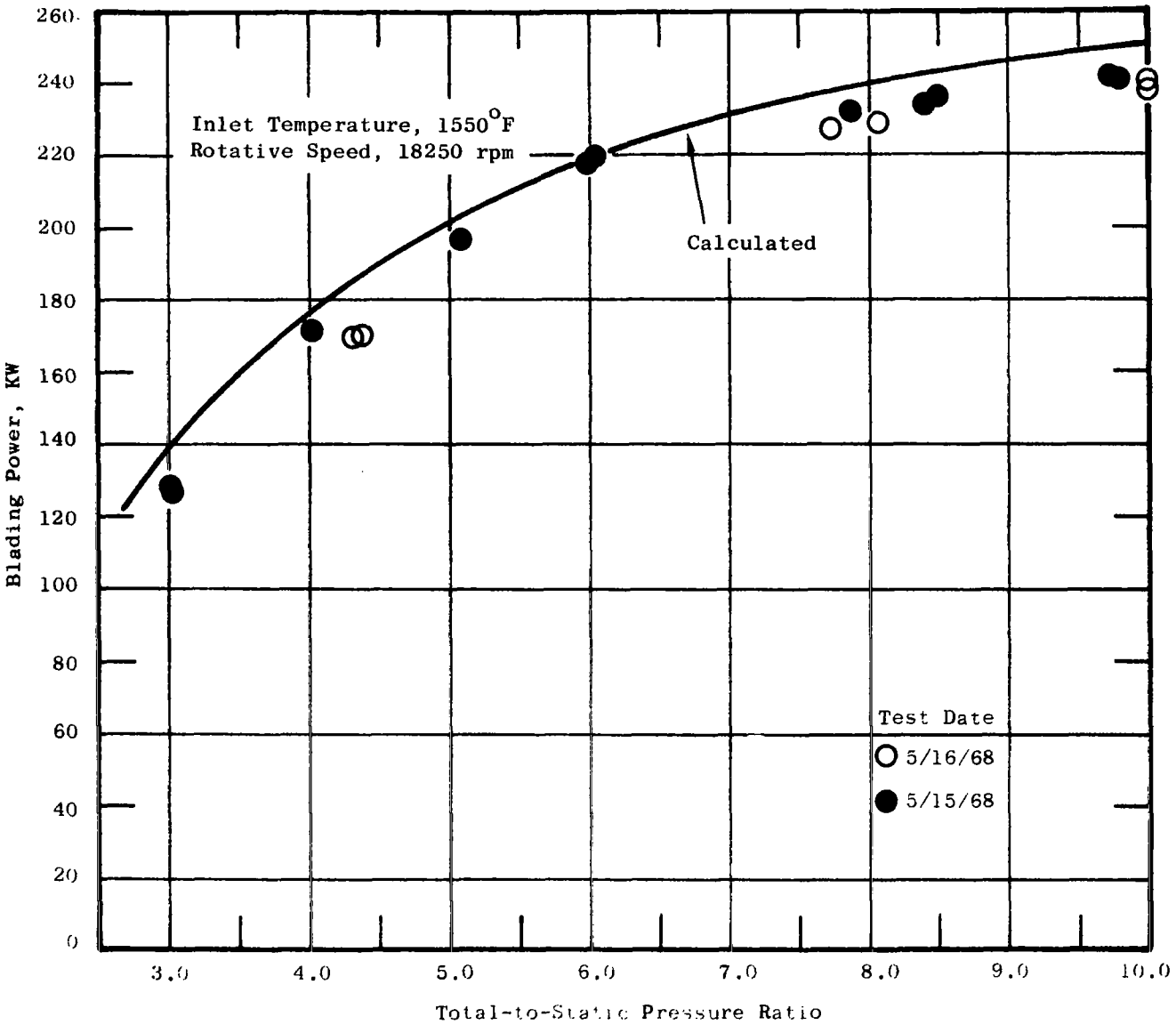

Figure 25. Comparison of Measured and Calculated Power. (Supersaturated Model)

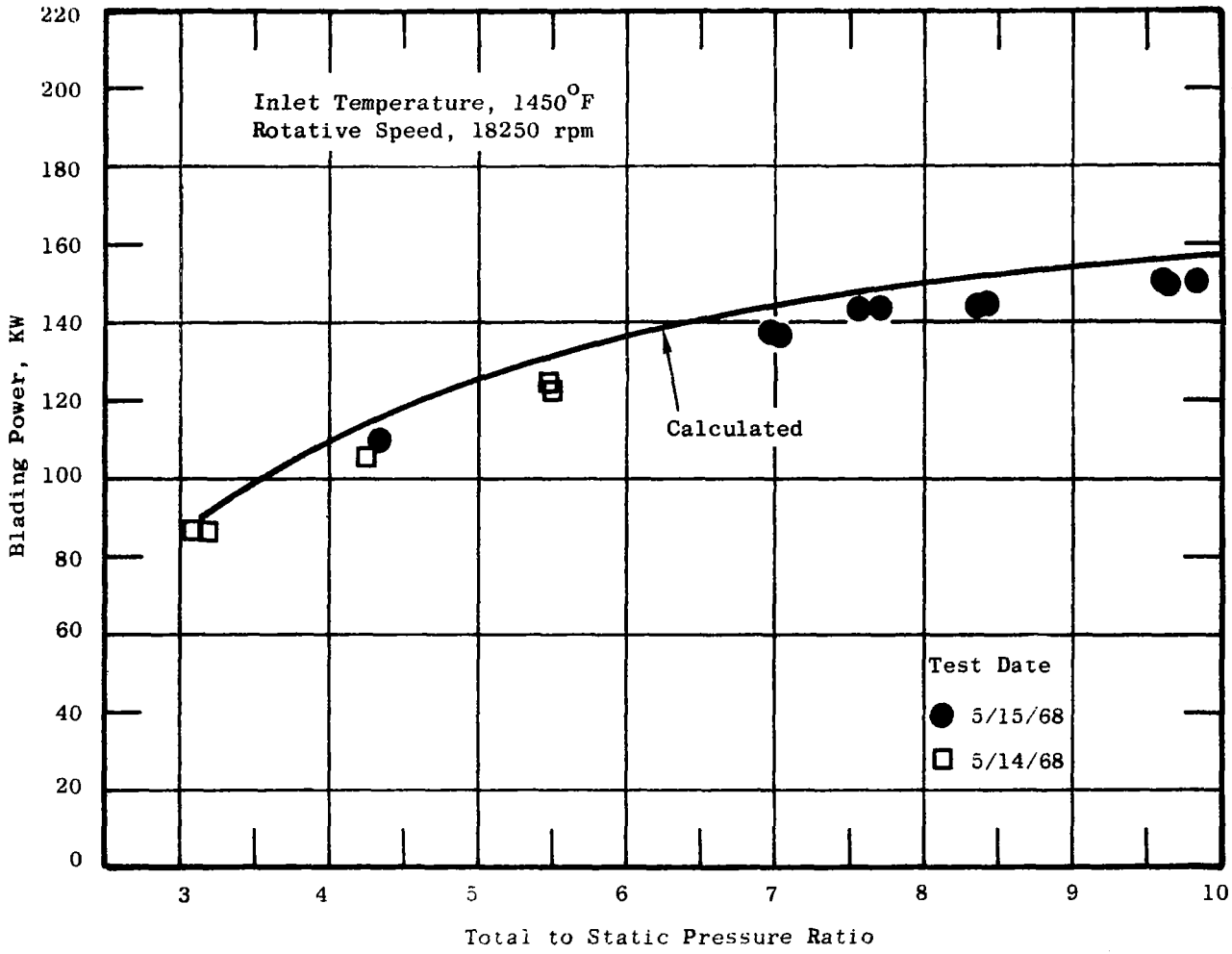

Figure 26. Comparison of Measured and Calculated Power. (Supersaturated Model)

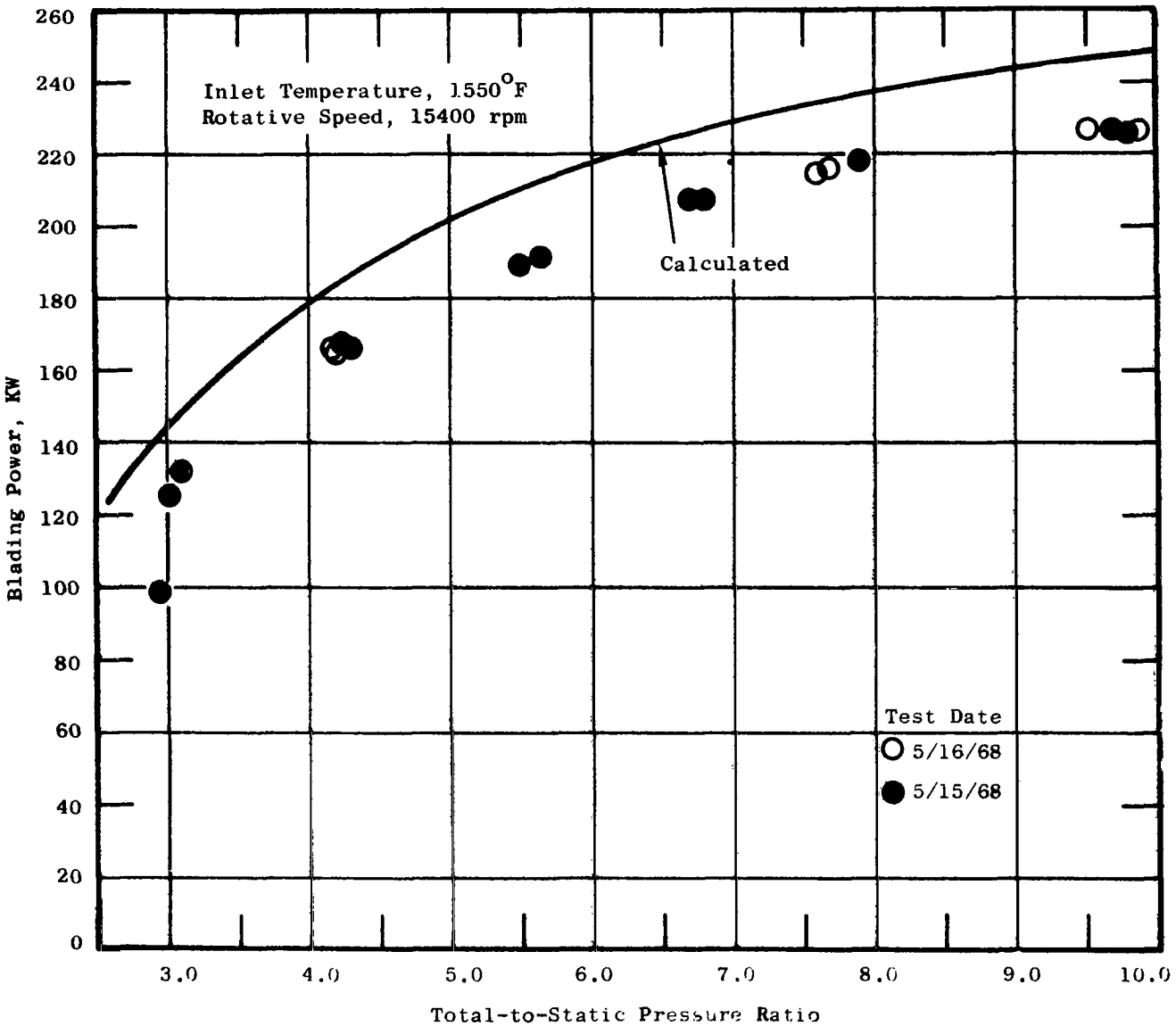

Figure 27. Comparison of Measured and Calculated Power. (Supersaturated Model)

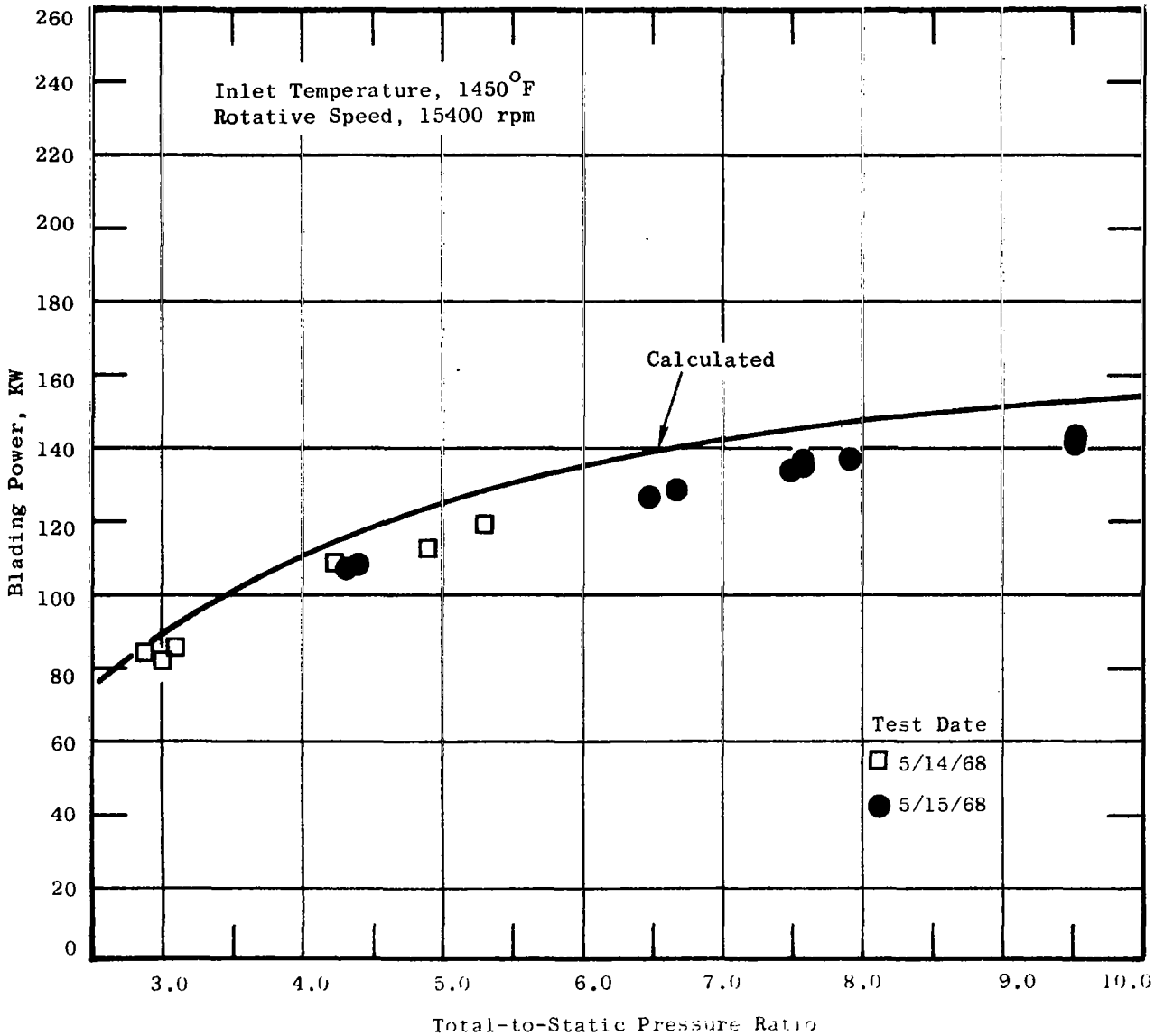

Figure 28. Comparison of Measured and Calculated Power. (Supersaturated Model)

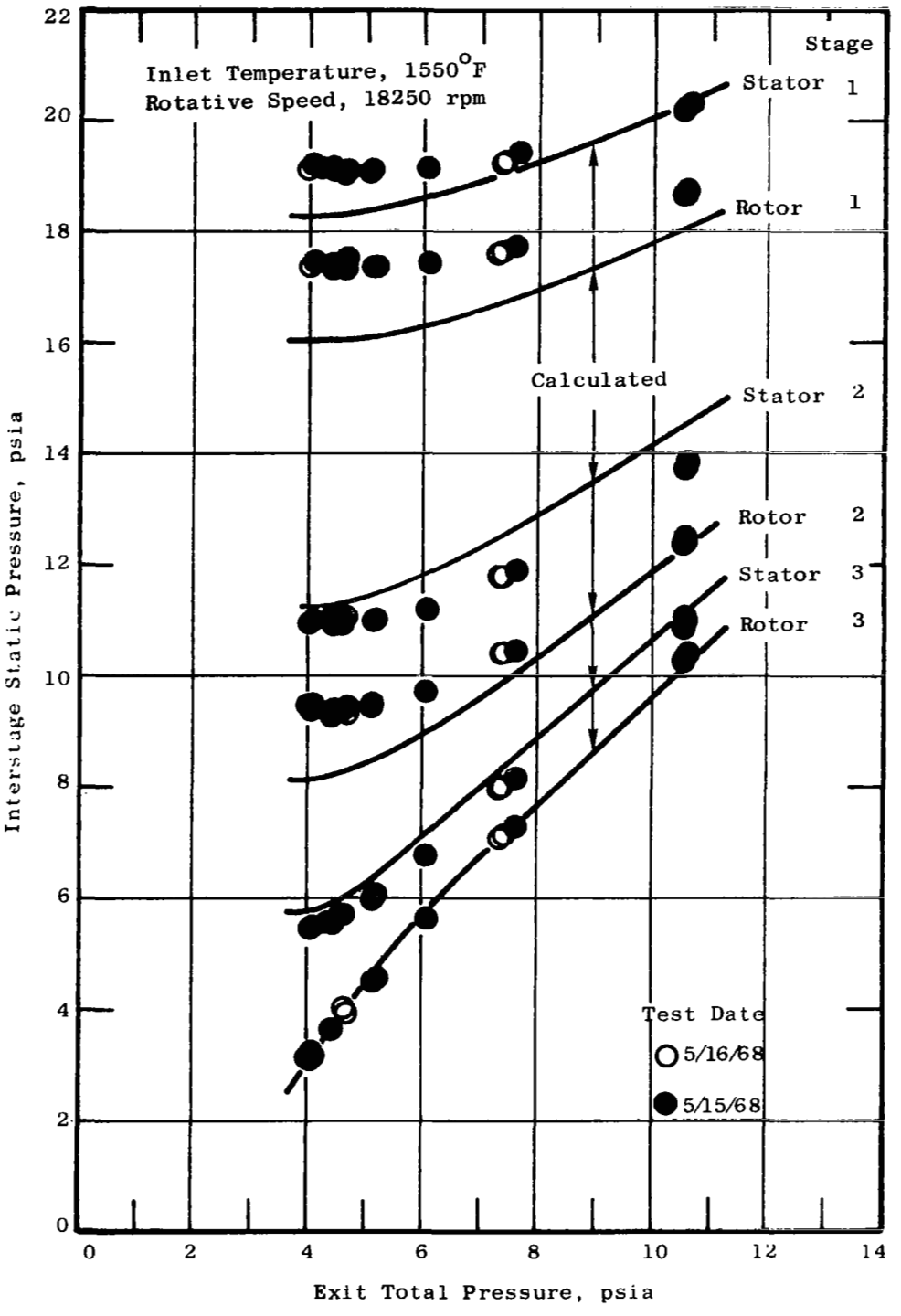

Figure 29. Comparison of Measured and Calculated Static Pressures. (Supersaturated Model)

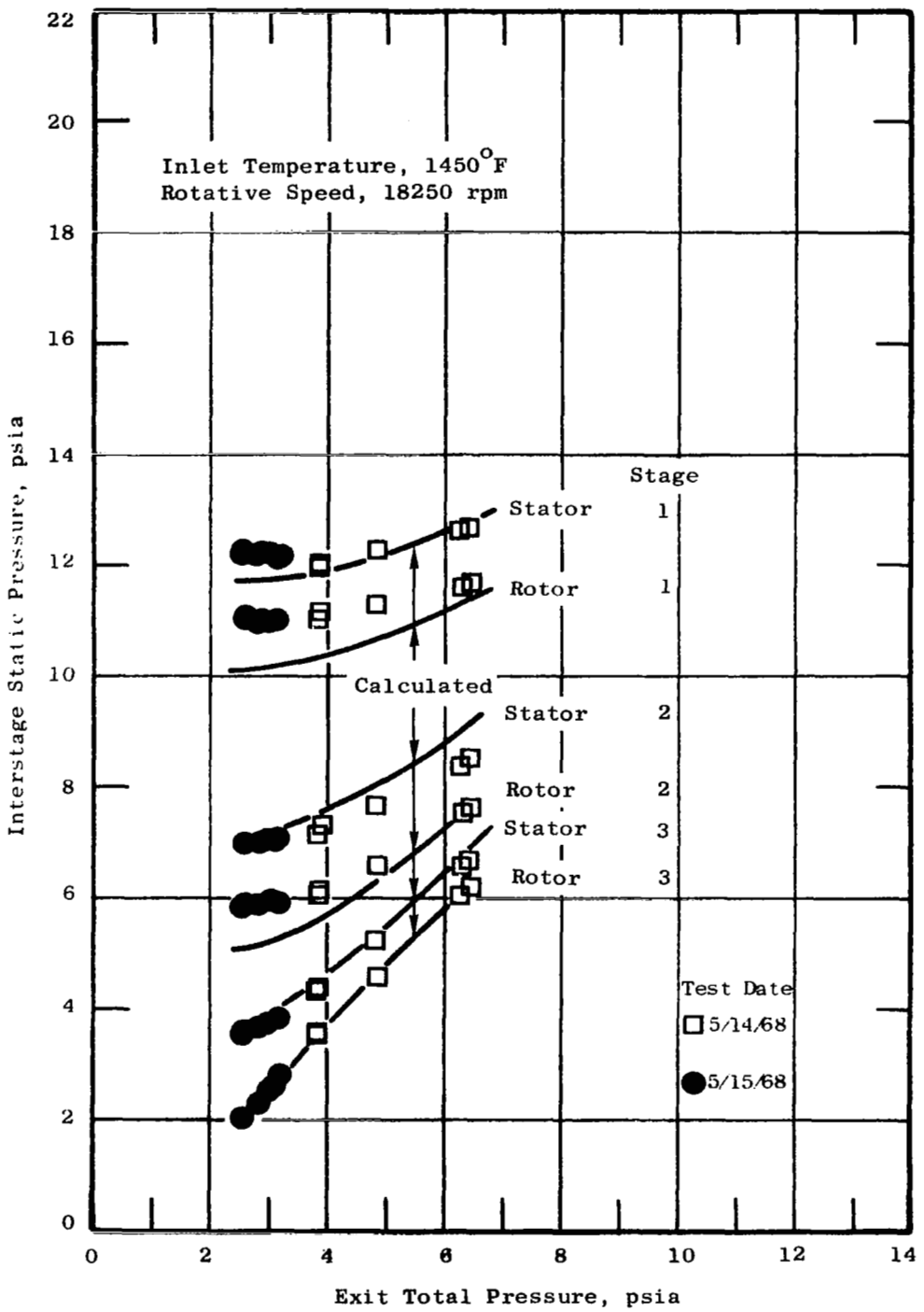

Figure 30. Comparison of Measured and Calculated Static Pressures. (Supersaturated Model)

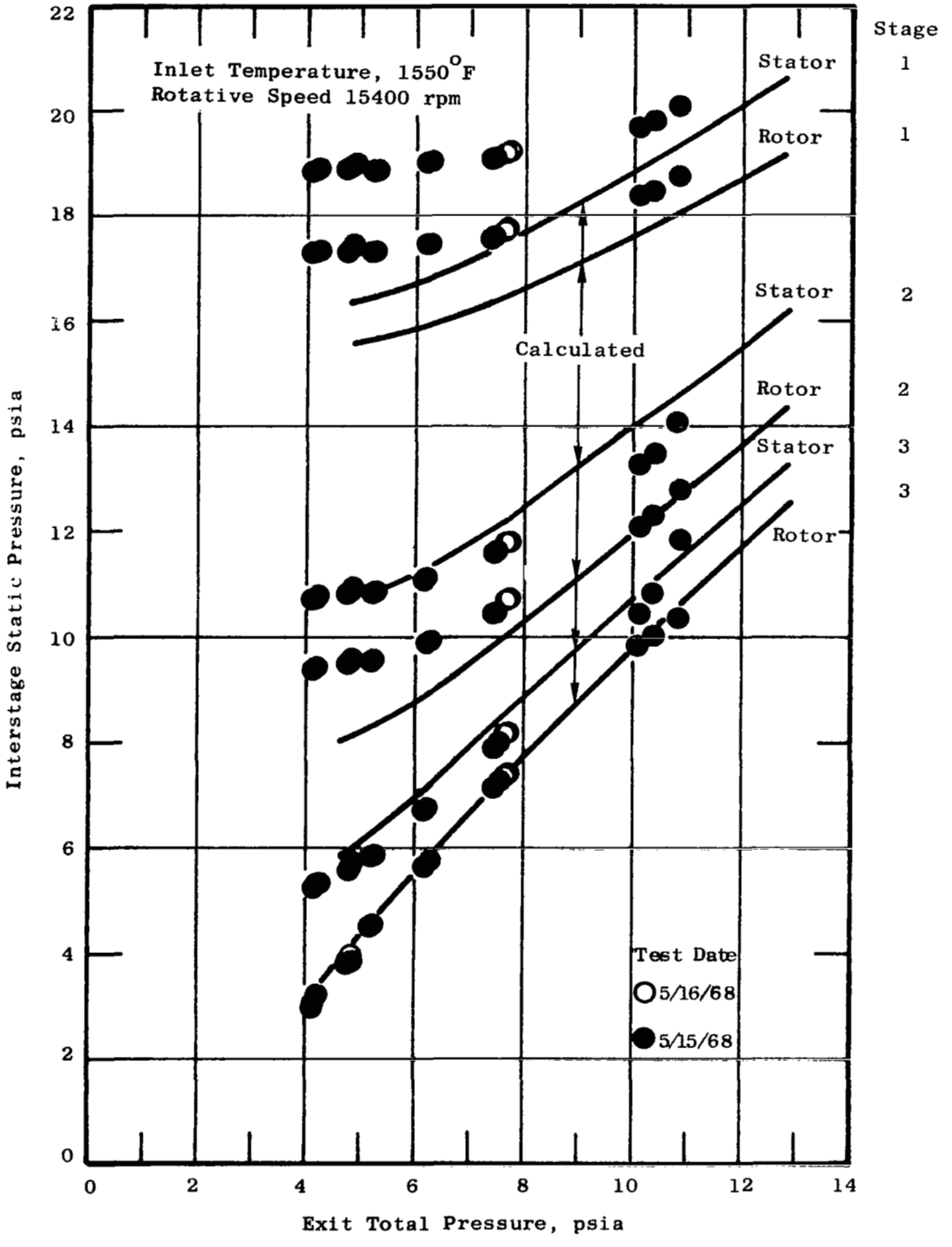

Figure 31. Comparison of Measured and Calculated Static Pressures. (Supersaturated Model)

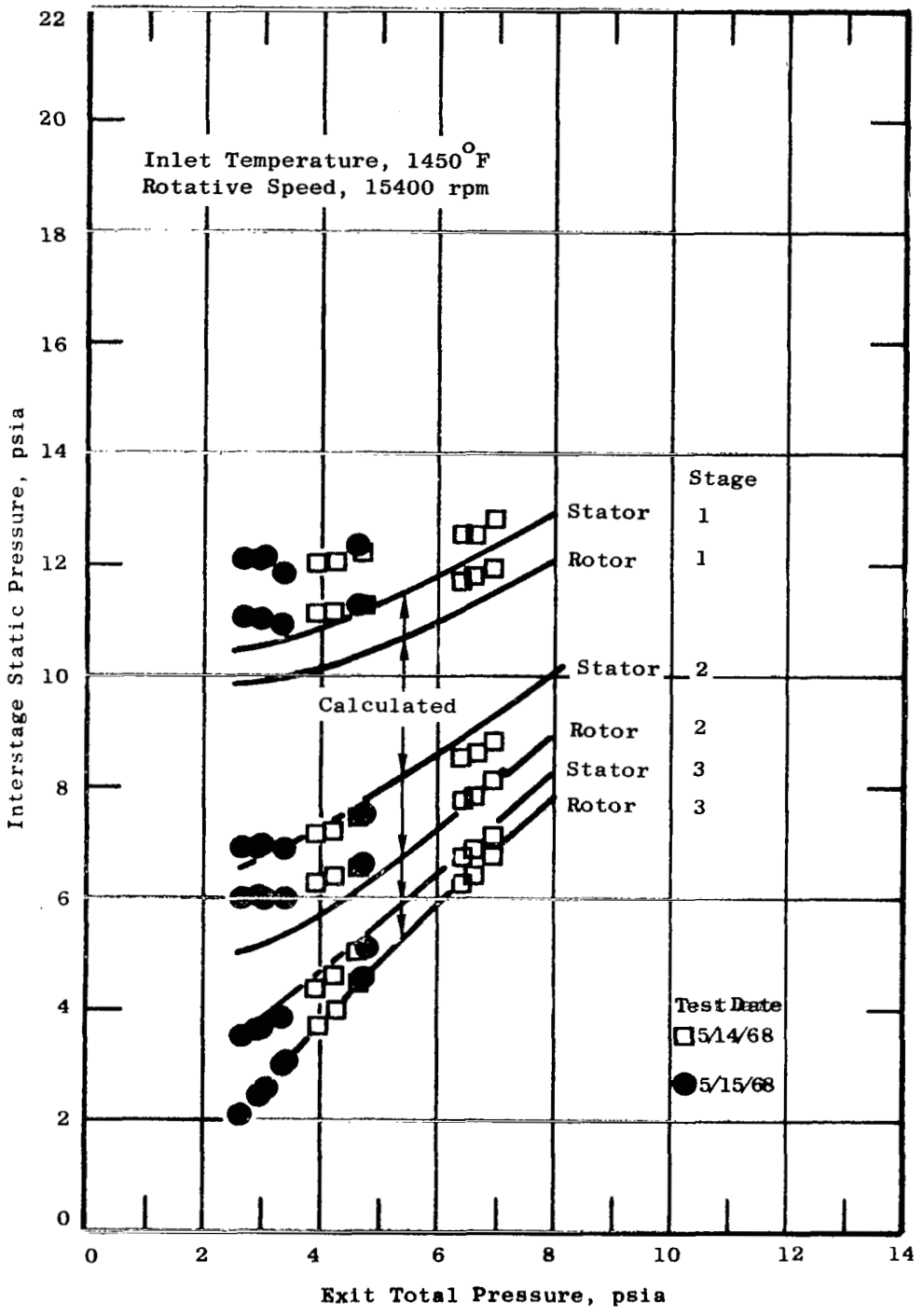

Figure 32. Comparison of Measured and Calculated Static Pressures. (Supersaturated Model)

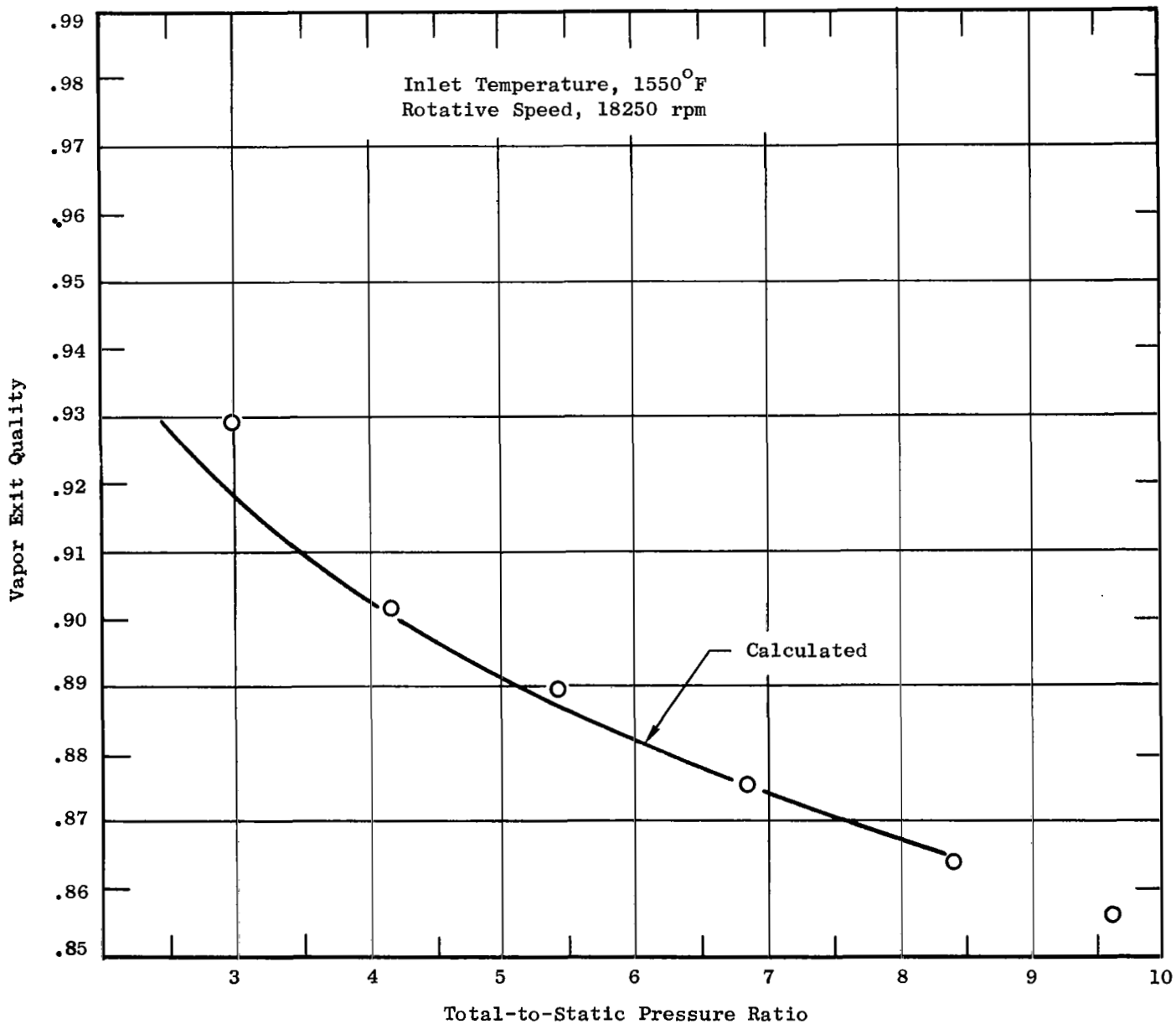

Figure 33. Comparison of Measured and Calculated Vapor Exit Quality. (Equilibrium Model)

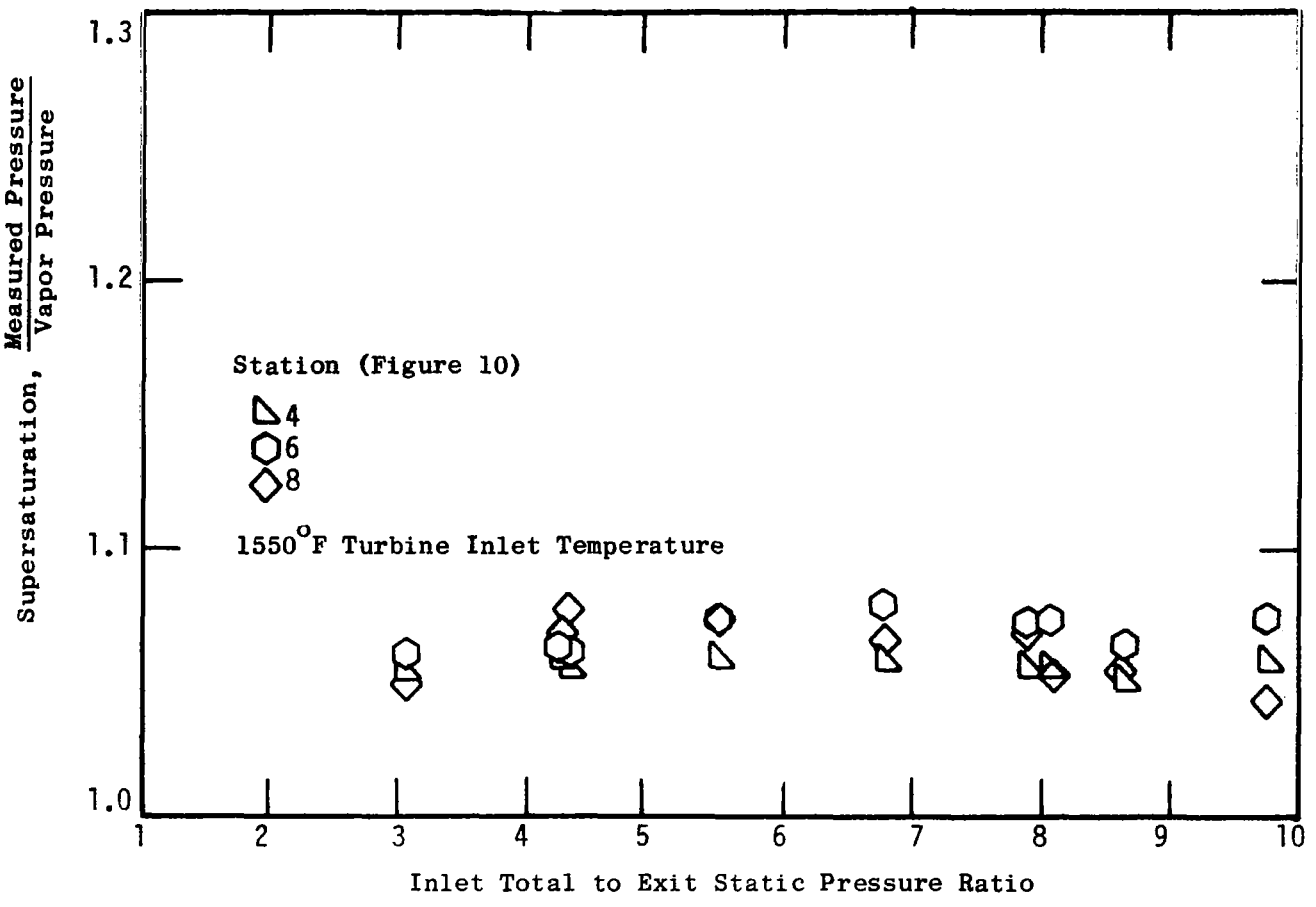

Figure 34. Supersaturation at Stator Blade Exit Stations.

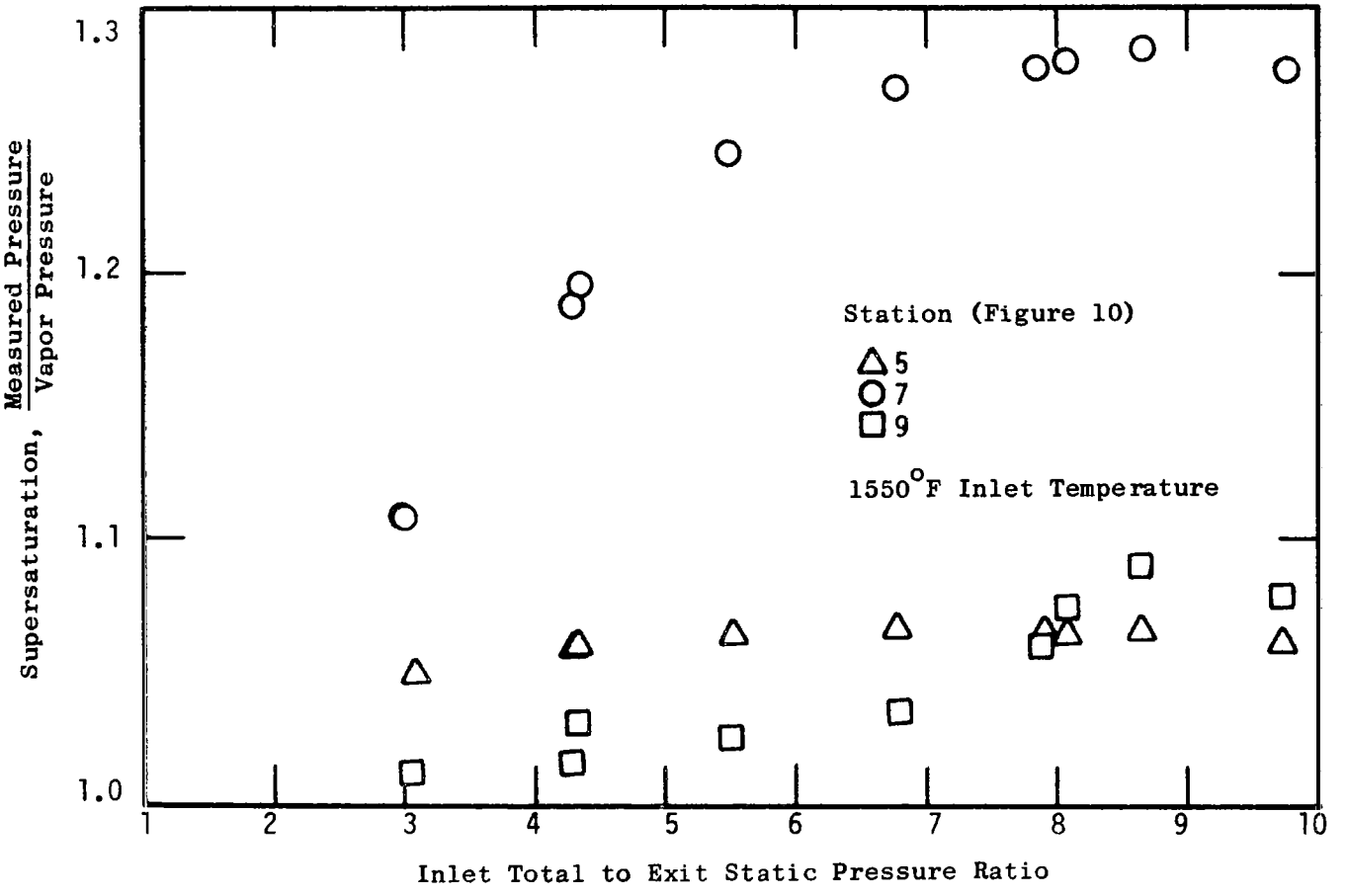

Figure 35. Supersaturation at Rotor Exit Stations.

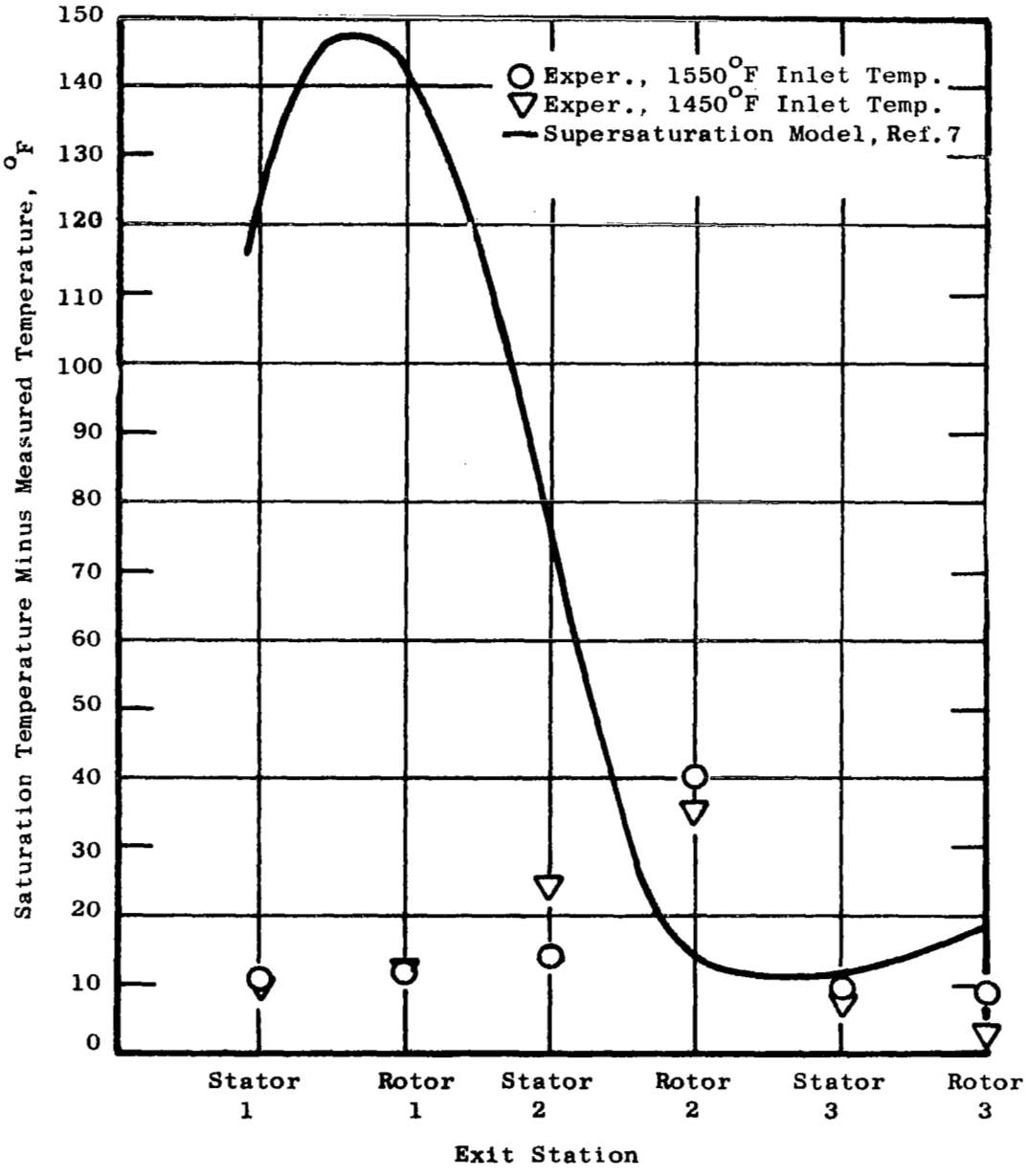

Figure 36. Subcooling in Three-Stage Turbine.

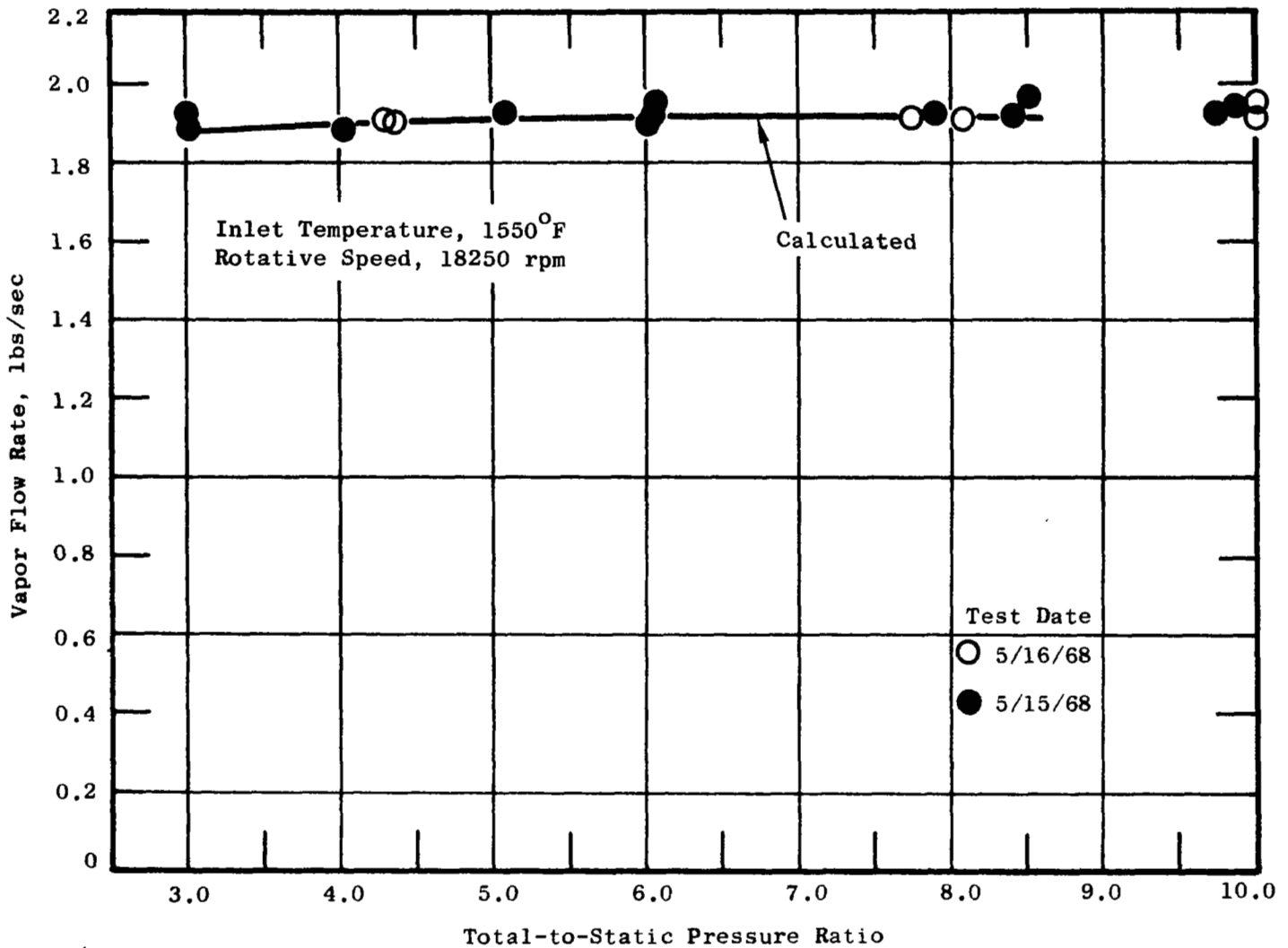

Figure 37. Comparison of Measured and Calculated Vapor Flow Rate. (Equilibrium Model)

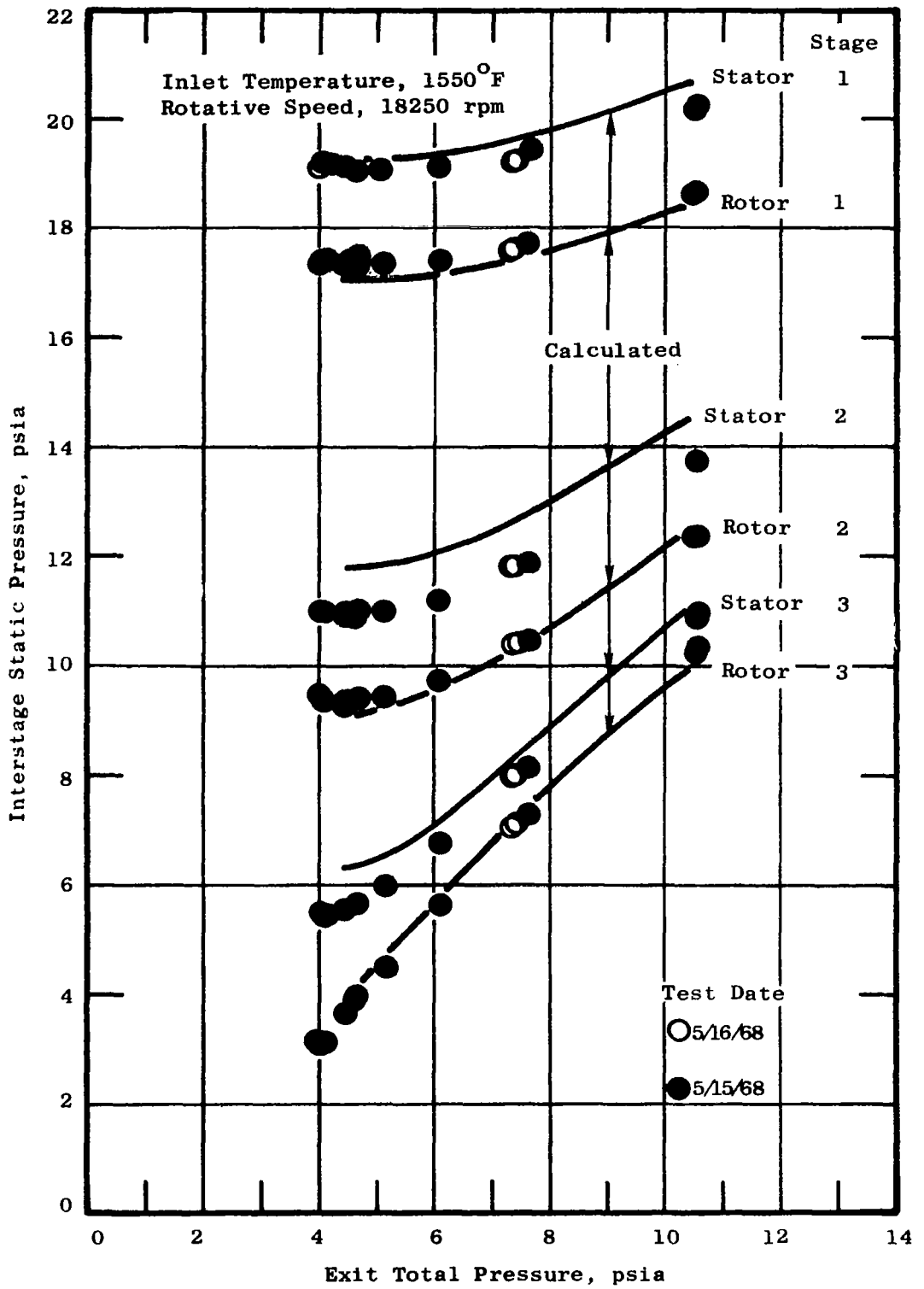

Figure 38. Comparison of Measured and Calculated Static Pressures. (Equilibrium Model)

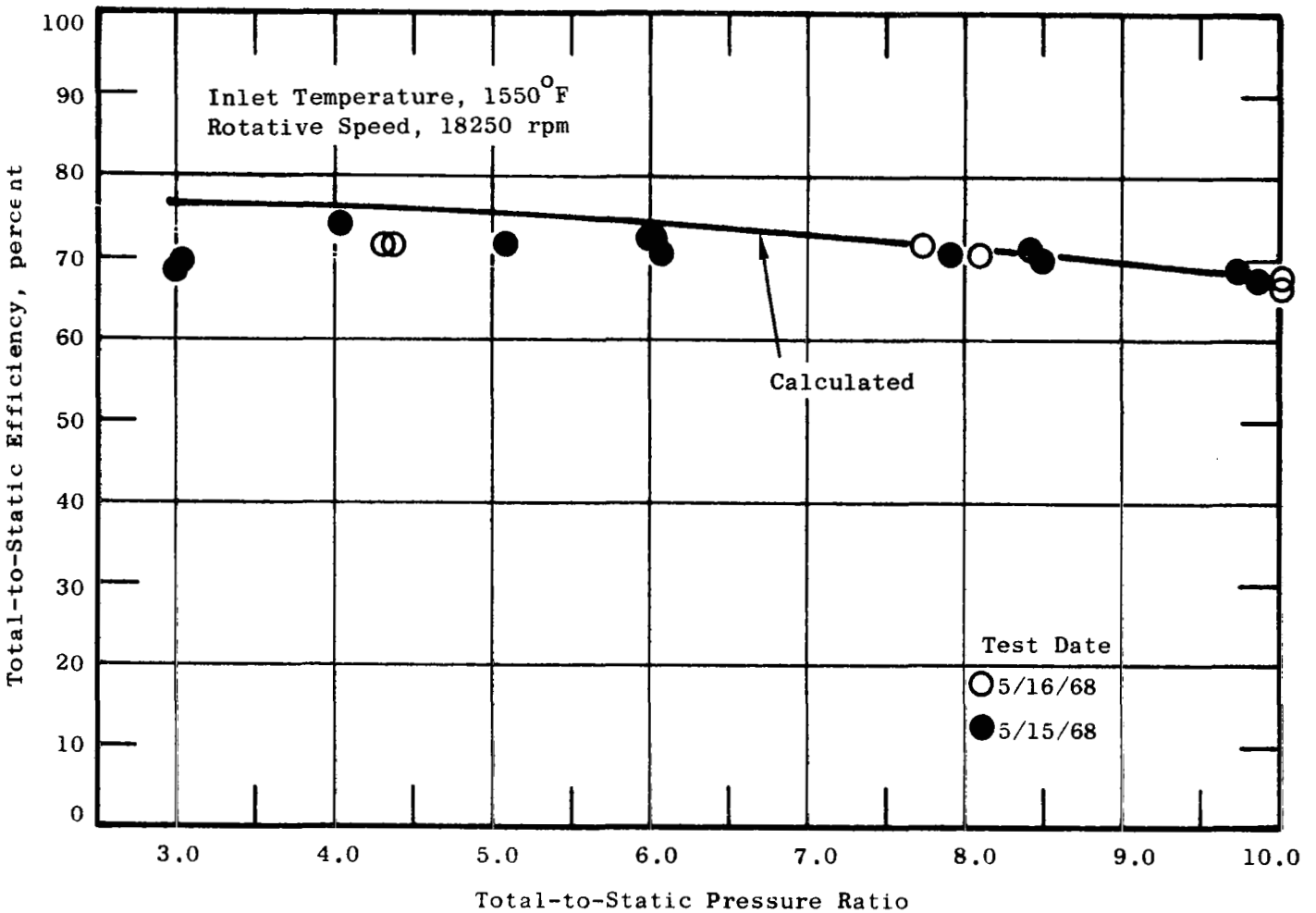

Figure 39. Comparison of Measured and Calculated Efficiency. (Equilibrium Model)

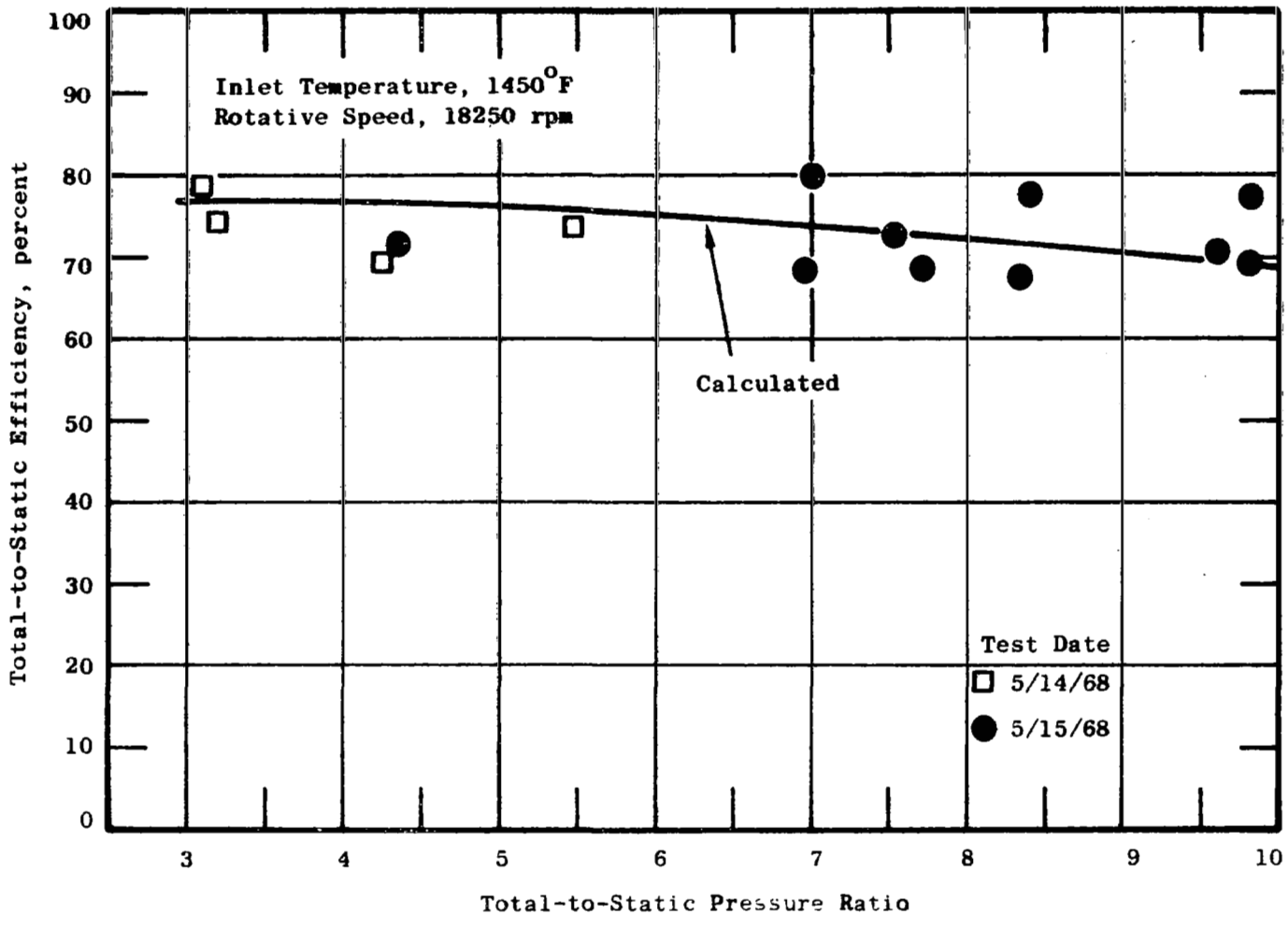

Figure 40. Comparison of Measured and Calculated Efficiency. (Equilibrium Model)

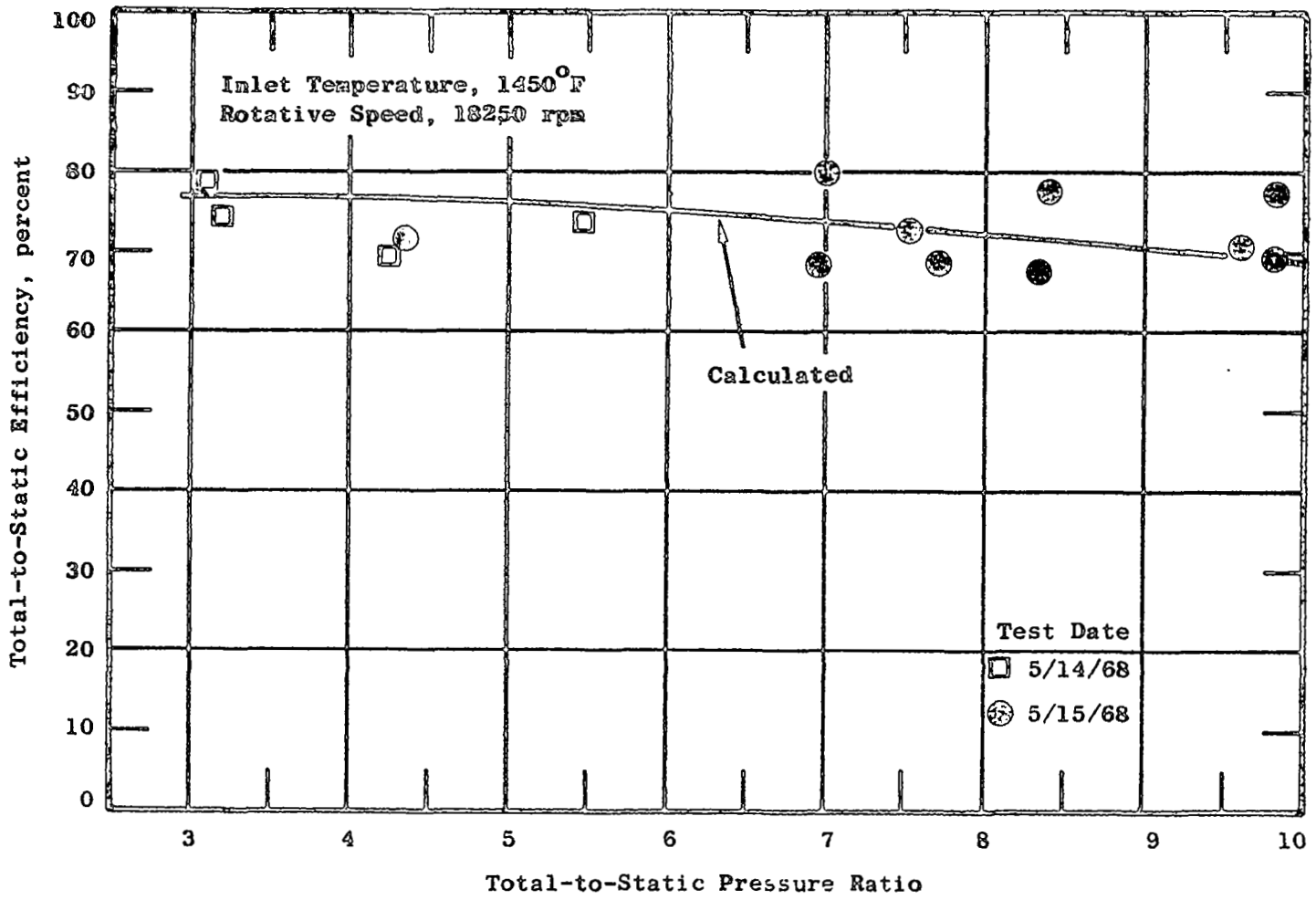

Figure 40. Comparison of Measured and Calculated Efficiency. (Equilibrium Model)

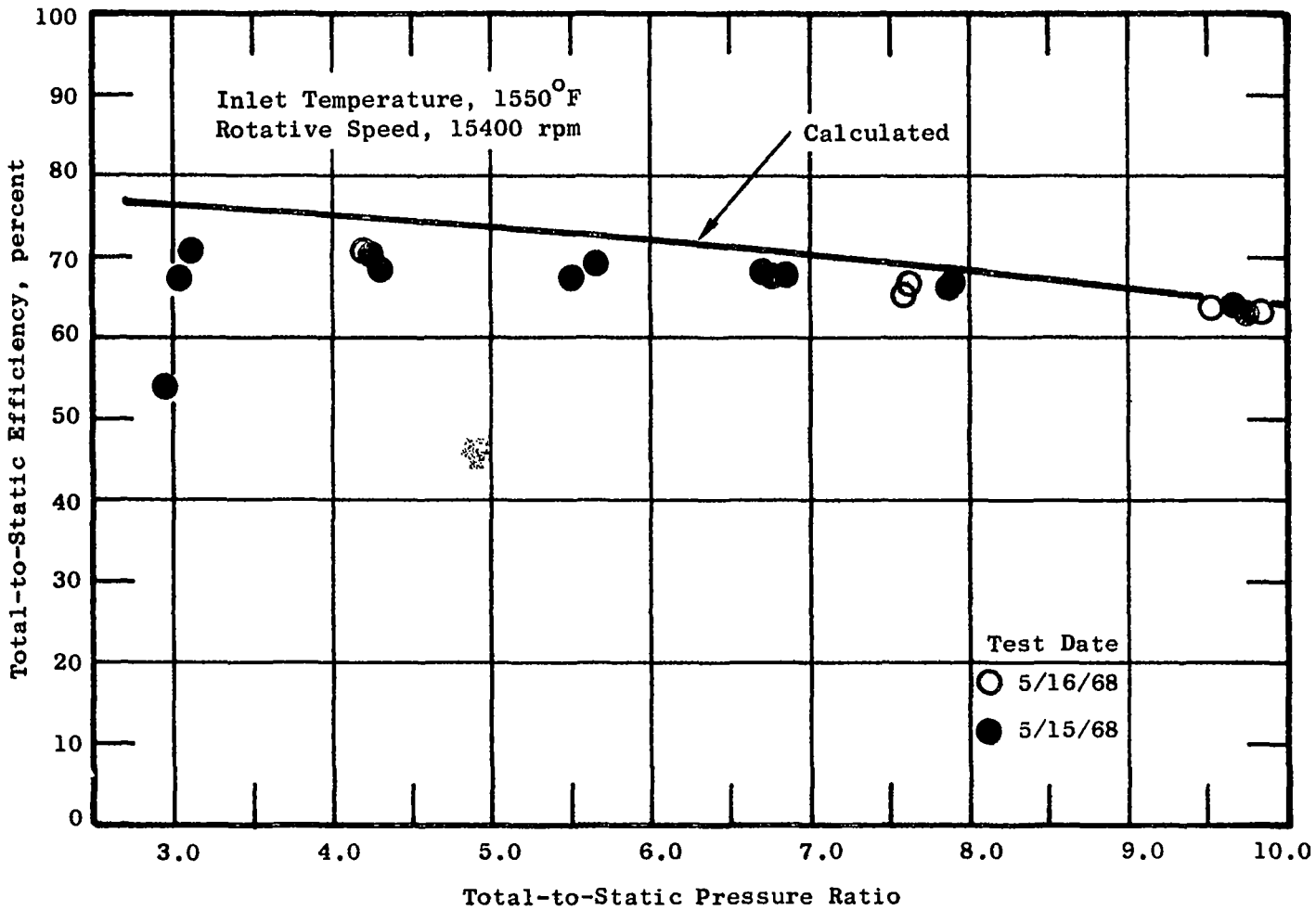

Figure 41. Comparison of Measured and Calculated Efficiency. (Equilibrium Model)

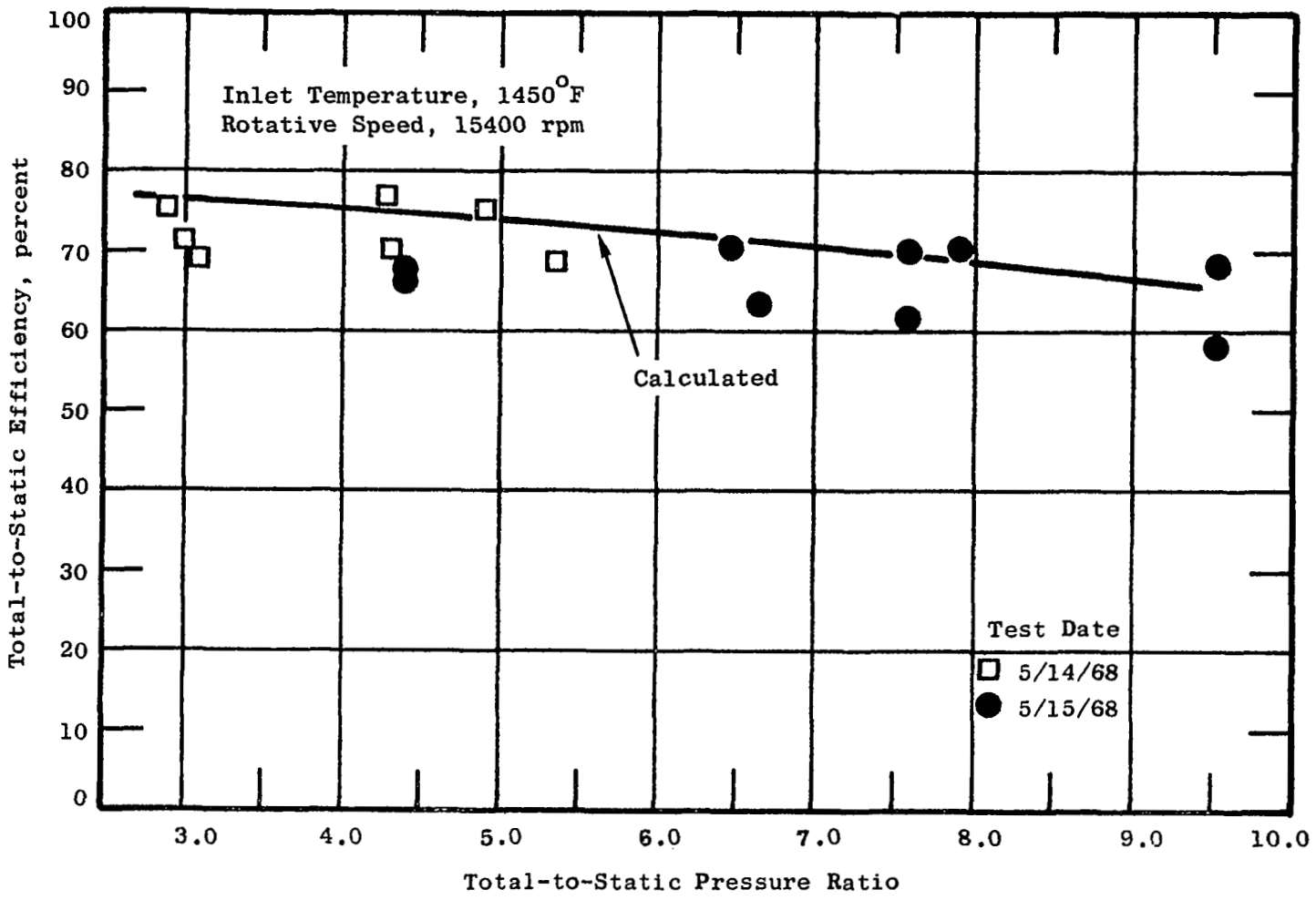

Figure 42. Comparison of Measured and Calculated Efficiency. (Equilibrium Model)

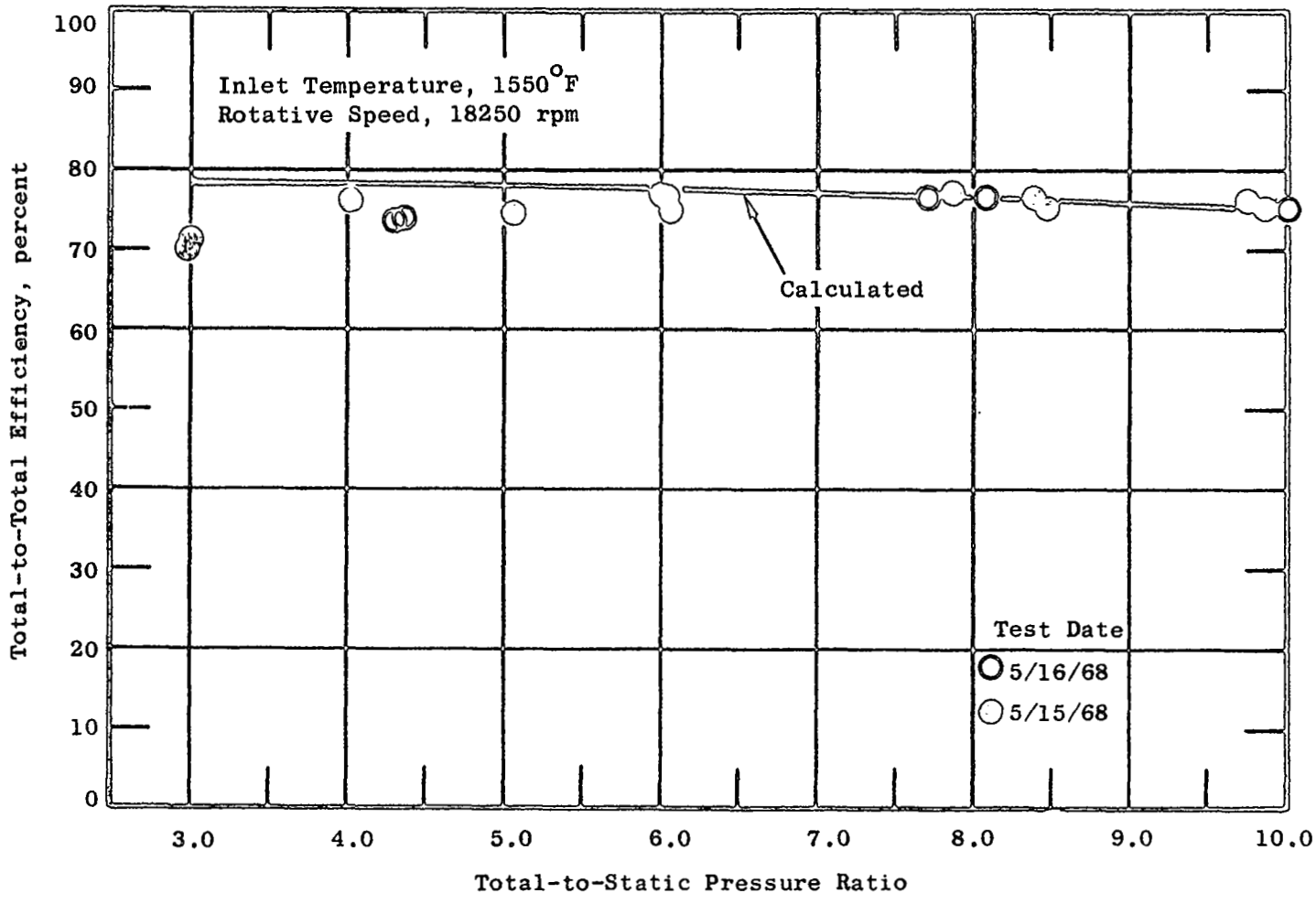

Figure 43. Comparison of Measured and Calculated Efficiency. (Equilibrium Model)

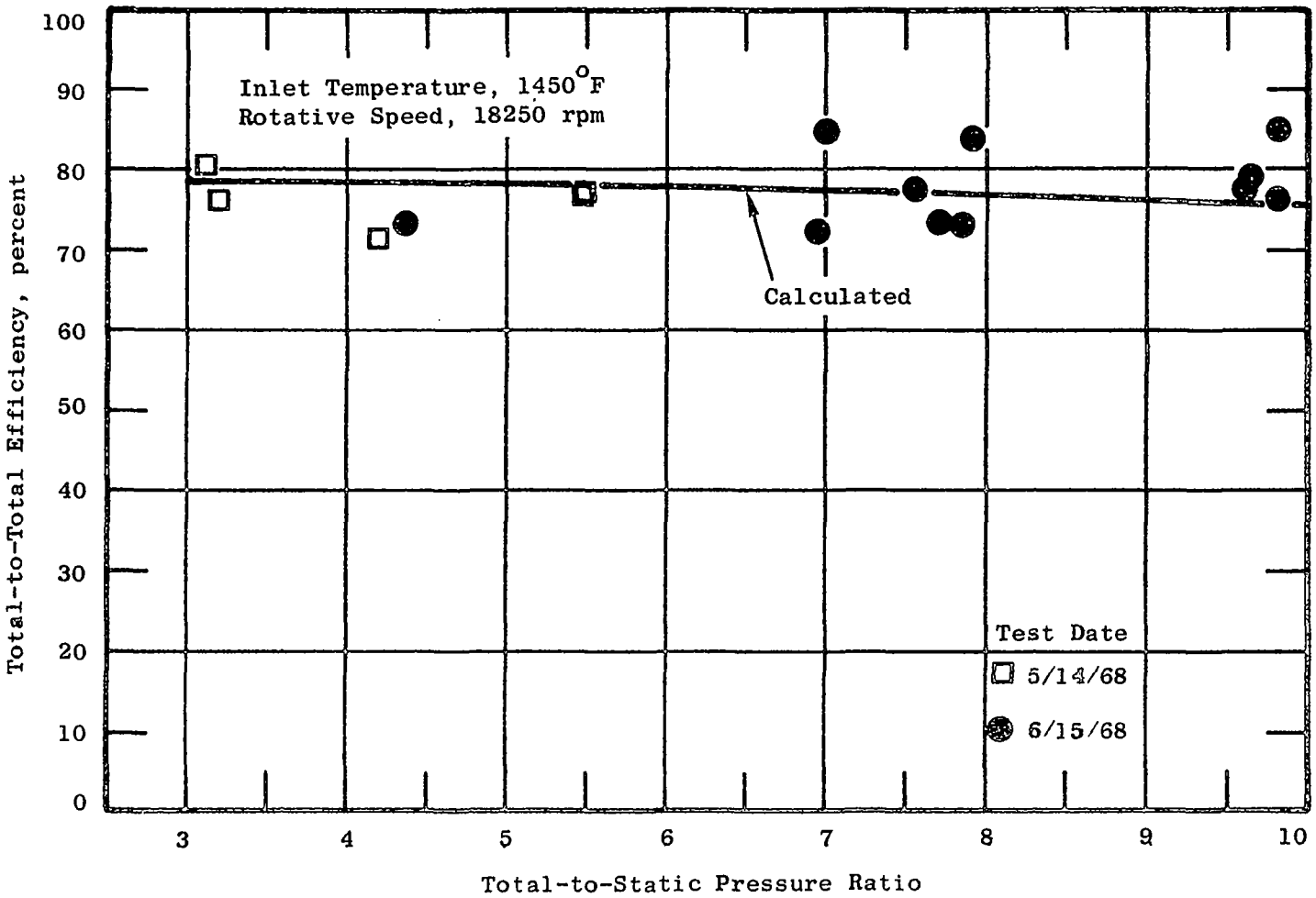

Figure 44. Comparison of Measured and Calculated Efficiency. (Equilibrium Model)

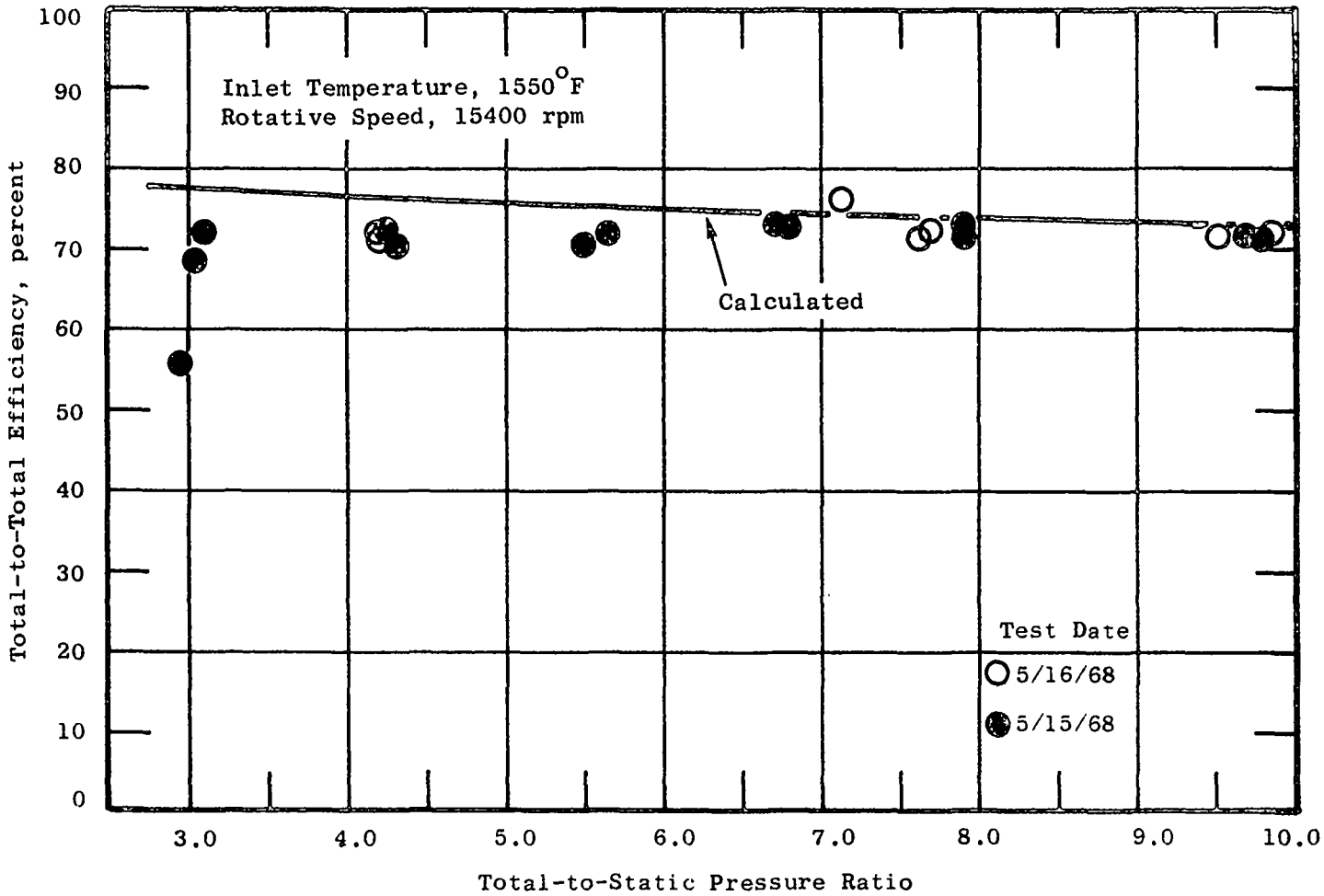

Figure 45. Comparison of Measured and Calculated Efficiency. (Equilibrium Model)

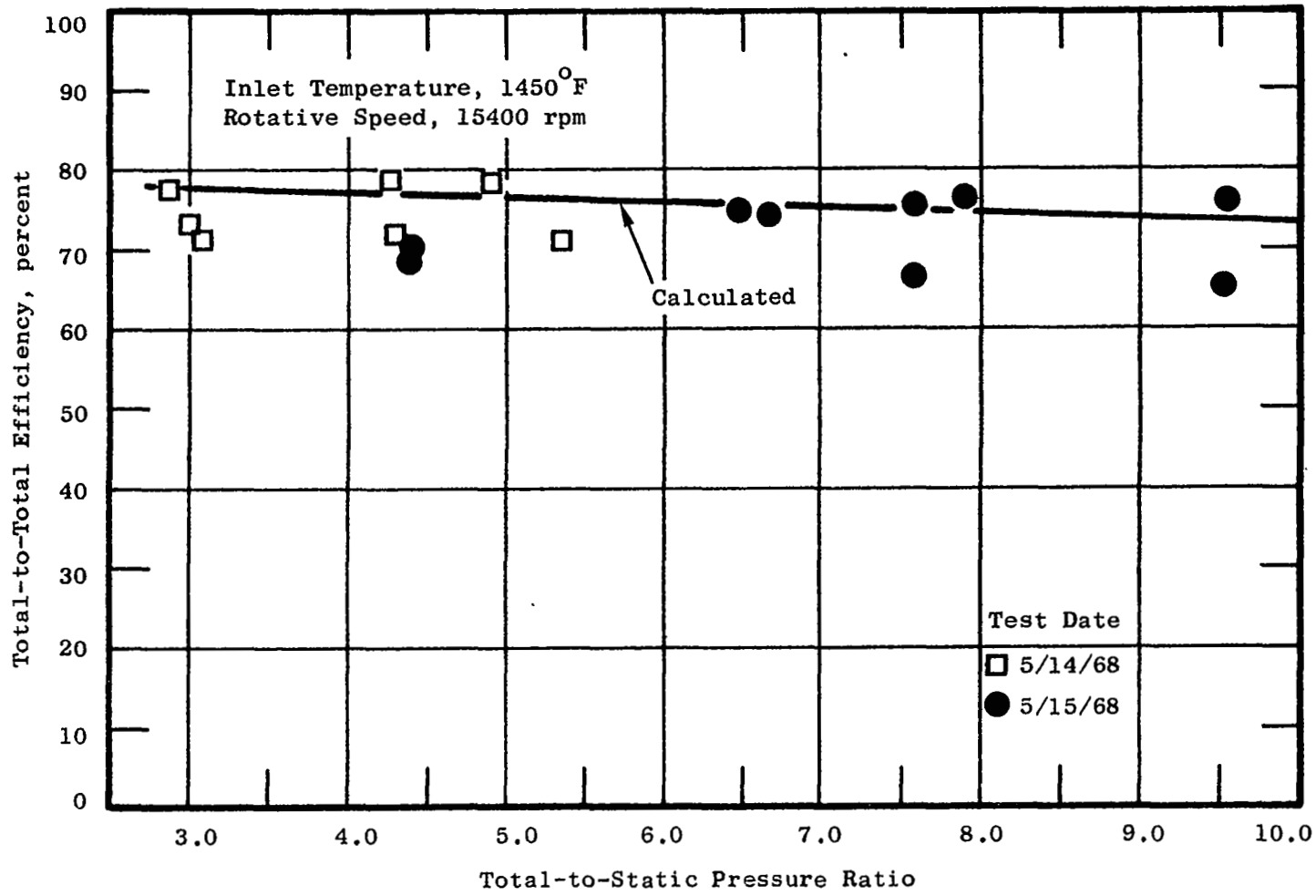

Figure 46. Comparison of Measured and Calculated Efficiency. (Equilibrium Model)

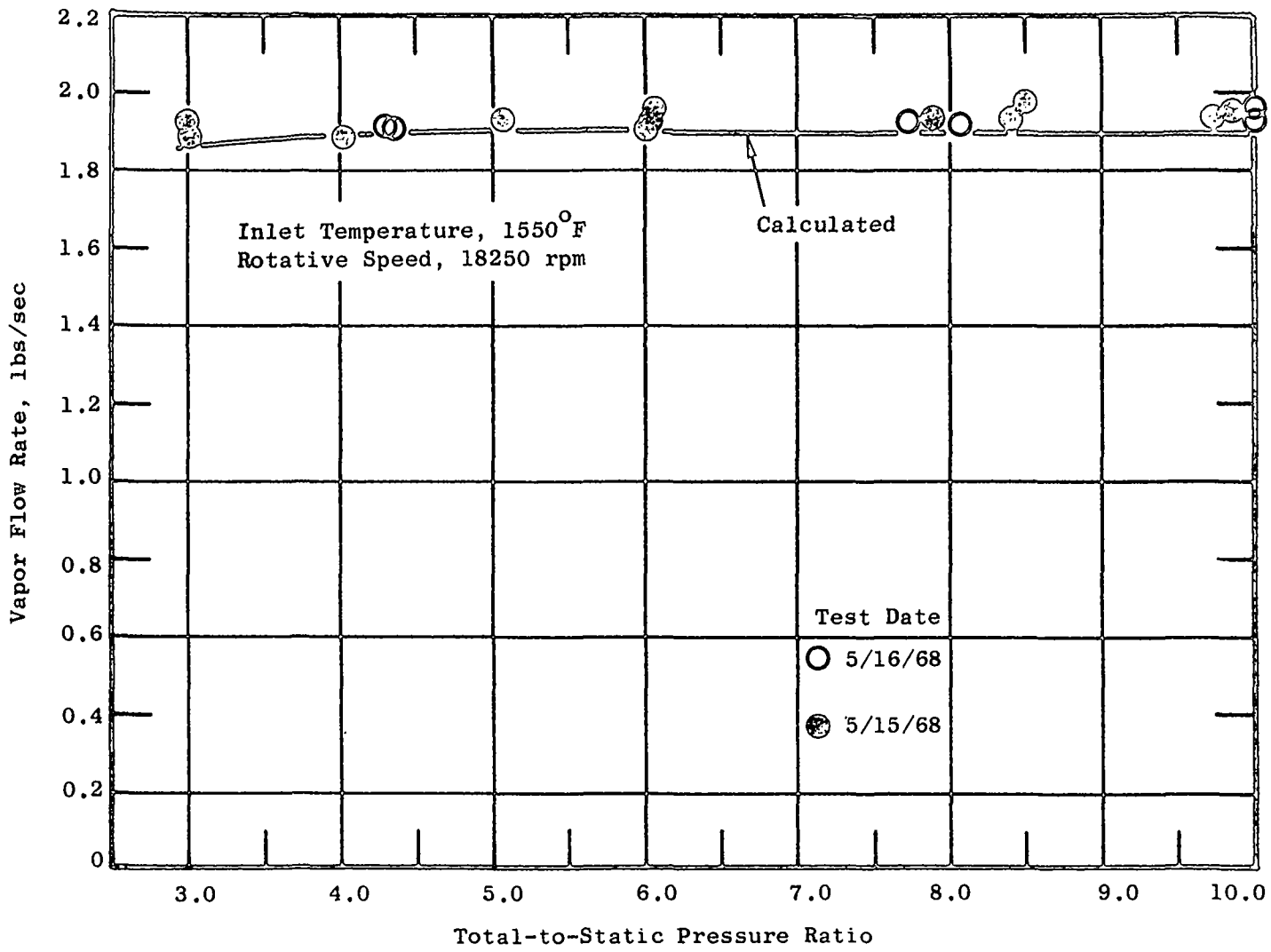

Figure 47. Comparison of Measured and Calculated Vapor Flow Rate. (Equilibrium Model)

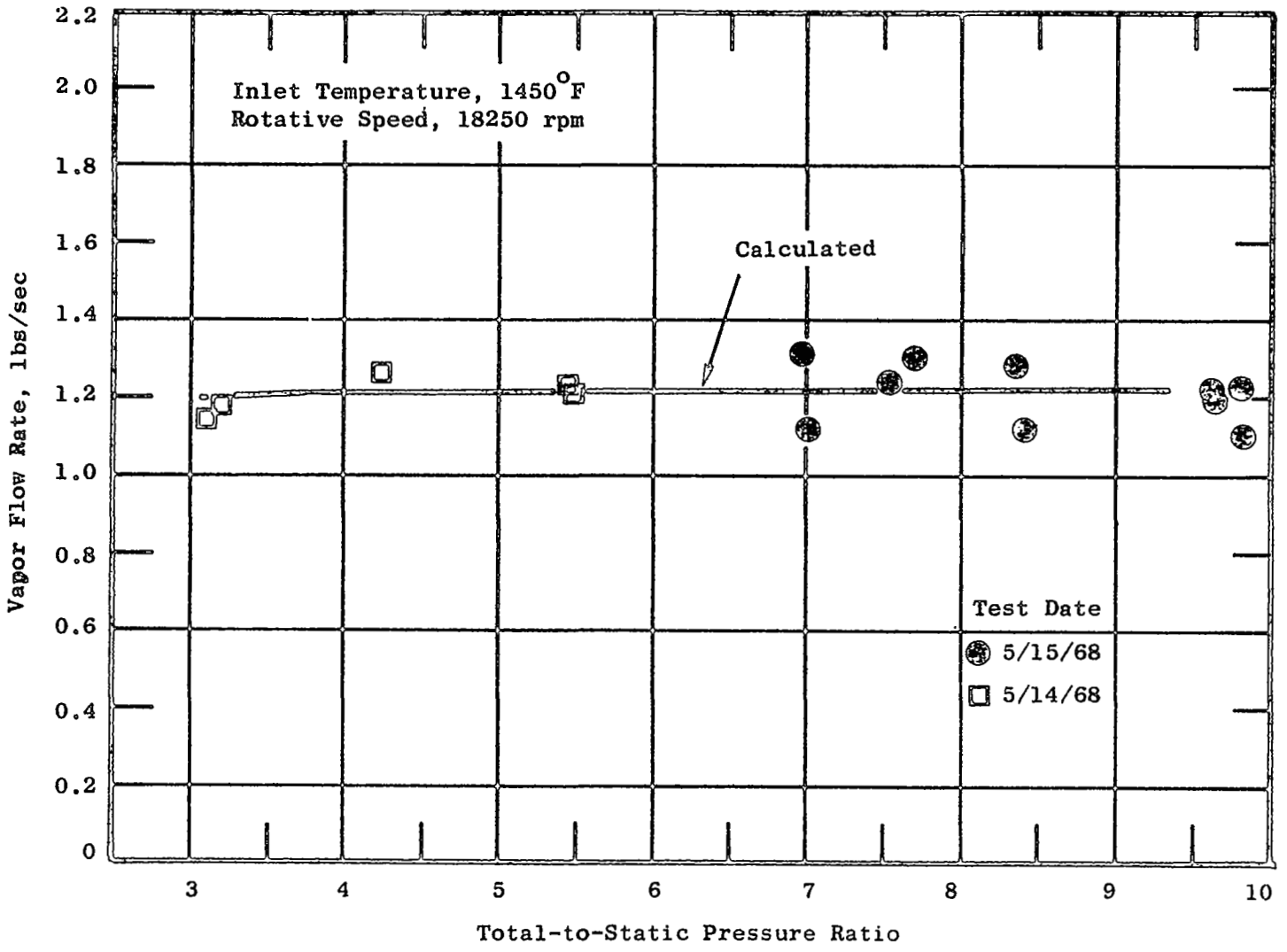

Figure 48. Comparison of Measured and Calculated Vapor Flow Rate. (Equilibrium Model)

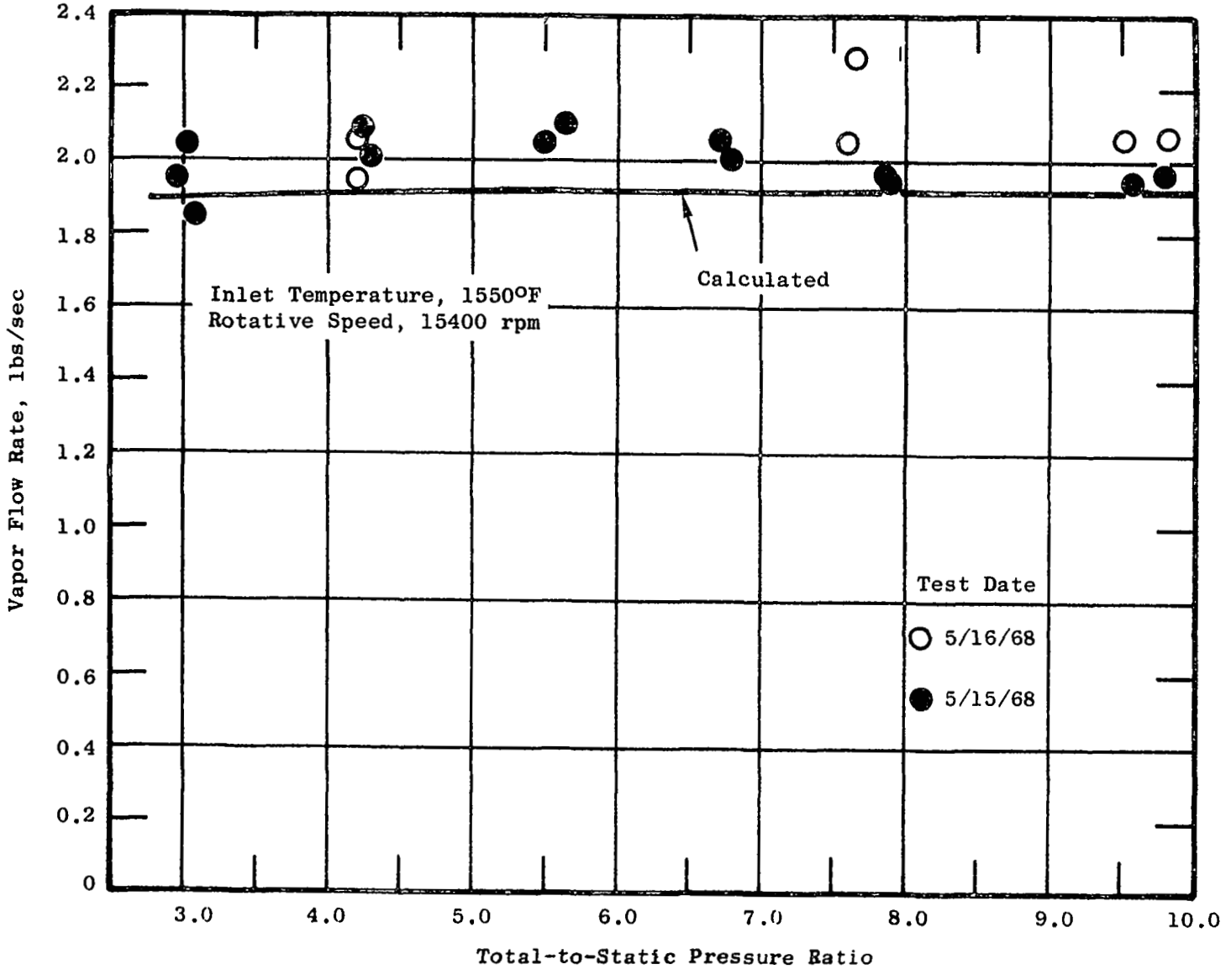

Figure 49. Comparison of Measured and Calculated Vapor Flow Rate. (Equilibrium Model)

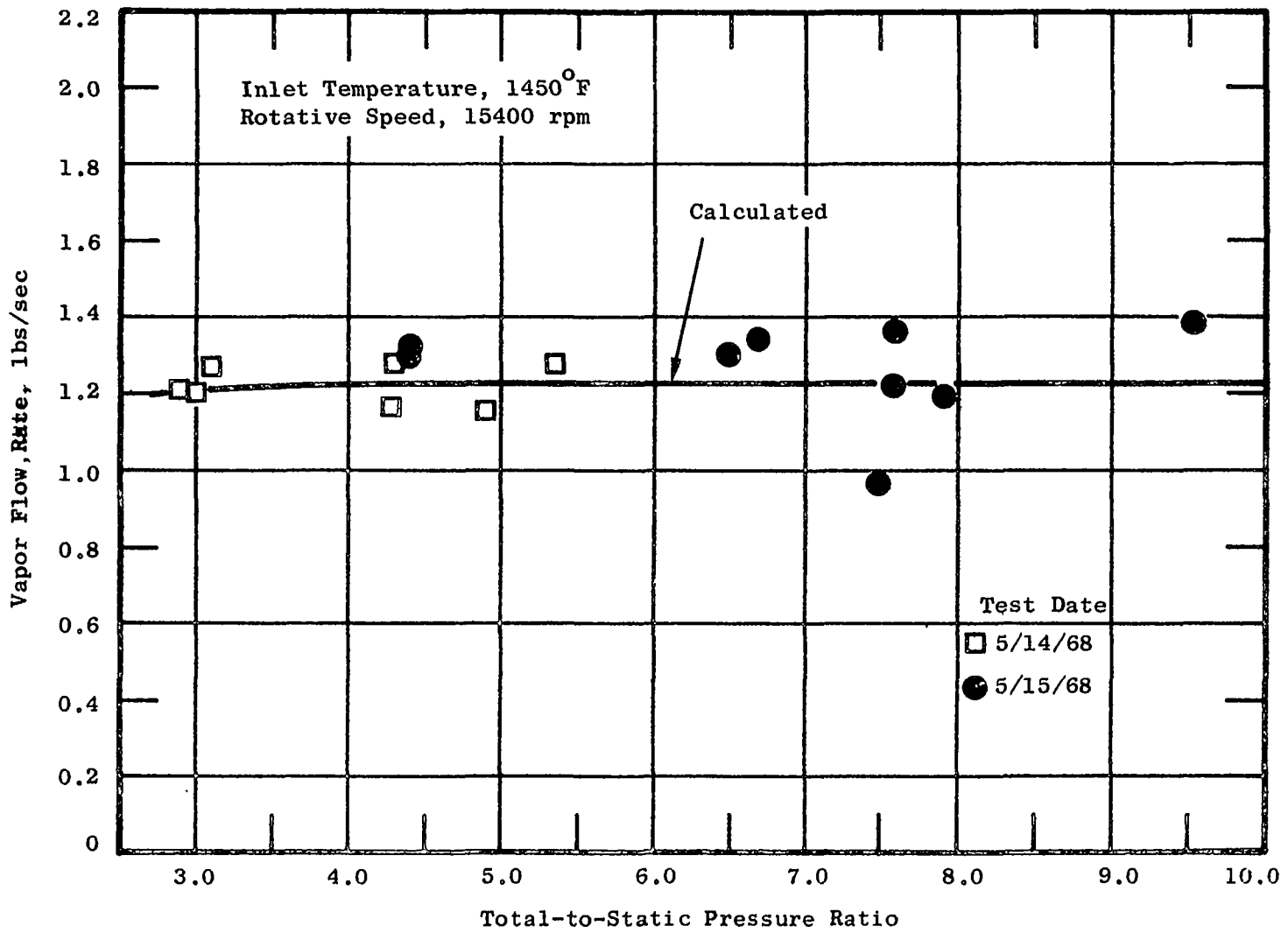

Figure 50. Comparison of Measured and Calculated Vapor Flow Rate. (Equilibrium Model)

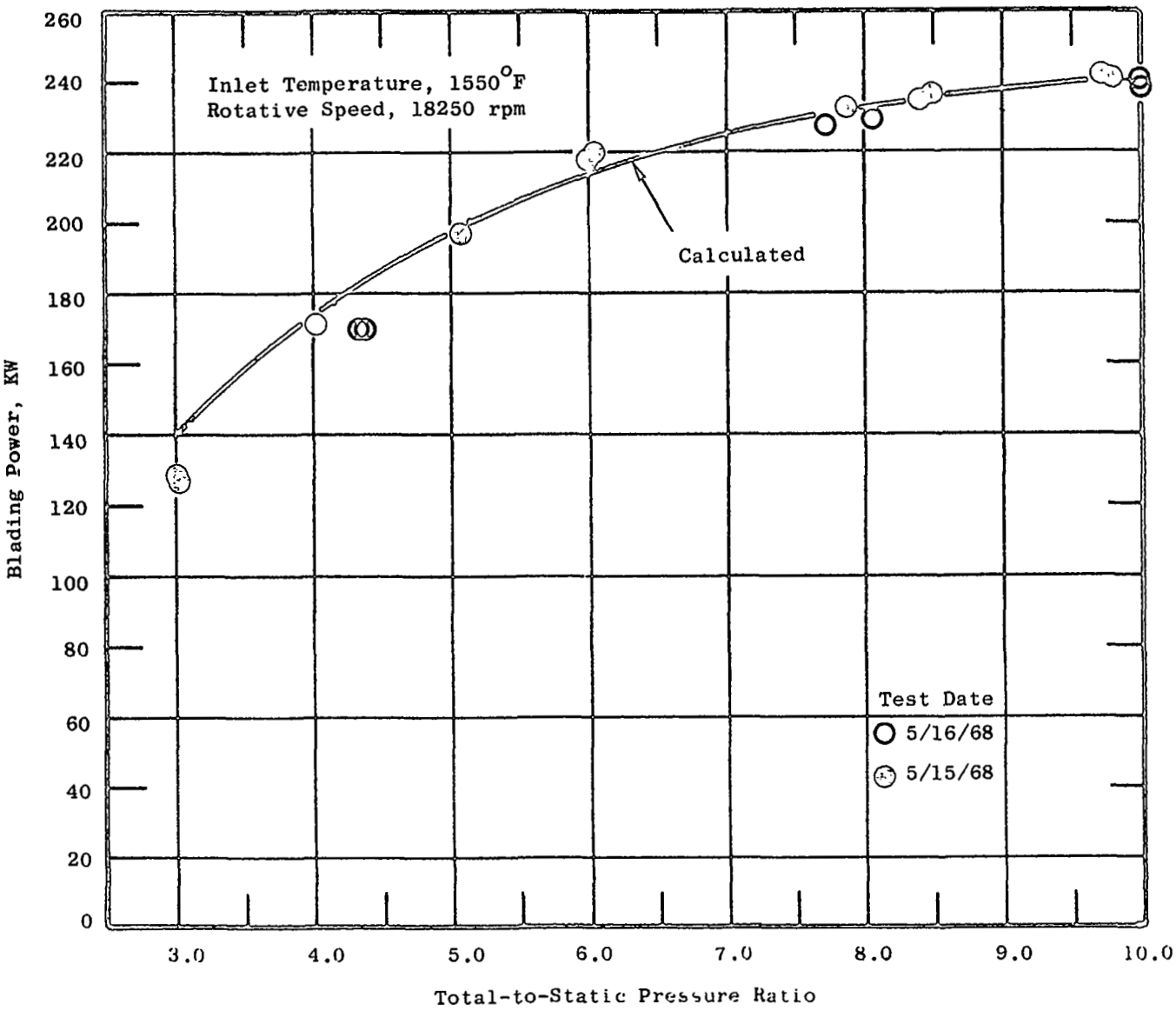

Figure 51. Comparison of Measured and Calculated Power. (Equilibrium Model)

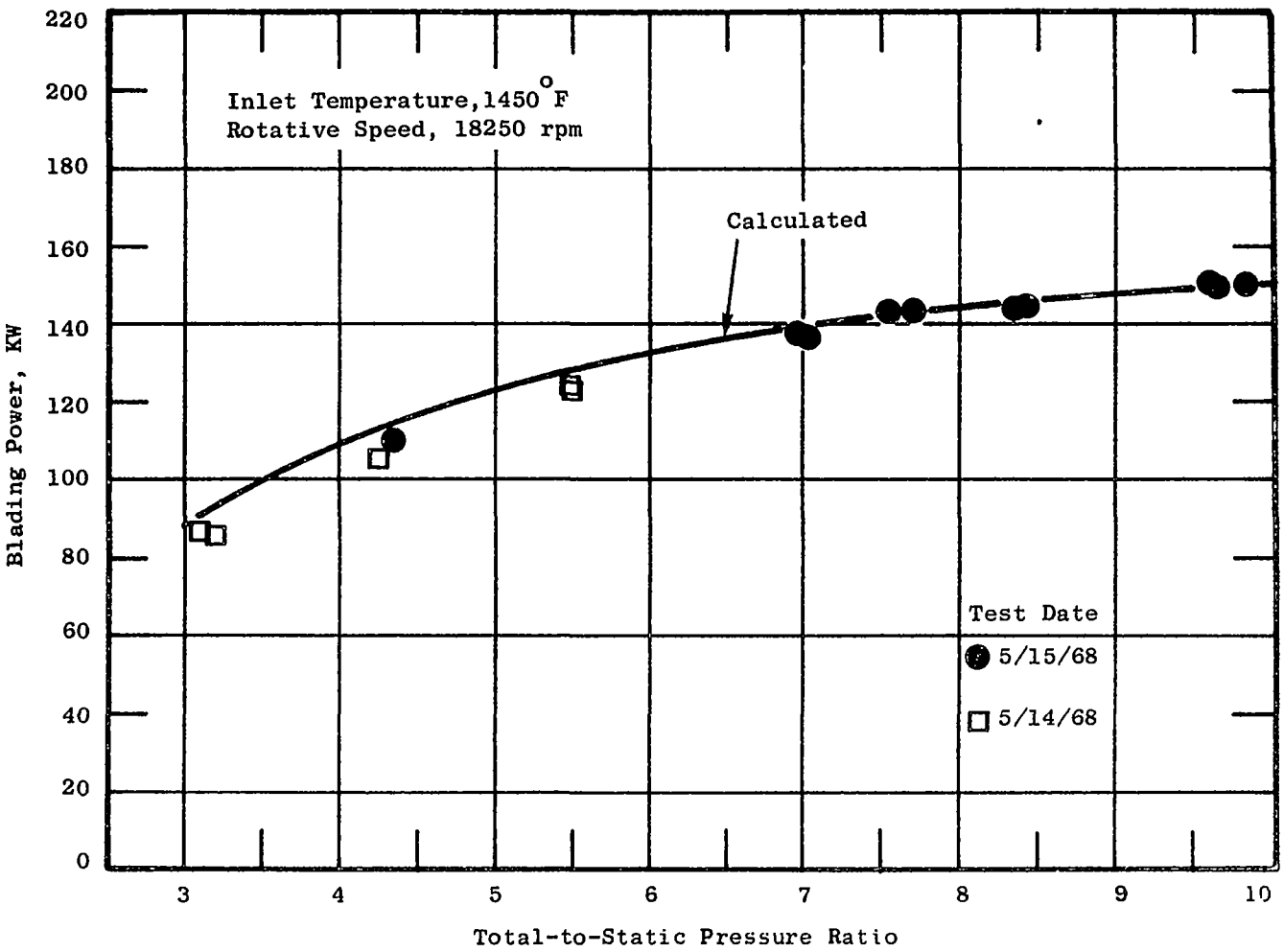

Figure 52. Comparison of Measured and Calculated Power. (Equilibrium Model)

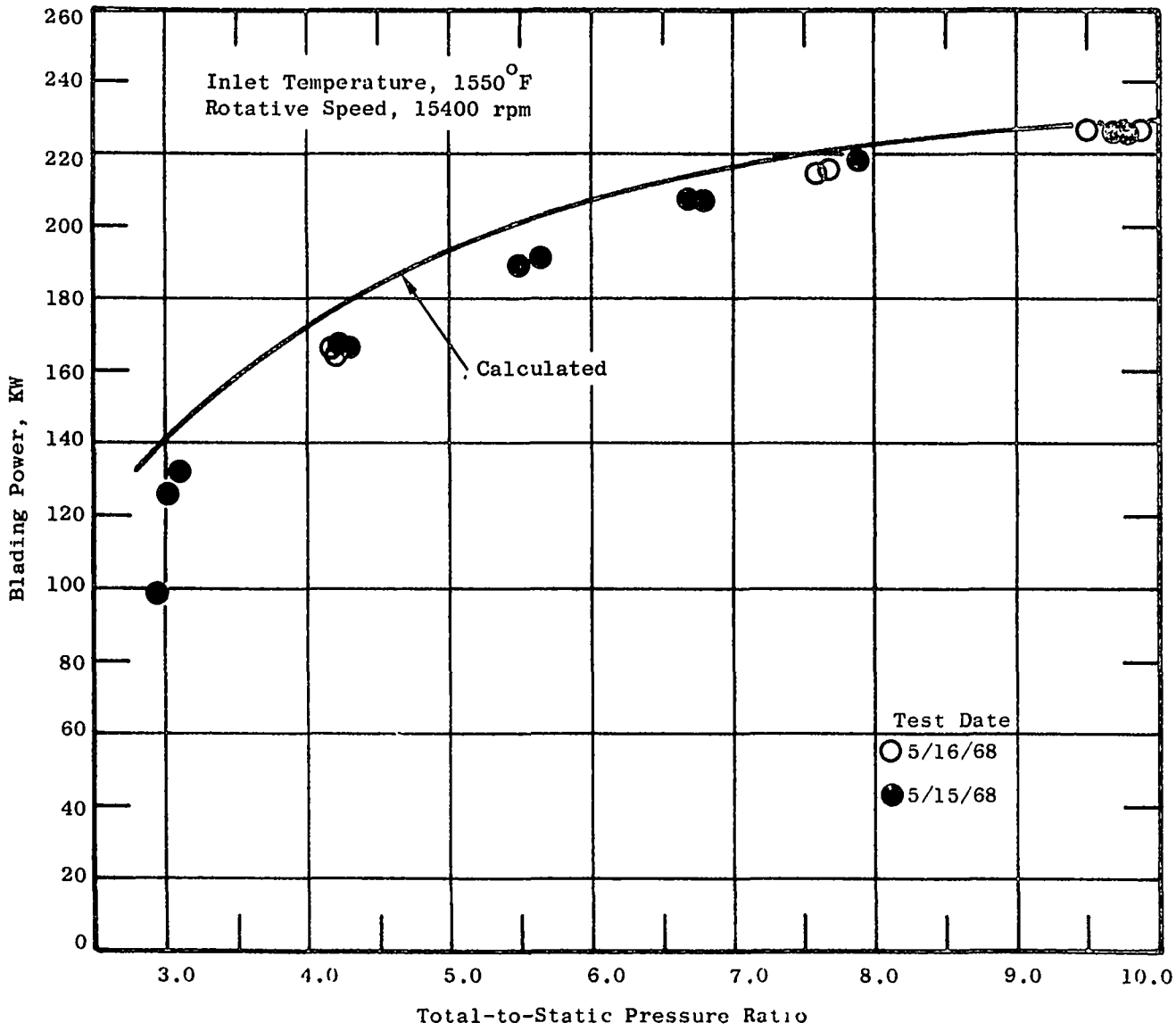

Figure 53. Comparison of Measured and Calculated Power. (Equilibrium Model)

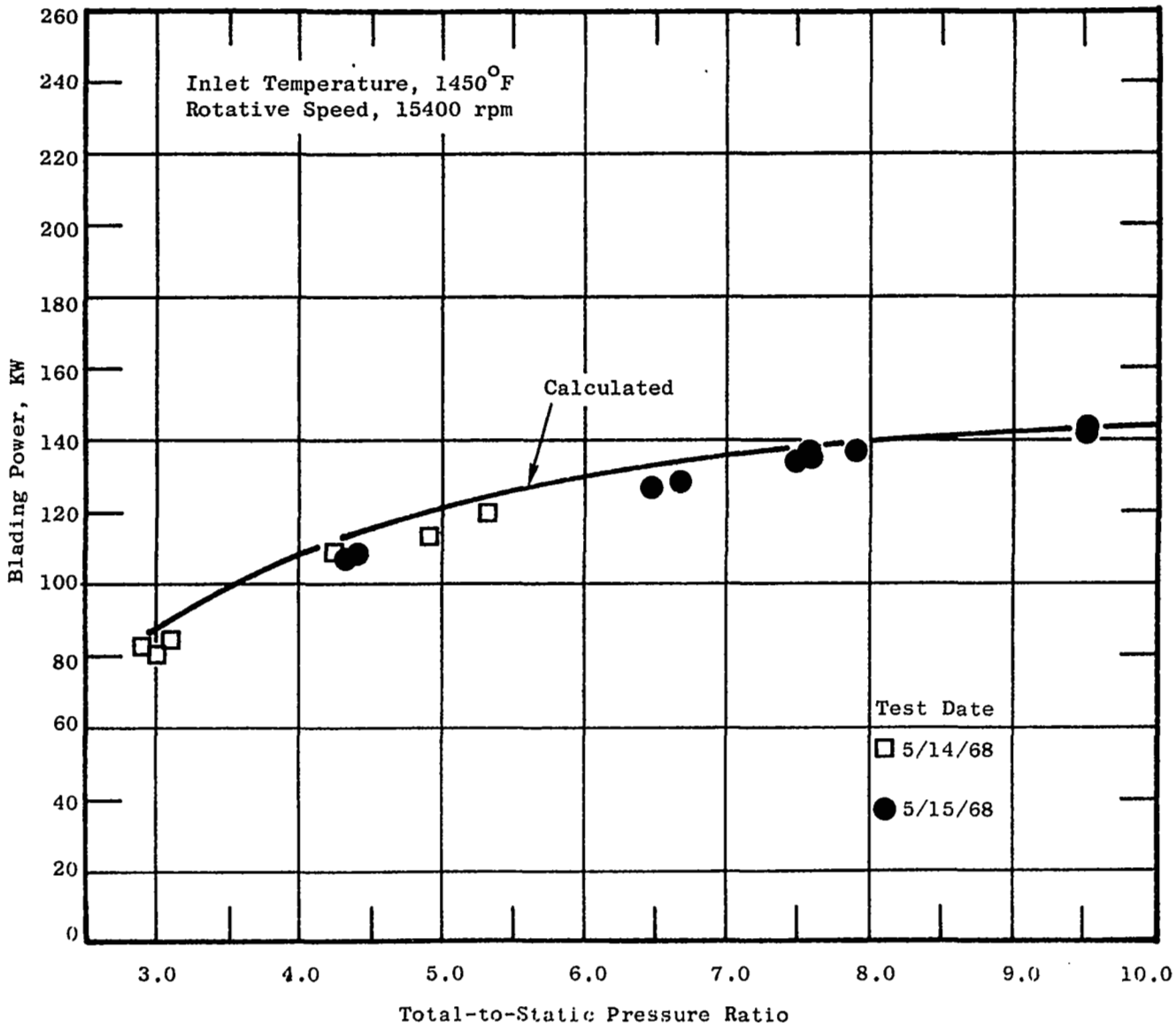

Figure 54. Comparison of Measured and Calculated Power. (Equilibrium Model)

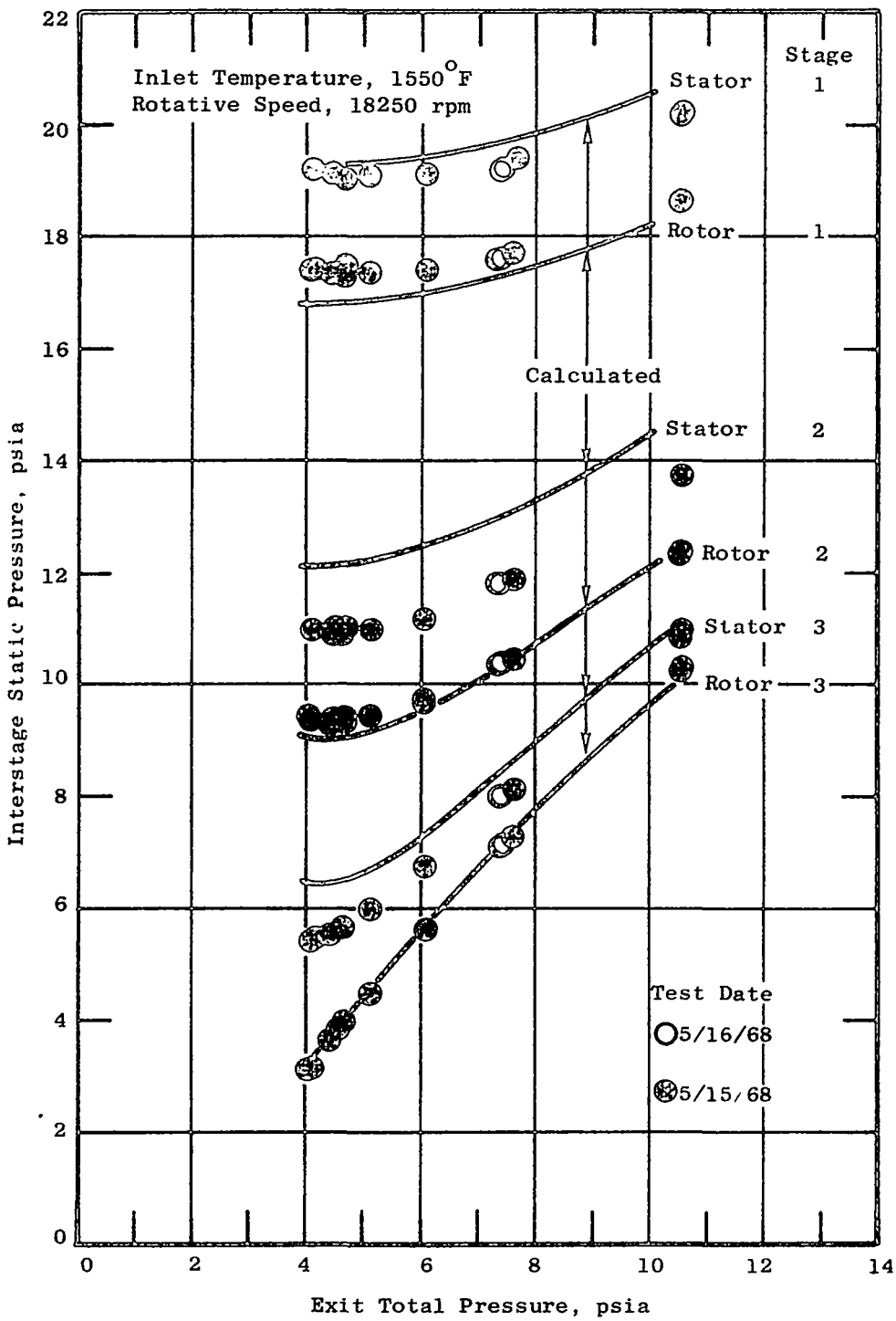

Figure 55. Comparison of Measured and Calculated Static Pressures. (Equilibrium Model)

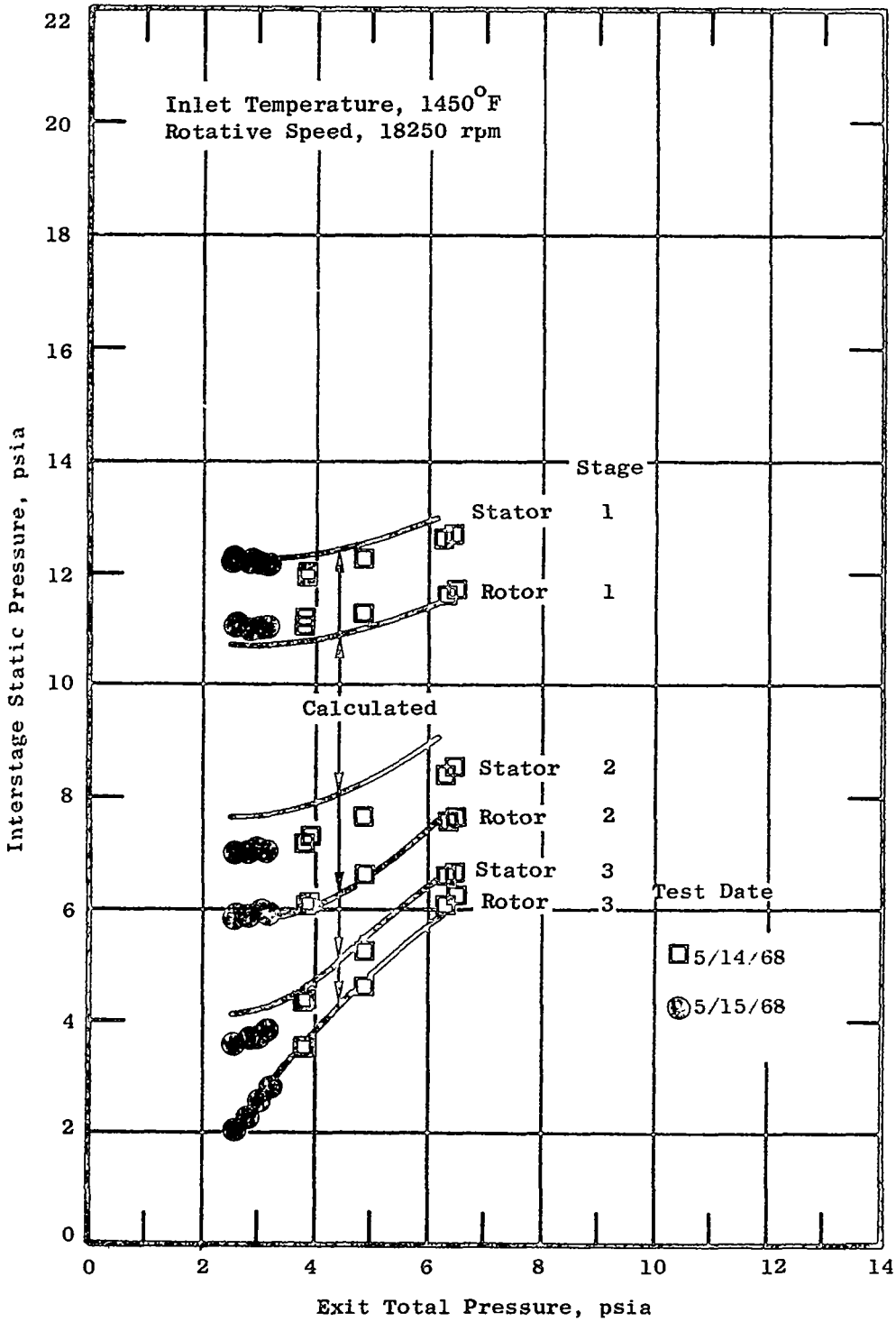

Figure 56. Comparison of Measured and Calculated Static Pressures. (Equilibrium Model)

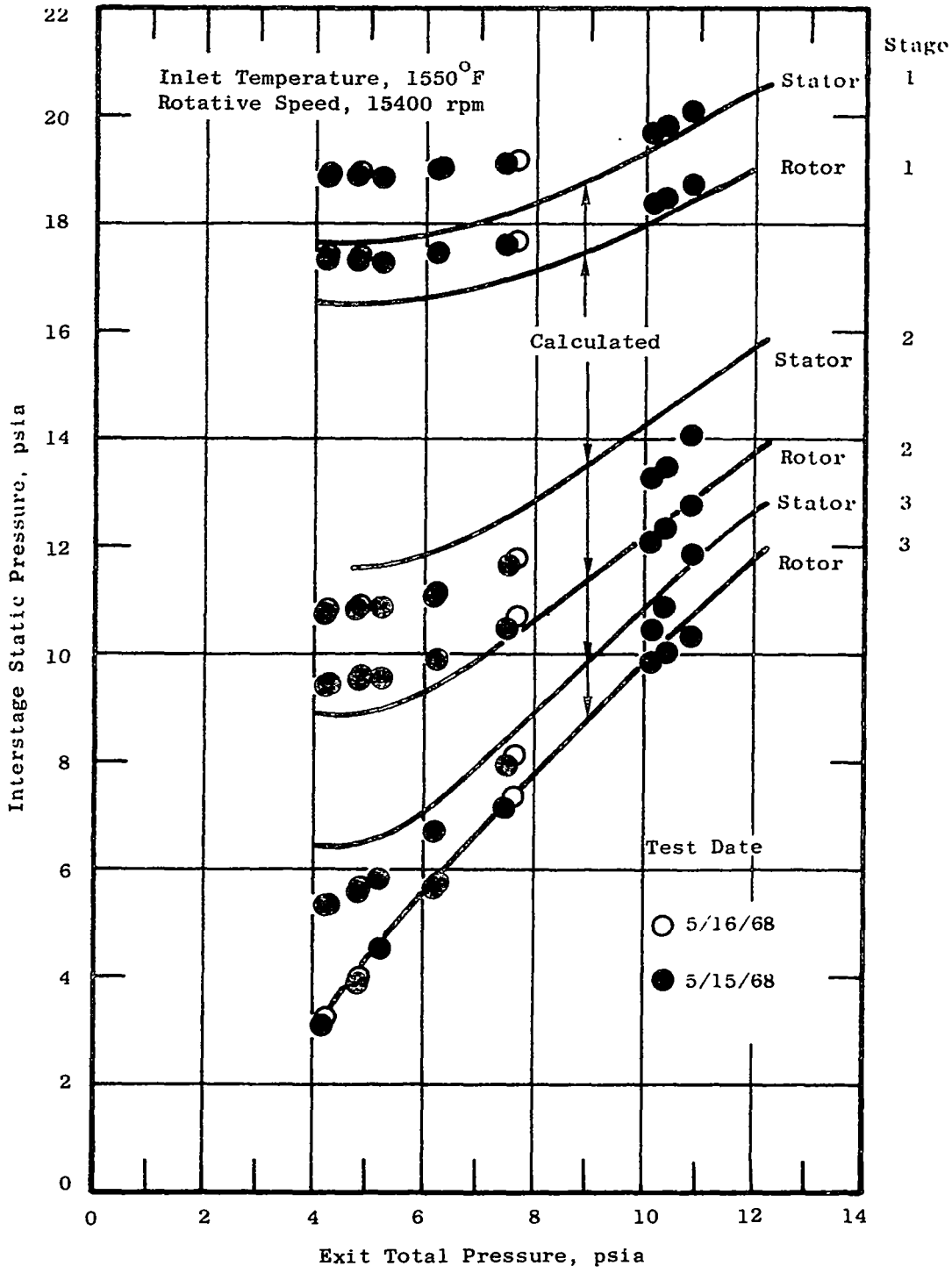

Figure 57. Comparison of Measured and Calculated Static Pressures. (Equilibrium Model)

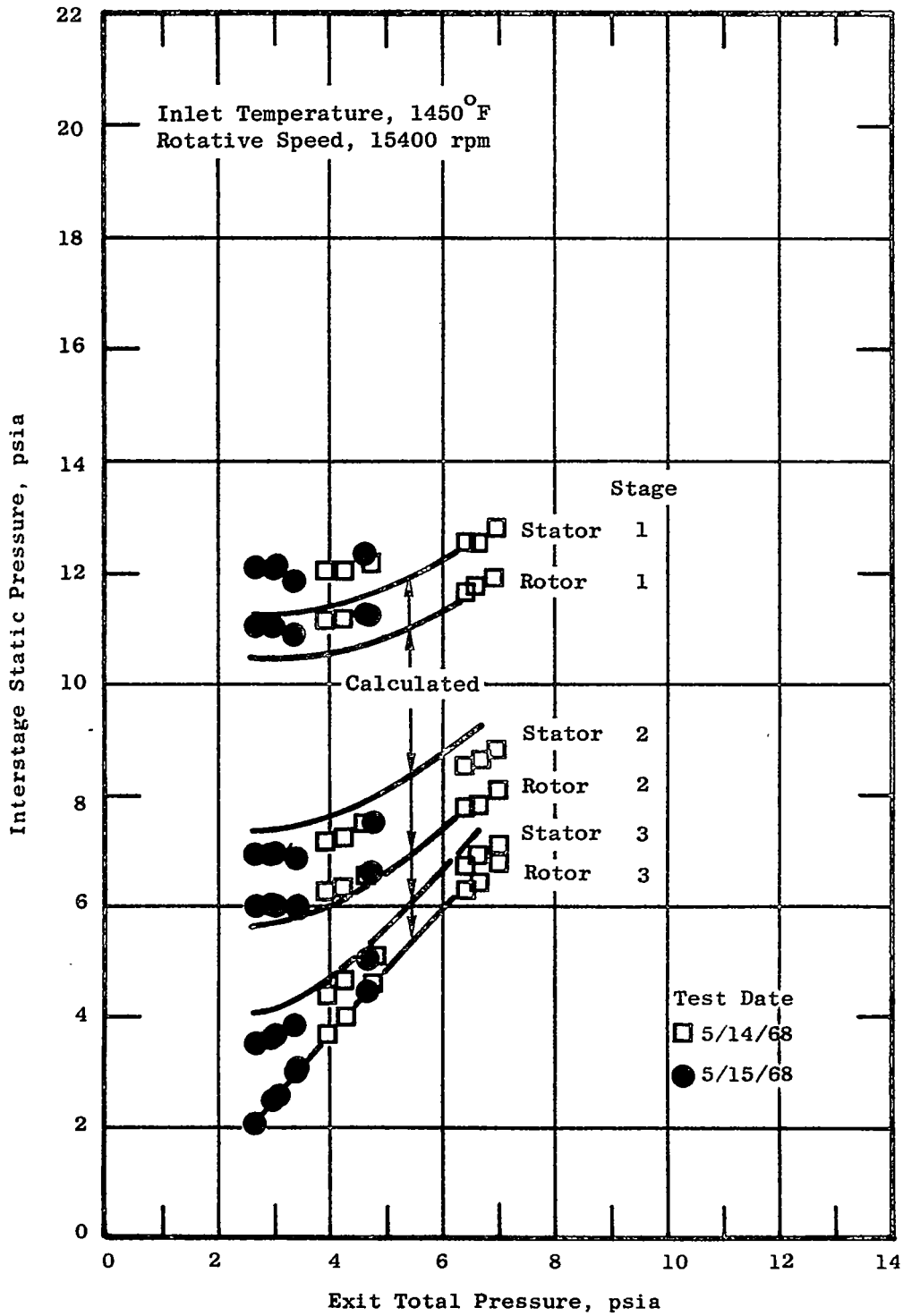

Figure 58. Comparison of Measured and Calculated Static Pressures. (Equilibrium Model)